A Fogging Scrubber to Treat Diesel Exhaust: Field Testing and a Mechanistic Model

Joseph Tabor

Thesis submitted to the faculty of the Virginia Polytechnic Institute and State University in partial fulfillment of the requirements for the degree of

Master of Science

In

Mining Engineering

Emily A. Sarver, Chair

John R. Saylor

Kramer D. Luxbacher

June 30, 2020

Blacksburg, VA

Keywords: Diesel Particulate Matter, DPM, fog, diesel exhaust, scrubber, underground mining, occupational health, mine ventilation

A Fogging Scrubber to Treat Diesel Exhaust: Field Testing and a Mechanistic Model

Joseph Tabor

Academic Abstract

Diesel particulate matter (DPM) is comprised of two main fractions, organic carbon (OC) and elemental carbon (EC). DPM is the solid portion of diesel exhaust and particles are submicron in size typically ranging from 10 to 1000 nanometers. DPM is a known respirable hazard and occupational exposure can lead to negative health effects. These effects can range from irritation of the eyes, nose, and throat to more serious respirable and cardiovascular diseases. Due to the use of diesel powered equipment in confined airways, underground mine environments present an increased risk and underground mine works can be chronically overexposed. Current engineering controls used to mitigate DPM exposure include cleaner fuels, regular engine maintenance, ventilation controls, and enclosed cabs on vehicles. However even with these controls in place, workers can still be overexposed.

The author's research group has previously tested the efficacy of a novel, fog-based scrubber treatment for removing DPM from the air, in a laboratory setting. It was found that the fog treatment improved DPM removal by approximately 45% by number density compared to the control trial (fog off). The previous work stated thermal coagulation between the fog drops and the DPM, followed by gravitational settling of the drops to be the likely mechanisms responsible for the DPM removal. The current work investigated the efficacy of the fog treatment on a larger scale in an underground mine environment, by using a fogging scrubber to treat the entire exhaust stream from a diesel vehicle. A total of 11 field tests were conducted.

Based on measurements of nanoparticle number concentration at the inlet and outlet of the scrubber, the fog treatment in the current work showed an average improvement in total DPM removal of approximately 55% compared to the control (fog off) condition. It was found that the treatment more effectively removed smaller DPM sizes, removing an average of 84 to 89% of the DPM in the 11.5, 15.4, and 20.5 nanometer size bins and removing 24 to 30% of the DPM in the 88.6, 115.5, and 154 nanometer size bins. These observations are consistent with expectations since the rate of coagulation between the DPM and fog drops should be greater for smaller diameters.

Further analysis of the DPM removal was aided by development of a mechanistic model of the fogging scrubber. The model uses the scrubber inlet data from the experimental tests as input parameters, and it outputs the outlet concentration of DPM for comparison to the experimental outlet data. Results provided support for the notion that DPM removal relies on DPM-fog drop coagulation, and subsequent removal of the DPM-laden drops as opposed to DPM removal by diffusion or inertial impaction of DPM directly to the walls. The model results suggest that inertial impaction of these drops to the scrubber walls is likely much more important than gravitational settling. Moreover, the ribbed geometry of the tubing used for the scrubber apparatus tested here appears to greatly enhance inertial impaction (via enhancement of depositional velocity) versus smooth-walled tubing. This is consistent with previous research that shows particle deposition in tubes with internally ribbed or wavy structures is enhanced compared to deposition in tubes with smooth walls.

A Fogging Scrubber to Treat Diesel Exhaust: Field Testing and a Mechanistic Model

Joseph Tabor

General Audience Abstract

Diesel particulate matter (DPM) describes the solid portion of diesel exhaust. These particles are in the nanometer size range (10-1000nm) and can penetrate deep within the lungs presenting a serious health hazard. Because of the use of diesel powered equipment in confined spaces, DPM presents an occupational hazard for underground mine workers. Even with the use of cleaner fuels, regular engine maintenance, proper ventilation, and enclosed vehicle cabs, workers can still be over exposed.

Previous work has shown that a water fog treatment can help to remove DPM from the air in a laboratory setting. This removal is due to the DPM particles attaching to the drops, followed by the drops settling out of the air due to gravity or impacting the walls of a tube. To explore a full scale exhaust treatment, a fogging scrubber was built using a fogger and a long tube, and was tested in an underground mine on vehicle exhaust. Experimental results showed that the fog treatment was effective at removing DPM from the exhaust. On average, the fog improved DPM removal by about 55% compared to when the treatment was not employed (fog off).

To better understand the mechanisms responsible for DPM removal in the scrubber, a computer model was generated. The model uses the inlet parameters from the field tests, such as inlet DPM and fog concentration and tube geometry, and predicts the scrubber outlet DPM concentration. The model results suggest that the primary way that DPM is removed from the system is by combining with fog drops, which then hit the scrubber tube walls. This effect is probably enhanced by the ribbed structure of the scrubber tubing used here, which may be important for practical applications.

Acknowledgements

I would like to thank first, my academic advisor Dr. Emily Sarver for her continuous support of my work and research. Her encouraging words and tenacious work ethic served as inspiration for me to push harder in my own research and lifted my spirits.

I would also like to thank my committee members with a special appreciation for Dr. John R. Saylor who shared his expertise and provided guidance, both of which proved invaluable in the completion of this work.

I would like to extend my thanks to the employees of the metal/nonmetal mine where I conducted my field tests. I am especially appreciative of Mark Luxbacher, Randal Simons, and Nathan Bench for taking time out of their day to accommodate my research needs and for coming and checking up on me during long testing sessions.

I would like to thank NIOSH and the CDC for sponsoring and funding my research under contract number 200-2014-59646.

I would like to thank my mother, Megan Pensack and my father David Tabor for their unconditional love and support. I would not have been able to receive such a great opportunity without their work and sacrifice.

Finally I would like to thank my friends I met in Blacksburg and my friends back home in Maryland for their companionship, and support. A special thank you to Morgen Leake who has been a roommate, a fellow researcher, and a life-long friend during my time here in graduate school. Thank you all for bolstering my spirits and supporting me.

Table of Contents

List of Figures

List of Tables

Preface

This thesis is composed of three chapters that collectively describe the work conducted to investigate the potential deployment of a fog-based scrubber in an underground mine environment to remove diesel particulate matter (DPM) from vehicle exhaust.

Chapter 1 discusses the field investigation of the fog-based scrubber treatment including its construction and its deployment in an underground mine environment, where data was collected on the concentration of nanoparticles at the inlet and outlet of the experimental apparatus. The results of the field testing are discussed in terms of total DPM removal and DPM removal for different sizes of DPM. Additionally, a discussion is offered on the role of fog drop settling in DPM removal.

Chapter 2 presents a model of the DPM removal measured in Chapter 1 and describes the inputs and mechanisms that are simulated. The results of the model are discussed and compared to results of the experimental data. The differences between the results and the experimental data are discussed in depth and previous literature is consulted to provide possible explanations. The discussion highlights the differences in the assumptions made for the equations used in the model and the actual environment inside the experimental apparatus.

Chapter 3 summarizes the thesis with a discussion of the lessons learned during the work conducted in Chapters 1 and 2 as well as a discussion of potential future work and the future potential of fog-based removal of DPM.

Chapter 1: Field Testing of a Fogging Scrubber for Diesel Vehicle Exhaust

1.1 Introduction

Diesel particulate matter (DPM) is the solid fraction of diesel exhaust. It is mostly comprised of carbonaceous solids and heavy hydrocarbons, and can also contain ash, silicates, sulfates, and metallic abrasion particles (Kittelson 1998). For the purpose of analytical measurements, the carbonaceous solids found in DPM are generally separated into two categories, organic (OC) and elemental carbon (EC), which are often summed to total carbon (TC) (Noll et al., 2007). These solid particles are typically found in the nanometer size range, with individual diameters less than 15 nm and agglomerates as large as about 1 µm (Kittleson, 1998).

Due to their size, respired DPM particles can penetrate deep within the lungs. Exposure to particles smaller than 2.5 µm has been linked to health effects such as irritation and damage to the lungs (Schwartz et al., 1996). Chronic exposures to DPM have been linked to more serious respiratory diseases such as asthma (Wade and Newman, 1993). Additionally, DPM is believed to be a possible carcinogen (Garshik et al., 1987) and single particles can infiltrate into the bloodstream (Campen et al., 2003). Exposures to higher concentrations of total diesel emissions have been associated with increased rates of cardiovascular disease and stroke (Wade and Newman, 1993; Campen et al., 2018).

Due to the use of diesel equipment in confined spaces, ambient DPM levels in underground mines can be higher than in most other work environments (Bugaski, Janisko, et al., 2011), which can lead to hazardous occupational exposures (Cantrell and Watts, 1997). In the United States, the Mine Safety and Health Administration (MSHA) has set regulatory limits on personal DPM exposures. For underground metal/non-metal mines, the limit is 160 µg/m^3 of TC determined as an 8-hour time weighted average (MSHA 2013).

Mine operators use a range of engineering and administrative controls to limit DPM exposures. These include frequent engine maintenance, optimization of operating conditions and fuel quality to reduce DPM generation (Bugarski, Janisko, et al., 2011; Kwon et al., 2001); exhaust after-treatments such as improved catalytic converters and diesel particulate filters to further limit DPM generation or particles from the exhaust (Howitt and Montierth, 1981); increased mine ventilation to dilute concentrations of DPM in the work environment (Bugarski, Janisko, et al., 2011); and use of enclosed equipment cabs, and policies and procedures that limit the amount of time miners can spend in high-DPM work areas (MSHA, 2013). Despite all of these options, DPM exposures can still be too high in some mines.

As an alternative approach to DPM abatement, the author's research group has been working on a novel scrubber concept, which seeks to use a high density of micron-scale water droplets (fog) to remove the particulates from a concentrated exhaust stream (Rojas-Mendoza et al., 2015; 2017a; 2017b). To date, the concept has been tested in a laboratory setting, using the experimental setup shown below in Figure 1.1 (Rojas-Mendoza et al., 2017a).

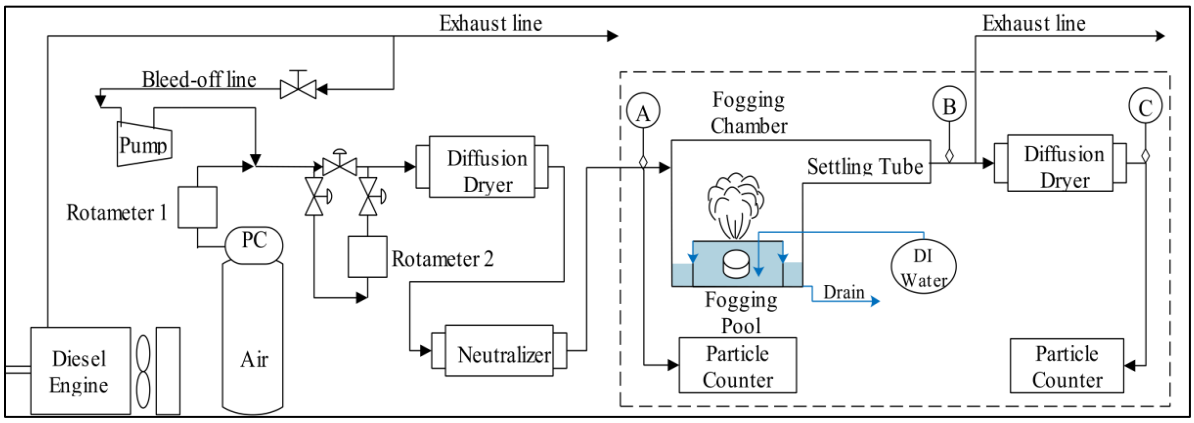

Figure 1.1. Laboratory setup used by Rojas-Mendoza et al (2017a).

In the lab testing, a bleed-off from the exhaust of a small diesel engine was diluted with ultra-pure air and neutralized, directed into a small chamber where fog droplets were introduced by an ultrasonic pond fogger, and then the DPM and fog-laden air moved through a long horizontal "settling" tube. A pair of nanoparticle sizers were used to measure the DPM concentration up- and downstream of the fog treatment (locations A and C, Figure 1.1), and filter samples were also collected (locations A and B). As illustrated in Figure 1.2, significantly more DPM was removed from the air when the fog treatment was applied relative to the control (fog-off) condition (Rojas Mendoza et al., 2017a; 2017b). It was proposed that the DPM removal during the treatment occurred via a two-step process, whereby the DPM quickly coagulates with the fog drops, which then settle by gravity.

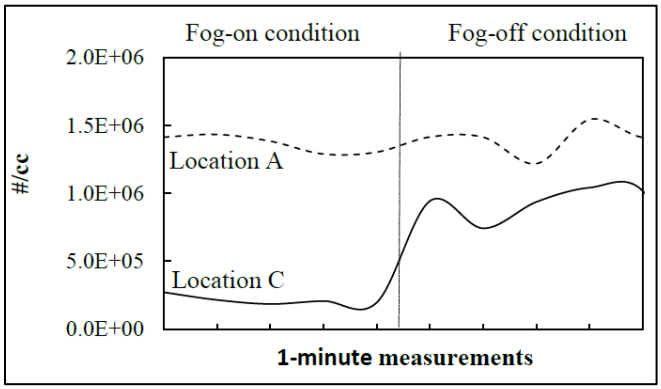

Figure 1.2 Nano-particle number concentration measured at points A and C in the experimental setup shown in Figure 1.1. (Taken from Rojas-Mendoza et al, 2017a.)

To determine if the fog treatment studied in the laboratory by Rojas-Mendoza et al. (2017a; 2017b) could be effectively scaled up for practical application as a vehicle exhaust treatment, a new scrubber apparatus was built and field tested in an underground stone mine.

1.2 Experimental Details

1.2.1 Field Site

The testing area was located approximately 600 feet underground in an inactive tunnel, about 100 linear feet off of the main entry ramp into the mine. This location is in a primary intake airway for the mine, which is characterized by low traffic and relatively low and consistent background particle concentrations in the nanometer size range. The depth of the testing location also ensured that the temperature (15 °C) and relative humidity of the air (around 95%) was constant during the tests.

1.2.2 Scrubber Apparatus

The experimental apparatus is shown in Figure 1.3, and a schematic of the primary components is shown in Figure 1.4. The DPM source used for these experiments was the exhaust of a diesel-powered vehicle. (It is noted that different vehicles were used in different tests based on availability of equipment at the mine, see Table A.1 in Appendix A). The exhaust was taken directly from the vehicle by placing the end of a section of ribbed, flexible Mylar tubing (diameter of 14 in, 35.6 cm) over the tailpipe. This section of tubing was 25 ft (7.26 m) long to promote mixing of the exhaust and any makeup air prior to particle measurement on the upstream (inlet) side of the fog treatment.

The fog was introduced to the exhaust airflow using an MHB12 Multi-function Ultrasonic Humidifier (Mainlandmart, Ocean Mist, CA), which is referred to as the "fogger" hereinafter. An external water tank was used to feed the fogger reservoir via gravity in an effort to maintain a consistent water level, since preliminary testing in the laboratory indicated that the fog drop concentration could vary with the water level (see Figure A.1 in Appendix A).

Just downstream of the fog introduction point was another 100 ft (30.5 m) section of the same Mylar tubing, referred to as the settling tube. At the outlet of the settling tube, particles were again measured before the air exited the apparatus through a small exhausting fan.

Figure 1.3 Scrubber apparatus setup in the underground mine.

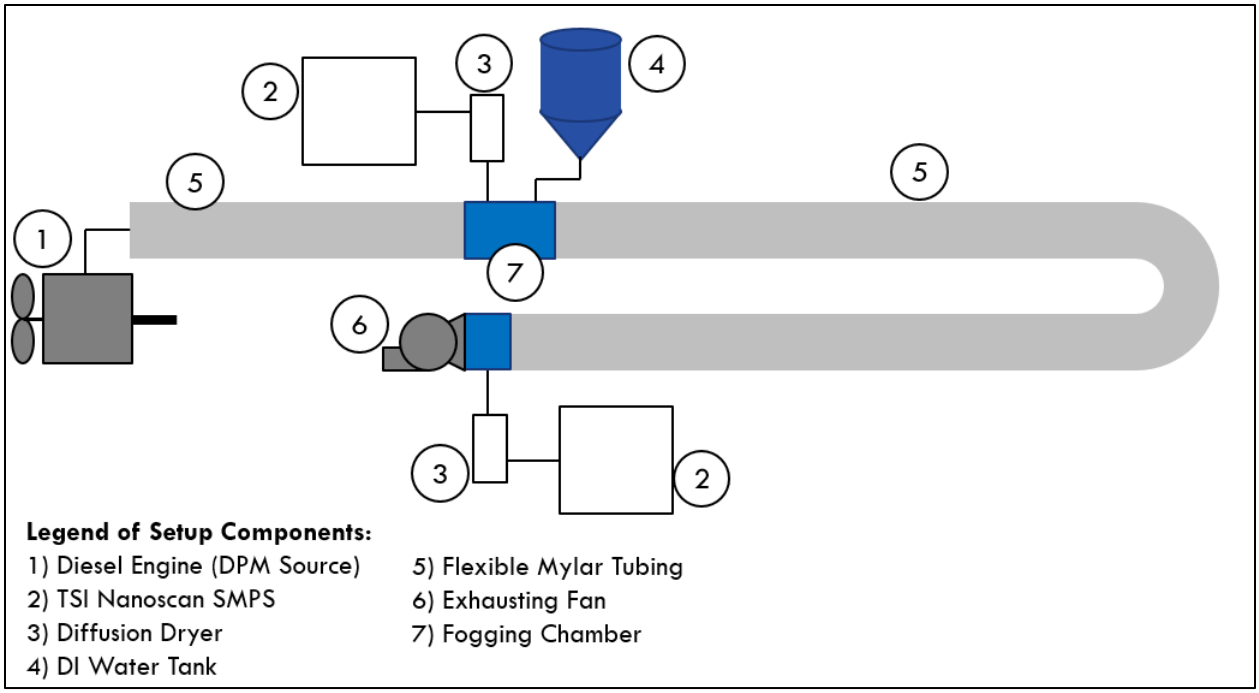

Figure 1.4 Schematic of scrubber apparatus.

Particle measurements were made using a pair of TSI 3910 SPMS NanoScan instruments (TSI, Shoreview, MN). The instruments sampled the air at the inlet and outlet locations using a standard flow rate of 1 L/min on 1-minute basis, and recorded the concentration of particles (#/cm^3) in size bins between 11.5 and 410 nm; only the 10 bins from 11.5 to 154 nm were used for this study since very few particles were observed in the larger bins, and those bins are also more susceptible to error. A diffusion dryer (DD Model 250; ATI, Owings Mill, MD) was used to remove moisture from the sample stream to each NanoScan.

The average flow through the scrubber apparatus was determined at the beginning of every field test by measuring the centerline velocity through the 14-in diameter tube. The average flow rate was approximately 105 ft^3/min (28,000 cm^3/s), yielding a residence time from inlet NanoScan to outlet NanoScan of 60.5 seconds. The characteristics of the airflow give a Reynolds number (Re) of 12,100, calculated from Equation 1.1.

$$Re = \frac{\rho V d_t}{\mu} \qquad 1.1$$

Where ρ is the air density (1.225 kg/m^3), V is the flow velocity (0.504 m/s), d_t is the scrubber tube diameter (0.356 m), and μ is the kinematic viscosity of the air (assumed to be $1.81\text{x}10^{-5}\text{kg} \cdot \text{m}^{-1} \cdot \text{s}^{-1}$). A Re value of 12,100 indicates turbulent airflow.

While fog drop measurements were not possible in the field, a TSI 3330 Optical Particle Sizer (TSI, Shoreview, MN) was used briefly in the laboratory to estimate the size of the drops. Figure 1.5 shows the resulting OPS data. From this, the average drop diameter ($d_{d\ avg}$) was determined using Equation 1.2.

$$d_{d\,avg} = \frac{\sum(d_{d\,j} C_{d\,j})}{\sum C_{d\,j}} \qquad 1.2$$

Where $d_{d\,j}$ and $C_{d\,j}$ are the mean drop diameter and measured number concentration in the j^{th} size bin, respectively. The average droplet diameter was found to be about 4.8 µm, which is in good agreement with the marketed 5 µm size for the fogger.

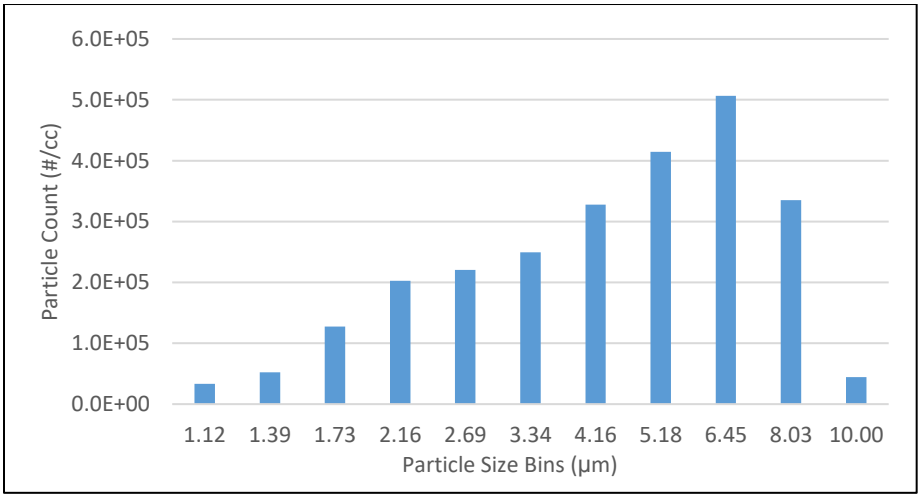

Figure 1.5. Fog drop size distribution based on laboratory data collected using the OPS

1.2.3 Scrubber Tests

A total of 11 field tests were conducted with the scrubber apparatus (Table A.1, Appendix A). Tests 1 through 4 were "continuous treatment" tests, which included two separate trial periods: a control period with the fogger turned off for a total of 2 consecutive hours, and a treatment period with the fogger turned on for a total of 2 consecutive hours. Tests 5 through 11 were "periodic treatment" tests and were conducted by cycling between fog-off and fog-on conditions on 20 minute intervals. All time series plots for the concentrations measured at the inlet and outlet of each test are found in Figure A.2 in Appendix A.

Before and after each test, the two NanoScans (inlet and outlet) were compared. For this, the sampling inlets of the two instruments were connected such that they sampled the same air stream for a minimum of 15 minutes. This was done in both a low and a high DPM environment to account for the differences in measurements between the two NanoScans at different DPM concentrations. For each comparison period, the average of the particle concentrations in each bin (C_j) were computed for both the inlet and outlet instrument, such that scaling factors (SF) for each bin could be calculated using Equation 1.3. Then, the outlet NanoScan data was adjusted by multiplying the raw concentration in a given bin (C_j) by its test-specific SF_j value per Equation 1.4. (Computations were also made to determine all-bin SF values to apply to total particle concentrations measured by the outlet Nanoscan.)

$$SF = \frac{\text{inlet } C_j}{\text{outlet } C_j} \qquad 1.3$$

$$\text{outlet } C_{j\_adj} = (SF)\text{outlet } C_j \qquad 1.4$$

The *SF* values for the total particle concentrations in each test (i.e., across all bins) ranged from 0.93 to 1.03, with an average of 1.00. The values for the individual bins varied more widely. All *SF* values for each test can be found in Table A.2 in Appendix A.

For all tests, the inlet fog drop concentration (C_d in $\#/\text{cm}^3$) was also estimated using Equation 1.5. Values of C_d for each test are shown in Table A.1 in Appendix A.

$$C_d = \frac{3R}{4Q\pi\left(\frac{d_d}{2}\right)^3} \qquad 1.5$$

Where R is the rate of water consumption measured each test (in cm^3/min), Q is the flowrate inside the settling tube (taken as 28,000 cm^3/min), and d_d is the average diameter of a single droplet (taken as 4.8 x 10^{-6} m).

1.4 Results

Table A.3 in Appendix A presents the average particle concentrations measured by the inlet and outlet NanoScans during the fog treatment (fog-on) and control (fog-off) periods for each of the 11 scrubber tests. Concentrations are reported for individual bins (11.5-154 nm), and all outlet NanoScan data has been adjusted as described above.

1.4.1 Total Particle Removal

Test results are first reviewed with respect to the effect of the fog treatment on total particle concentrations (i.e., across all bins, 11.5-154 nm). Figures 1.6 and 1.7 show example time series data for the total particle concentration measured with the inlet and outlet NanoScans in a continuous test and a periodic test, respectively. (The time series data for all tests can be found in Figure A.2 in Appendix A.) From these plots, it is evident that the fog treatment significantly reduced the DPM concentration in the exhaust stream as compared to the control case.

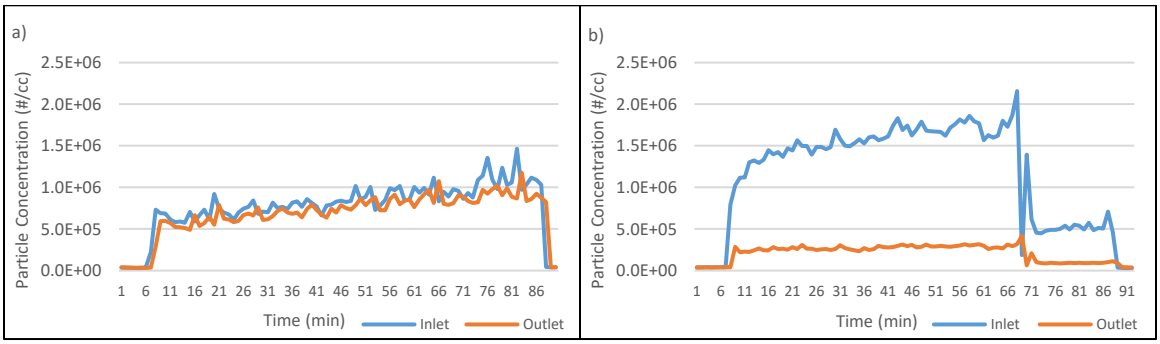

Figure 1.6.Total particle concentration at the inlet and outlet of the scrubber apparatus for Test 4. Plot a) shows the control (fog off) condition and b) shows the treatment (fog on) condition.

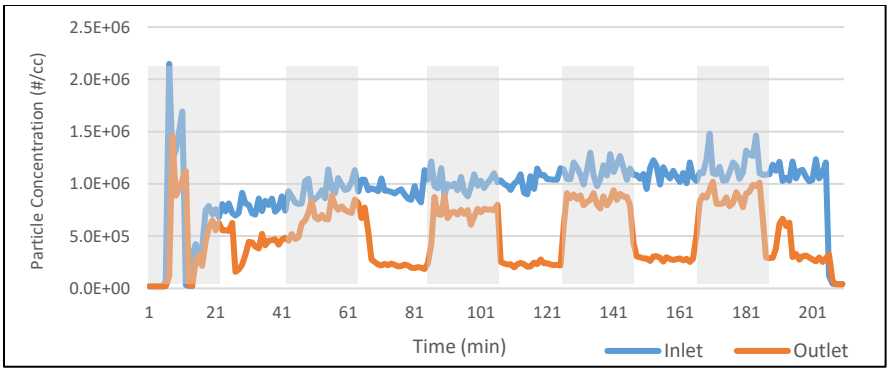

Figure 1.7. Total particle concentration at the inlet and outlet of the scrubber apparatus for Test 11. Control (shaded) and treatment conditions were tested on 20 minute intervals.

The total particle removal efficiency (E_D) was determined for each test using Equation 1.6 for both the treatment and control periods using the DPM concentration measured at the inlet ($inlet\ C$) and the DPM concentration measured at the outlet and adjusted for *SF* ($outlet\ C_{adj}$). Results are tabulated in Table 1.1.

$$E_D = \left(\frac{inlet\ C - outlet\ C_{adj}}{inlet\ C}\right) * 100\% \tag{1.6}$$

Table 1.1. Average E_D computed for control and treatment periods of each scrubber field test.

Test	Control (Fog-off)	Treatment (Fog-on)
1	12%	73%
2	4%	61%
3	13%	64%
4	11%	82%
5	16%	57%
6	20%	60%
7	34%	76%
8	22%	57%
9	18%	18%
10	24%	78%
11	26%	69%

Except for Test 9, the fog treatment yielded *E* between 57 and 82% (average of 63%), representing an overall improvement in E_D between 34 and 71% (average of 50%) versus the control condition. (Test 9 showed almost no difference between the treatment and control conditions. No conclusive explanation was

found for this, but this test did have very low inlet particle concentrations, which may have been a factor.) Notably, E_D for the control condition (average of 24%, excluding Test 9) in the periodic tests were consistently higher than those determined for the continuous tests (average of 10%). This is likely due to the fact that the scrubber tube walls were wetted as the fogger was cycled on and off during the periodic tests.

In general, the total particle removal observed in the field tests is consistent with observations by Rojas-Mendoza et al. (2017a) in the laboratory. In those experiments, average E_D for the control and fog treatment conditions were about 40 and 87%, respectively, representing an improvement in E_D of about 45% due to the fog. Similarities between the Rojas-Mendoza et al. (2017a) work and the field tests in this work include the average drop size and concentration; the prior work estimated these as 3.9 μm and 5.0×10^5 #/cm^3, respectively. However, some differences between the present and prior work that might contribute to differences in removal efficiencies include Reynolds number, inlet particle concentrations, and tube geometry. In the current work, there is a higher volume of air to surface area of tube ratio, which might have resulted in less diffusion-controlled particle removal under control conditions. This difference in geometry may have also contributed to somewhat less particle removal under treatment conditions here, since the fog drops had further to settle. Additionally, the inlet particle concentrations used by Rojas-Mendoza (2017a) generally exceeded those used here. Higher DPM concentrations should promote higher DPM-drop coagulation efficiencies. Finally, the Rojas-Mendoza (2017a) apparatus included a TSI Kr-85 Neutralizer to eliminate surface charges on the DPM particles, which may have also impacted particle removal efficiency.

1.4.2 Particle Removal as a Function of Particle Size

Results were also evaluated with respect to particle size. Figure 1.8 shows the average size distribution of particles (across all 11 field tests) measured by the inlet and outlet NanoScans during the control and fog treatment conditions, respectively (data for each separate test is included in Table A.3 in Appendix A). The size distribution at the inlet was generally observed to be unimodal, with a peak in the in 36.5 nm bin. At the outlet, the size distribution was also unimodal, but appears to have shifted slightly to the right—meaning, on average, the particles at the outlet were slightly larger than those at the inlet. This was observed during both control and treatment conditions. In the control trials, this is likely due to agglomeration of DPM particles as they move through the scrubber apparatus.

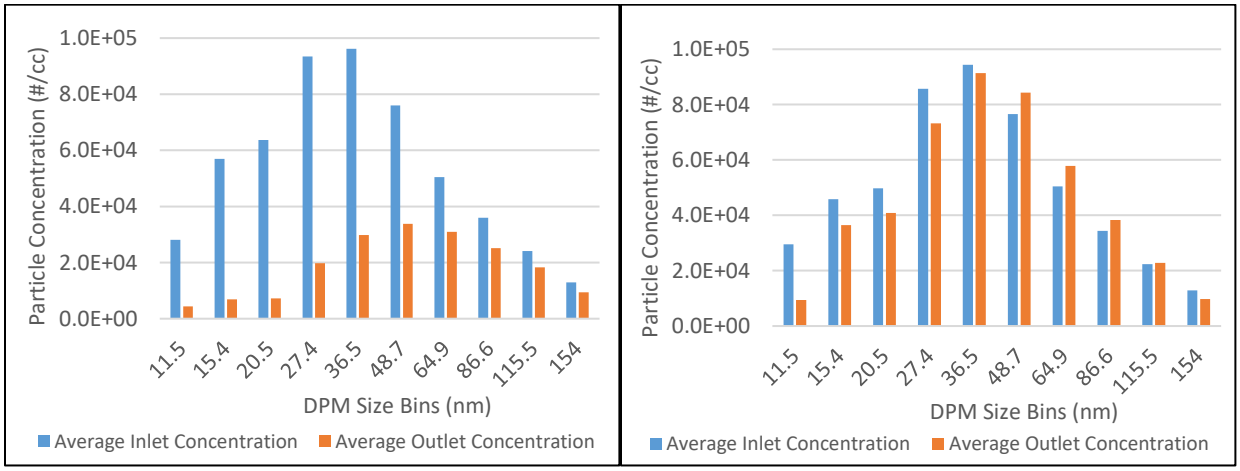

Figure 1.8. Average particle concentrations across all tests in each size bin at the inlet and outlet for a) the treatment (fog on) and b) the control (fog off) condition

E was also determined by size bin. Figure 1.9 shows the results averaged across all 11 field tests for both control and fog treatment conditions. (Table A.4 in appendix A shows the results for each separate test). In general, *E* was observed to be highest for the smallest size bins. This is expected since the smallest particles should experience the highest diffusion rates and thus coagulate more efficiently with the drops. The negative values for *E* shown for the control case in Figure 1.9 (bin sizes between 48.7 and 115.5nm) are likely due to the aforementioned shifting particle size distribution between the inlet and outlet, given that particles should not be generated inside the apparatus.

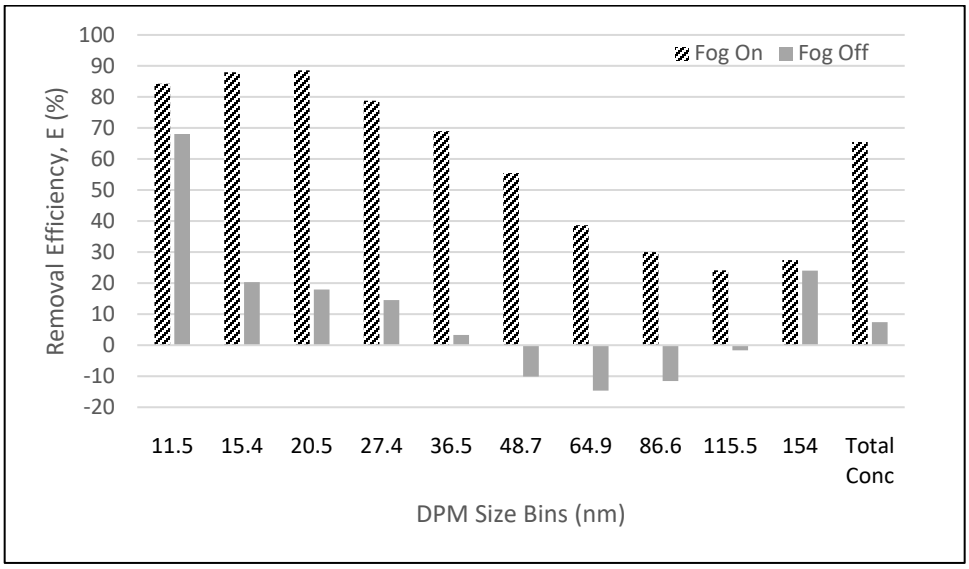

Figure 1.9. Average E across all tests, shown by bin size and across all bins (total concentration), for both the control (fog off) and treatment (fog on) conditions.

1.5 Discussion

The results of the field tests presented here can provide more insight to the DPM removal mechanisms at play within the fogging scrubber. Based on results under control conditions, diffusion of free DPM (i.e., not coagulated with a drop) should only account for a minor fraction of the total removal. With fog, Rojas-Mendoza et al. (2017a) proposed that additional removal occurs when DPM particles coagulate with the fog drops, which are subsequently settled due to gravity.

According to Merrell and Saylor (2017), the fraction of particles (in this case, drops) that settle due to gravity in a horizontal tube (G) in the time step can be predicted by Equation 1.7.

$$G = \left(1 - \frac{\left(\frac{{d_t}^2}{2}\right)\operatorname{acos}\left(\frac{l_d}{d_t}\right) - \left(\frac{l_d}{2}\right)\sqrt{\left({d_t}^2 - {l_d}^2\right)}}{\pi\left(\frac{d_t}{2}\right)^2} \right) \tag{1.7}$$

Where d_t is the diameter of the settling tube (0.356 m), and is l_d, the distance that the drops fall (in meters).

$$l_d = tV_s \tag{1.8}$$

Where t is the residence time in the tube (60.5 s) and V_s is the Stoke's settling velocity of the drops (in m/s), which can be calculated using Equation 1.9.

$$V_s = \frac{\rho_d (d_d)^2 g}{18\mu} \tag{1.9}$$

Where g is the acceleration of gravity (9.81 m/s^2) and ρ_d is the density of the droplet (taken as 997 kg/m^3), and d_d is the drop diameter (taken as 4.8 µm). Using Equations 1.7-1.9, only about 15% of the drops are expected to settle in the scrubber apparatus under the conditions tested here. However, the observed DPM removal with fog treatment suggests that significantly more of the drops were removed. Given the flow conditions in the scrubber apparatus, it is likely that inertial impaction of drops to the tube walls was also significant and could account for the increased DPM removal. This mechanism is explored further in the next chapter of this thesis.

While removal of the fog drops themselves could not be directly determined for the field tests reported here, it stands to reason that E_d should be similar to E_D under the following conditions:

- Removal of free DPM, for example by diffusion to the scrubber walls, gravitational settling or coagulation with other DPM particles, is relatively insignificant. In the case where fog drops are present, most DPM is expected to coagulate with the drops very quickly, thereby reducing the free DPM concentration subject to removal mechanisms that are unrelated to drop removal.
- The DPM-drop coagulation also happens quickly relative to the drop removal—and to the retention time of the scrubber. This should mean that the DPM removal can be approximated by drop removal, since drop removal happens after DPM-drop coagulation. This condition is more likely for smaller DPM sizes, for which coagulation with drops should occur faster.
- The initial DPM concentration is significantly greater than the initial drop concentration and the two aerosols are well mixed, such that coagulation results in a situation where all drops take up similar numbers of DPM particles. This would mean that each drop removes the same number of DPM particles.
- The DPM contained in drops that are not removed within the scrubber (i.e., by settling or inertial impaction) do not significantly agglomerate as the drops are dried out before being counted by the NanoScan. Such agglomeration would effectively be observed as DPM removal since there would be fewer (but larger) particles.

Qualitatively, the above conditions are probably best satisfied for small DPM particles (i.e., fast coagulation with drops), but perhaps not the smallest particles (i.e., subject to free DPM diffusion to the scrubber tube walls). Per Table A.3 in Appendix A and Equation1.6, (excluding Test 9) E_D for the total particles in the three size bins between 20.5 and 35.6 nm ranged from 70 to 88% (average of about 78%). It is thus expected that E_d should also be within this range. In the next chapter, E_d will be further considered using a mechanistic model of the scrubber apparatus field tested here.

Assuming that DPM removal in the scrubber is indeed primarily due to fog drop removal subsequent to DPM-drop coagulation, the reduction in DPM particle number concentration with time should follow a decay trend with the same rate constant (K) as the reduction in drop number concentration. For drop removal

mechanisms such as gravitational settling and inertial impaction, the concentration decay should be a first-order process where K is given by Equation 1.10.

$$K = \ln\left(\frac{C_o}{C(t)}\right)\left(\frac{1}{t}\right) \quad 1.10$$

For the scrubber tests, t is the total residence time (60.5 s), and $C_o/C(t)$ is simply the ratio of the drop concentration at the inlet to that at the outlet—which is assumed to be equal to the ratio for DPM particle concentration. Based on Equation 1.10, K values were determined for each scrubber test (Table 1.2) using the measured particle concentrations (bins 20.5-35.6 nm) at the inlet and outlet.

Aside from variability in the inlet drop and DPM particle concentrations, if all other conditions were exactly the same between tests, then K values would be expected to be the same for all tests. However, the variability in K values shown in Table 1.2 suggests that some factors did change between tests. The data presented in Table A.1 in Appendix A does not show a definite trend between E_D and droplet concentration or DPM concentration, which would be the most likely variables affecting particle removal. It is possible that the drop size varied somewhat between tests, although this quantity could not be measured in the field. Equation 1.5 shows that the concentration of drops is heavily dependent on the drop diameter. Larger drops would decrease the drop concentration but increase settling, whereas smaller drops would yield the opposite effects.

Table 1.2. Expected E_d and K values for each field test, based on measured particle concentrations at the scrubber inlet and outlet in bins 20.5, 27.4 and 35.6 nm.

Test	$E_{20.5-36.5} = E_d$	K (s^{-1})
1	0.869	0.0372
2	0.786	0.0266
3	0.726	0.0227
4	0.837	0.0296
5	0.727	0.0220
6	0.767	0.0253
7	0.876	0.0364
8	0.699	0.0199
9	0.334	0.00715
10	0.799	0.0321
11	0.713	0.0193

1.6 Conclusions

Respiratory exposures to DPM present a serious health hazard for underground miners. While administrative and engineering controls can be used to reduce the concentration of DPM in the air, these controls are not always sufficient to prevent overexposure. Prior work has shown that a water fog treatment can effectively remove DPM particles from concentrated diesel exhaust in a laboratory setting (Rojas-Mendoza et al., 2017a). The current study tested a modified scrubber apparatus in the field to prove its efficacy in a real work environment. The treatment was shown to be effective at removing DPM particles from an exhaust stream at various initial concentrations. The treatment was found to be highly effective at

removing the DPM particles in the smallest measured size ranges. This finding is significant to mitigating health risks of DPM exposure as smaller particles can penetrate deeper within the lungs and some may even translocate from the lungs into the bloodstream.

Results for a practical application of this treatment are promising and the highly effective removal of the smallest particles show potential for coupling this treatment with current technology like diesel particulate filters, which are more effective at capturing larger particles. However, the fogging scrubber needs to be optimized from here. Moreover, the lack of concrete data on the effect of initial drop size and concentration deserves further investigation. The fog treatment represents a novel approach to DPM abatement, which may be beneficial for use in underground mines or other environments where DPM exposure risks are high.

References

1) Kittleson, D. (1998). Engines and Nanoparticles: a review. *Journal of Aerosol Science*. Vol 29 (5). Pages 575-588.
2) Wade J.F. 3rd, Newman L.S. (Febuary, 1993). Diesel Asthma. Reactive Airways Disease Following Overexposure to Locomotive Exhaust. *Journal of Occupational Medicine.* Vol 35(2). Pages 149-154.
3) Garshick E, Schenker M, et al. (1987) A Case-Control Study of Lung Cancer and Diesel Exhaust Exposure in Railroad Workers. *American Review of Respratory Disease.* Vol 135 (6). Pages 1242-1248.
4) Noll, J.D., Burgarski, A.D., Patts, L.D., Mischler, S.E., McWilliams, L. (2007). Relationship between Elemental Carbon, Total Carbon, and Diesel Particulate Matter in Several Underground Metal/Non-metal Mines. *Environmental Science & Technology.* 41(3). Pages 710-716.
5) Schwartz, J, Dockery, D, Neas, L. (1996). Is Daily Mortality Associated with Fine Particles? *Journal of the Air & Waste Management Association.* Vol 46 (10). Pages 927-939.
6) Cantrell, B, Watts, W. (1997). Diesel Exhaust Aerosol: Review of Occupational Exposure. *Applied Occupational and Environmental Hygiene.* Vol 12 (12). Pages 1019-1027.
7) Kwon Y., Mann N., Rickeard D.J., (2001). Fuel Effects on Diesel Emmissions- A New Understanding. *SAE Technical Paper*. 2001-01-3522.
8) Howitt, J., & Montierth, M. (1981). Cellular Ceramic Diesel Particulate Filter. *SAE Transactions.* Vol 90(1). Pages 493-501.
9) Mine Safety and Health Administration. (2013). Limit on Exposure to Diesel Particulate Matter. Title *30 CFR 57*.5060.
10) Code of Federal Regulations Title 30 Part 57 Section 5060 (30CFR57.5060), Limit on Exposure to diesel particulate matter. 2013.
11) Bugarski, A, Janisko, S, et al. (2011). Diesel Aerosols and Gases in Underground Mines: Guide to Exposure Assessment and Control. *NIOSH Report of Investigations 9687.*
12) Campen, M.J., McDonald, J.D., Gigliotti, A.P. et al. (2003). Cardiovascular effects of inhaled diesel exhaust in spontaneously hypertensive rats. *Cardiovascular Toxicology.* Vol 3. Pages 353–361.
13) MHSA, OSHA. (January, 2013). Diesel Exhaust/Diesel Particulate Matter. Retrieved from: https://www.osha.gov/Publications/OSHA-3590.pdf. Retrieved on May, 2020.

14) Rojas-Mendoza, L, Sarver, E, et al. (2015). *A preliminary Investigation of DPM Scavenging by Water Sprays.* 15th North American Mine Ventilation Symposium.

15) Rojas-Mendoza, L, et al. (2017a). Removal of DPM from an Airstream Using Micron-Scale Droplets. *Aerosol and Air Quality Research.* Vol 17. Pages 1865-1874.

16) Rojas-Mendoza, L, et al. (2017b). Laboratory Demonstration of DPM Mass Removal From an Exhaust Stream by Fog Drops. *Mining Engineering.* 2017. Vol 69(11). Pages 55-60.

17) Hinds, W.C. (1999). *Aerosol Technology: Properties, Behavior, and Measurement of Airborne Particles, 2nd Edition.* New York: Wiley-Interscience.

18) TSI. (January, 2013). NanoScan SPMS Nanoparticle Sizer Model 3910 Operational and Service Manual. TSI Incorporated.

19) Merrell, T. M. and Saylor, J. R. (2017). *Demisting using an Ultrasonic Standing Wave Field*. Journal of the Acoustical Society of America. Vol 141. Pages 171-182.

Chapter 2: Mechanistic Model of Particle Removal in the Fogging Scrubber

2.1 Introduction

Diesel engine exhaust contains solid nanoparticles commonly referred to as diesel particulate matter. The experimental results presented in Chapter 1 showed that application of micron-scale fog drops to concentrated diesel exhaust in a long tube "scrubber" could effectively remove between 56-82% of DPM (11.5-154 nm) from the exhaust stream. Removal is thought to be primarily due to a two-step process, whereby the DPM must first coagulate with the fog drops, which are then removed from the air flow by gravitational settling and/or inertial impaction with the tube walls. Given that DPM-drop coagulation is expected to be relatively quick and complete (i.e., most DPM particles do coagulate with drops), it was also posited that the removal efficiency of the fog drops themselves (E_d) should be roughly equal to that of the DPM (E_D); although, E_d could not be directly determined from field measurements.

In order to test the plausibility of the above ideas and further explore the mechanisms underlying DPM removal in the scrubber, a model was built in Matlab (version R2018a; Mathworks, Natick, MA) (hereby referred to as the model). (The code for the model is given in Appendix C). It simulates the DPM-drop coagulation, and reduction in DPM and drops due to gravity and wall diffusion/impaction, in a series of narrow time steps that correspond to incremental flow distance along the scrubber length. At each time step, the model tracks the fractions of suspended and removed DPM and drops, ultimately allowing comparison with experimental measurements at the scrubber outlet.

2.2 Model Development

Figure 2.1 conceptualizes the DPM and drop interactions and removal mechanisms included in the model: coagulation of DPM and drops, diffusion of un-coagulated ("free") DPM to the tube walls, gravitational settling of free DPM, inertial impaction of drops to the tube walls, and gravitational settling of drops. Each mechanism is discussed and defined by its governing equation(s) in the following sections.

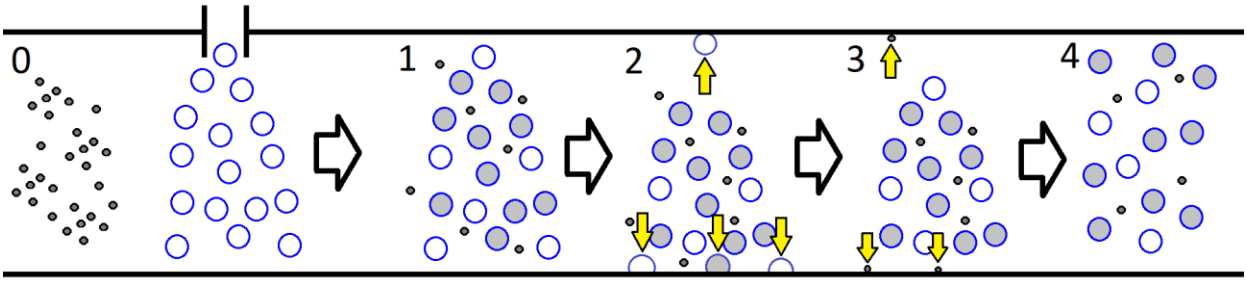

Figure 2.10. Mechanistic stages included in the model. At Stage 0, the DPM (small black particles) and drops (large blue particles) are introduced into the same air flow, after which they are assumed to be homogenously distributed. At Stage 1, a fraction of the DPM coagulates with the drops to form DPM-laden drops (large grey particles). At Stage 2, a fraction of the drops are reduced by gravitational settling to the tube floor and inertial impaction to the tube walls. At Stage 3, a fraction of any uncoagulated (free) DPM is removed by gravitational settling to the tube floor and turbulent diffusion to the tube walls. At Stage 4, the drops and DPM are homogeneously redistributed. After the first time step increment in the model, stages 1-4 repeat for each time step.

Based on the experimental data collected in Chapter 1, the primary input parameters for the model are the concentration of DPM particles in 10 nominal size bins (11.5, 15.4, 20.5, 27.4, 36.5, 48.7, 64.9, 86.6, 115.4,

and 154 nm), and the concentration of fog drops with a fixed mean diameter and size distribution. Table 2.1 provides a full list of input and output variables for the model.

Table 2.3. List of variables for the model of the fogging treatment.

Quantity		Value	Units	Origin
Scrubber tube length	l_t	30.48	m	Measured (see Chapter 1)
Scrubber tube diameter	d_t	0.356	m	Measured (see Chapter 1)
Scrubber flow rate	Q	3	m^3/min	Measured (see Chapter 1)
Inlet drop size distribution	--	1.1 to 10.0	µm	Fixed based on measurement (see Chapter 1)
Inlet drop diameter	d_d	4.8	µm	Fixed based on calculation (See Chapter 1 Equation 1.2)
Inlet droplet concentration	C_d	variable	#/cm^3	Input from measurements (See Chapter 1 Equation 1.5)
Inlet DPM diameter	d_D	10 bins with nominal sizes 11.5-154	nm	Fixed (see Chapter 1)
Inlet DPM concentration (by bin)	C_D	variable	#/cm^3	Input from measurements (see Chapter 1)
Reynolds Number	Re	12154	None	Calculated (See Chapter 1 Equation 1.1)
Mean free path of air	λ	0.068	µm	Assumed
Time step	t_s	0.005	seconds	Fixed
Viscosity of air	ν	1.81	kg/(m · s)	Assumed
Acceleration of gravity	g	9.81	m/s^2	Assumed
Density of water drops	ρ_d	997	kg/m^3	Assumed
Density of DPM particles	ρ_D	1225	kg/m^3	Assumed (Virtanen, et al., 2002)
Boltzman Constant	k	1.38×10^{-23}	$m^2 \cdot kg/K \cdot s^2$	Assumed
Temperature	T	286	Kelvin	Measured (see Chapter 1)
Residence time in tube	t_{res}	60.5	seconds	Calculated (see Chapter 1)
DPM diffusion coefficient	D_D	4.2×10^{-8} to 3.4×10^{-10}	m^2/s	Calculated (See Equation 2.3)
Droplet diffusion coefficient	D_d	2.1×10^{-11} to 2.3×10^{-12}	m^2/s	Calculated (See Equation 2.3)
Average DPM fall distance per time step	l_{DPM}	1.99×10^{-11} to 3.56×10^{-9}	m	Calculated (See Equation 2.12)
Average droplet fall distance per time step	l_d	1.87×10^{-7} to 1.50×10^{-5}	m	Calculated (See Equation 2.7)
DPM deposition velocity	V_{dep_D}	3.85×10^{-5} to 1.545×10^{-6}	m/s	Calculated (Equation 2.15)
Drop deposition velocity	V_{dep_d}	2.4×10^{-7} to 5.6×10^{-8}	m/s	Calculated (Equation 2.10)

Deposition velocity enhancement factor	R_V	Variable, (initial value of 1.0)	None	Input
Fraction of DPM settled by gravity	G_D	Variable based on input test data	%	model output (Equation 2.11)
Fraction of drops settled by gravity	G_d	Variable based on input test data	%	model output (Equation 2.6)
Fraction of free DPM diffused on wall	W_D	Variable based on input test data	%	model output (Equation 2.14)
Fraction of drops impacted on wall	W_d	Variable based on input test data	%	model output (Equation 2.9)
DPM removal efficiency	E_D	Variable based on input test data	%	model output (Equation 1.6)
Drop removal efficiency	E_d	Variable based on input test data	%	model output (Equation 1.6)

The time step length was set to 5 ms to approximate simultaneous (rather than stepwise) mechanisms, and the model evaluates from t=0 to the scrubber residence time (t = 60.5 s). Within each time step, each DPM size is treated separately such that stages 1-4 shown in Figure 2.1 are evaluated for 11.5 nm particles, then for 15.4 nm particles, and so on. At the end of each time step, the number fraction of DPM (of each size) and drops is calculated in all possible classes (Table 2.2). Then, the DPM and drops remaining suspended in the air flow are assumed to be evenly redistributed before computations begin for the next time step.

Table 2.4. Possible classes for DPM particles and drops calculated by the model. The number percentages of particles or drops in all classes must sum to 100%.

DPM classes	Drop classes
• Free DPM: un-coagulated DPM, suspended in air flow. Calculated as • Coagulated DPM: DPM combined with drops, suspended in air flow • Wall deposition: free DPM removed to the tube wall by diffusion • Grav settled: free DPM removed by gravitational settling to the tube floor • Drop Removal (Wall): DPM coagulated with drop, removed by drop impacting tube wall due to inertia • Drop Removal (Grav): DPM coagulated with drop, removed by gravitational settling of drop	• suspended: drops suspended in air flow • impacted: drop removed by inertial impaction to tube wall • settled: drop removed by gravitational settling

2.2.1 DPM-drop Coagulation

The first mechanism considered by the model is DPM-drop coagulation (stage 1 in Figure 2.1). The model determines the fraction of the DPM in each of the ten size bins that collide with a drop, effectively being taken up by the drops in an irreversible process. The collision between drops and DPM particles is predicted based on the relative motion between the two aerosols, as described by Pruppacher and Klett (1978). Equation 2.1 defines the fraction of the DPM particles (ϕ) that collide with the much larger water drop:

$$\phi = 1 - e^{-\Lambda_c t} \qquad 2.1$$

Where t is time (in seconds) and Λ_c is the fractional particle removal rate (in s^{-1}) defined by Equation 2.2:

$$\Lambda_c = 2\pi D_{DPM} \int_0^{\infty} d_d N(d_d) d(d_d) \quad 2.2$$

Where $N(d_d)$ is the size distribution of the drops, d_{drop} is the mean diameter of the drops, and D_D is the diffusion coefficient of the DPM particle given by Equation 2.3.

$$D_D = \frac{k_c T C_c}{3\pi\mu_a d_D} \quad 2.3$$

Where k_c is the Boltzmann constant (1.38×10^{-23} $m^2 \cdot kg/(s^2 \cdot K^1)$), T is the ambient temperature (taken as 286 K), d_D is the diameter of the DPM particle (in m), μ_a is the dynamic viscosity of air (1.81×10^{-5} $kg/(s \cdot m)$, and C_c is the Cunningham correction factor:

$$C_c = 1 + \left(\frac{\lambda}{d_D}\right)\left(2.34 + 1.05 \exp\left(0.39 \frac{d_D}{\lambda}\right)\right) \quad 2.4$$

Per Hinds (1999), C_c corrects for the non-continuous effect that air resistance has on relatively small-diameter particles (diameter < 1 μm) and can be calculated by Equation 2.4 using the diameter of the particle and the mean free path of air, λ (0.068 μm).The Cunningham Correction factor only applies to particles in the submicron size range and approaches 1 for the fog droplets (Hinds, 1999).

At the end of stage 1 the fraction of "coagulated DPM" (from Table 2.2) increases by the fraction of DPM that was removed from the "free DPM".

It should be noted that, for this model, drop-drop and any combination of DPM-DPM coagulation is assumed to be insignificant. This is because the relative coagulation coefficients, $K_{1,2}$, for these combinations are much smaller than $K_{1,2}$, for DPM-drop combinations (see Table B.1 in Appendix B). The coagulation coefficient, $K_{1,2}$, is described by Hinds (1999) as the rate at which the concentration of two monodisperse aerosols are reduced due to coagulation with each other. $K_{1,2}$ can be calculated using Equation 2.5.

$$K_{1,2} = \pi\big((D_D d_D) + (D_D d_d) + (D_d d_D) + (D_d d_d)\big) \quad 2.5$$

Where d_D and d_d are the diameters of the DPM particle and of the fog drop, respectively; and D_D and D_d are the diffusion coefficients for the DPM particle and of the fog drop, respectively. D_d can be determined by Equation 2.3 given that the diameter used in the denominator is d_d.

2.2.2a Droplet Reduction, Gravitational Settling

At stage 2, the fraction of drops that are removed during the time step is determined. Drops are removed by two mechanisms, by gravitational settling and by inertial impaction to the tube walls. The fraction of drops that settle out due to gravity (G_d) is determined by the following equation based on work by Merrell and Saylor (2017):

$$G_d = \left(1 - \frac{\left(\frac{{d_t}^2}{2}\right)\text{acos}\left(\frac{l_d}{d_t}\right) - \left(\frac{l_d}{2}\right)\sqrt{\left({d_t}^2 - {l_d}^2\right)}}{\pi\left(\frac{d_t}{2}\right)^2} \right) \tag{2.6}$$

Where d_t is the diameter of the scrubber tube (0.356 m), and l_d is the vertical distance that the drops fall (in m). Equation 2.7 is determines l_d which uses the time step and the Stoke's settling velocity of the drop, V_{s_d}, which can be calculated using Equation 2.8

$$l_d = t_s V_{s_d} \tag{2.7}$$

$$V_{s_d} = \frac{\rho_d (d_d)^2 g}{18\mu_a} \tag{2.8}$$

Where g is the acceleration of gravity (9.81 m/s^2) and ρ_d is the density of the drop (997 kg/m^3). Due to the turbulent mixture of DPM and drops within the tube, the DPM is assumed to coagulate evenly with the available drops. Due to this assumption, the fraction of total drops removed is equal to the fraction of total coagulated DPM removed. The fraction of coagulated DPM removed by the gravitational settling of the droplets is added to the "Drop Removal (Grav)" DPM category from Table 2.2. The fraction of settled droplets is removed from the "suspended" drops and added to the "settled" drops category from Table 2.2.

2.2.2b Droplet Reduction, Inertial Impaction

Along with gravitational settling, the drops can also be removed from the air by inertial impaction to the walls of the settling tube, which is assumed to be irreversible (i.e., an impacted drop and any DPM it is carrying are permanently removed from the air flow). The model calculates the fraction of drops that impact the walls (W_d) of the tube using Equation 2.9 given by Hinds (1999):

$$W_d = 1 - P = 1 - e^{-\frac{\left(4V_{dep_d} t\right)}{d_t}} \tag{2.9}$$

Where P is defined as the penetration fraction of particles that exit a tube with diameter d_{tube} after time, t (Hinds, 1999). The model uses the time step (0.005 s) for t to determine the fraction of particles that impact the walls. V_{dep} is the deposition velocity of the particles per Hinds (1999) for a straight walled tube. It was assumed that the deposition velocity would be enhanced by an internal rib structure inside tube so the equation for V_{dep} from Hinds (1999) was adapted to have an enhancement factor, R_V, shown below as Equation 2.10 for the depositional velocity of the droplets, V_{dep_d}:

$$V_{dep_d} = R_V \frac{0.04V}{Re^{1/4}} \left(\frac{\rho_d D_d}{\mu_a}\right)^{\frac{2}{3}} \tag{2.10}$$

Where V is the velocity of the flow in the tube (0.504 m/s), ρ_d is the density of the drop (taken as 997 kg/m^3), and D_d is the diffusion coefficient of the drop given by Equation 2.2. The enhancement factor was initially set to 1.0 but was varied later to explore the effect V_{dep_d} enhancement has on DPM removal.

The fraction of drops that impact the walls is removed from the suspended drops and added to the impacted drops category. Due to the assumption of even coagulation, this same fraction is removed from the coagulated DPM and added to the "Drop Removal (Wall)" DPM category from Table 2.2.

2.2.3a Free DPM Reduction, Gravitational Settling

In Stage 3, the model calculates the fractions of free DPM that are removed by from the air. While it is expected to be a small fraction, the fraction of free DPM that settles out due to gravity is determined. The fraction is determined by rewriting Equations 2.6, 2.7, and 2.8 using the density and diameter of the DPM particle in place of the drop characteristics as Equations 2.11, 2.12, and 2.13. This fraction of settled DPM is removed from the remaining free DPM and added to the "Grav settled" DPM category in Table 2.2.

$$G_D = \left(1 - \frac{\left(\frac{{d_t}^2}{2}\right)\operatorname{acos}\left(\frac{l_D}{d_t}\right) - \left(\frac{l_D}{2}\right)\sqrt{{d_t}^2 - {l_D}^2}}{\pi\left(\frac{d_t}{2}\right)^2}\right) \tag{2.11}$$

$$l_D = t_s V_{s_D} \tag{2.12}$$

$$V_{s_D} = \frac{\rho_p (d_D)^2 g}{18\mu_a} \tag{2.13}$$

2.2.3b Free DPM Reduction, Turbulent Diffusion

Along with gravitational setting, the free DPM can also be removed by turbulent diffusion to the tube walls. This fraction is determined in the same way that the fraction of drops removed by inertial impaction is determined. Equations 2.9 can be rewritten as Equation 2.14 and used to determine the fraction of free DPM lost to the walls by rewriting Equation 2.10 as Equation 2.15 which accounts for both the turbulent diffusion and inertial impaction of particles to the walls of a straight tube (Hinds, 1999). The difference in removal mechanism (diffusion versus impaction) is a property of the size of the particles in each aerosol (Hinds, 1999). The turbulently diffused fraction of DPM is removed from the free DPM category and added to the "wall deposition" DPM category shown in Table 2.2.

$$W_D = 1 - P = 1 - e^{-\frac{(4V_{dep}t)}{d_t}} \tag{2.14}$$

$$V_{dep_D} = \frac{0.04V}{Re^{1/4}}\left(\frac{\rho_d D_D}{\mu_a}\right)^{\frac{2}{3}} \tag{2.15}$$

2.2.4 Turbulent Redistribution

The last stage shown in Figure 2.1 explicitly illustrates the assumption that the drops and DPM particles are evenly redistributed at the end of the time step. At this point, the model advances by another 0.005 seconds and starts over at stage 1. During the course of each loop the fractions of the free DPM, the coagulated DPM, the DPM that diffuses to the wall, and the DPM removed by the impaction and settling of the drops are adjusted based on the assumed behavior of the two aerosols within the current time step.

2.3 Results and Discussion

The model was used to simulate the DPM removal measured in the scrubber apparatus in Chapter 1. The model was run using inlet DPM and fog drop concentrations determined in all 11 field tests, and results from the model using input data from Test 6 are shown here to illustrate key points. This test was chosen because its inlet concentrations were most representative of the average concentrations across all tests. The simulated results for all other field test conditions are shown in Appendix B.

2.3.1 Relative Impact of Different Mechanisms on DPM Removal

While the outlet concentration of DPM (total or by size bin) is the only simulated quantity that can be directly compared to experimental results from Chapter 1, one benefit of the model developed here is the ability to gain insight about what happens to the DPM particles as they move through the scrubber tube. Figure 2.2 shows the fractionation of DPM between possible classes (See Table 2.2) as a function of the residence time which at a constant air speed is comparable to the distance air has moved down the length of the scrubber tube. Figure 2.2 shows the time series results for three of the 10 size bins modeled, the smallest bin (11.5 nm), the largest bin (154 nm), and a middle size bin (36.5 nm). For the model results shown in Figure 2.2, inlet concentrations of DPM and drops were those measured in Test 6 in Chapter 1, and the R_V was set at 1.0. (The same plots using conditions from all other tests in Chapter 1 are presented in Figures B.1-B.9 in Appendix B.)

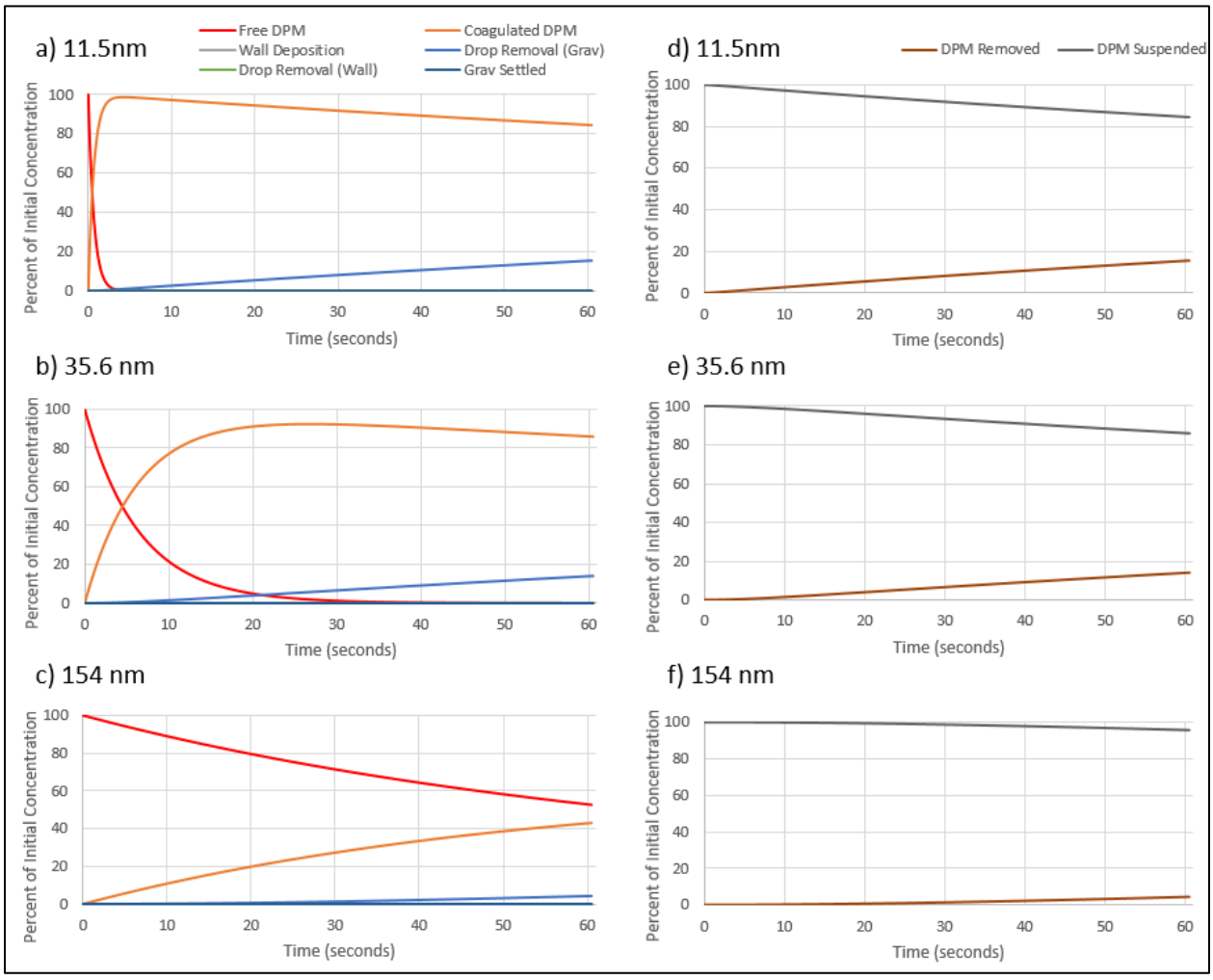

Figure 2.11 Simulated DPM classes shown across the length of the scrubber tube using initial conditions from Test 6. a), b) and c) show results for the 11.5, 36.5, and 154 nm size bin, respectively, with particles fractionated between the six possible DPM classes defined in Table 2.2. d), e) and f) show the total DPM removed and still suspended in the air flow for the same three size bins.

From Figure 2.2, it is clear that gravitational settling and diffusion of free DPM to the tube walls are expected to remove negligible amounts of DPM of any size. Rather, DPM removal is primarily due to removal of fog drops that have coagulated with the DPM. This coagulation happens most rapidly for the 11.5 nm DPM particles, which is evident by comparing the orange "coagulated DPM" lines in Figure 2.2a-c. However, it is important to note that, regardless of the DPM size the coagulated DPM is not predicted to be efficiently removed from the air flow; as shown in Figure 2.2d-f, most of the DPM remains suspended in the air flow at the scrubber tube outlet (at t=60.5 s). For comparison with experimental data, Figure 2.3 shows the simulated DPM concentration distribution at the scrubber outlet for the same test conditions shown in Figure 2.2.

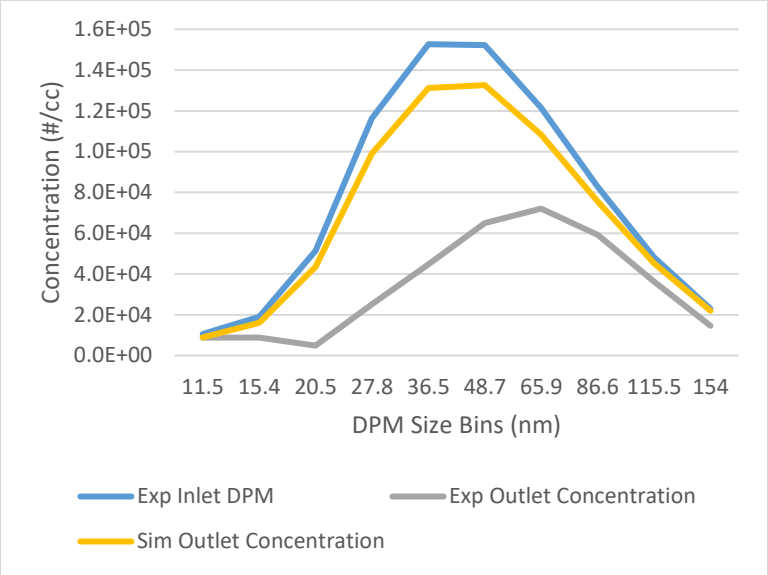

Figure 2.12. Experimental and simulated scrubber outlet DPM concentration by size bin for inlet conditions measured in Test 6 in Chapter 1. The measured inlet DPM concentration by size bin is also shown, and the inlet fog drop concentration was taken as $2.53 \times 10^5 \#/cm^3$ *per Chapter 1.*

The underestimation of DPM removal by the model shown in Figure 2.3 is also observed when using scrubber inlet concentrations measured in other tests reported in Chapter 1 (see Figures B.10-B.18, Appendix B). This is related to the predicted removal of DPM-laden drops. Though estimates for gravitational settling (per Equation 2.6) should be reasonably accurate, estimates for drop removal by inertial impaction to tube walls are likely not. Equations 2.9 and 2.10 from Hinds (1999) are meant for a straight smooth-walled tube. However, as can be seen in Figure 2.4, the Mylar tube used for the experimental scrubber apparatus has a helical rib structure imparted by a thin steel-coil. This structure makes the tubing flexible in terms of length and rigid in terms of keeping the cross-sectional diameter open; but the effect on air flow dynamics might significantly enhance V_{dep_d}. Thus, to more accurately model DPM removal in the fog scrubber, the V_{dep_d} enhancement factor R_V should be increased.

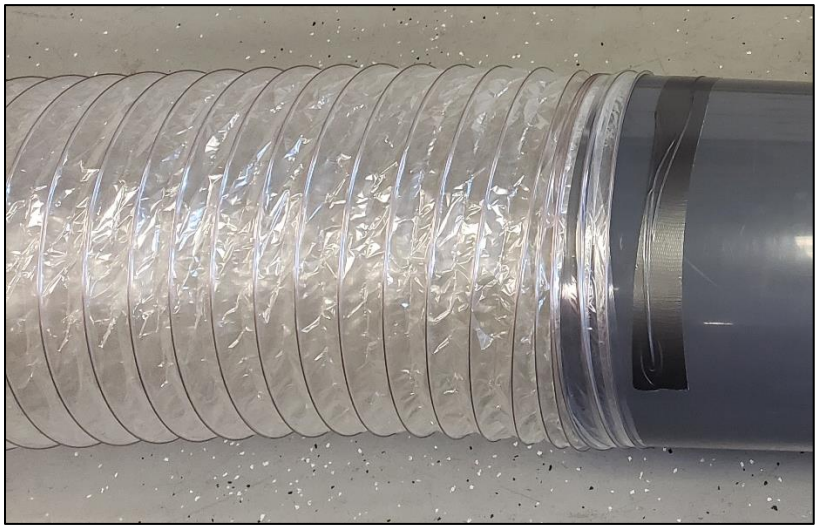

Figure 2.13. A section of the Mylar tubing used in the scrubber apparatus.

2.3.2 Analysis of Depositional Velocity

Because of its importance in many systems such as ventilation ducts, particle deposition in turbulent flows has been well researched for smooth ducts (e.g., see Chamberlain, et al., 1984). A review of the literature shows that the value of V_{dep_d} can be significantly enhanced in tubes with rough, ribbed or wavy walls (El-Shobokshy and Ismail, 1979; Sippola and Nazaroff, 2010; Lu and Lu, 2015; 2016; Lai et al., 1999; Lu and Wang, 2019; Hyati et al., 2019).

Figures 2.2 and 2.3 show simulated results for the fog scrubber assuming a smooth-walled tube (R_V= 1.0), with average V_{dep_d} calculated to be 1.29×10^{-5} cm/s (Equation 2.10). To estimate the effective V_{dep_d} for the fog scrubber apparatus, the model was run using increasing values for V_{dep_d} (by increasing R_V up to 150,000). Figure 2.5 shows the simulated outlet concentration (total DPM) as a function of V_{dep_d} for the inlet DPM and drop concentrations measured in Test 6 from Chapter 1. The figure also shows the outlet concentration measured during the test. (The same plots corresponding to other tests reported in Chapter 1 are given in Figures B.19-B.27 in Appendix B.)

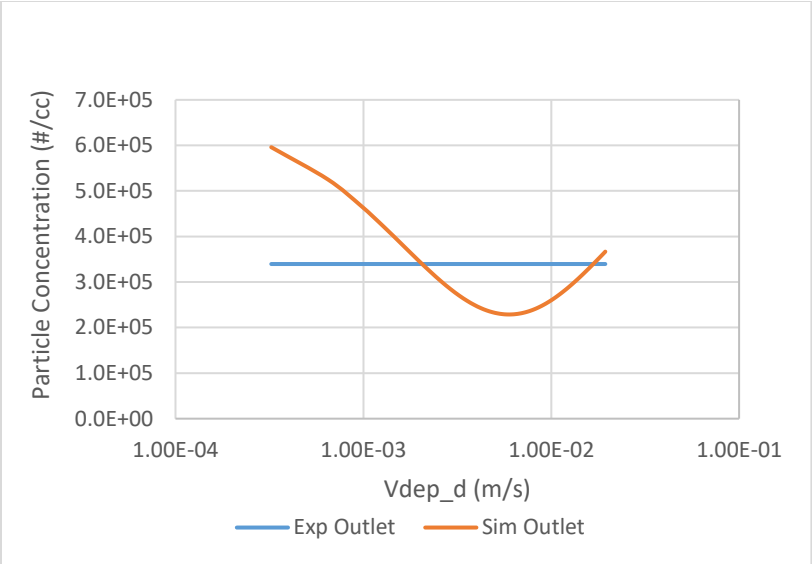

Figure 2.14. Simulated DPM concentration at the scrubber outlet as a function of V_{dep} for the inlet DPM and fog drop concentrations measured in Test 6 in Chapter 1. The experimental outlet concentration is also shown.

Figure 2.5 indicates that two different values of V_{dep_d} (termed from here as "low fitted V_{dep_d}" and "high fitted V_{dep_d}") will produce simulated scrubber results that agree with the results observed in the field test. (Values of low and high fitted V_{dep_d} can be found in Table B.2 in Appendix B.) The V-shaped curve and the two fitted V_{dep_d} values are the result of competing mechanisms between DPM-drop coagulation and drop removal. At the low fitted V_{dep_d}, there is more time for coagulation before too many drops are removed by impaction. At the high fitted V_{dep_d}, the drops are removed so rapidly by the enhanced impaction that they are less available for coagulation. These points are evident in Figure 2.6, which predicts that suspended DPM at the scrubber outlet will include significant fractions of coagulated

particles for the low fitted V_{dep_d} but will be entirely free DPM at the high fitted V_{dep_d}. Figure 2.6 uses the low and high fitted V_{dep_d} values from Test 6 seen in Figure 2.5. The category breakdown of DPM for the low and high fitted V_{dep_d} values from the other tests are shown in Figures B.28-B.36 in Appendix B.

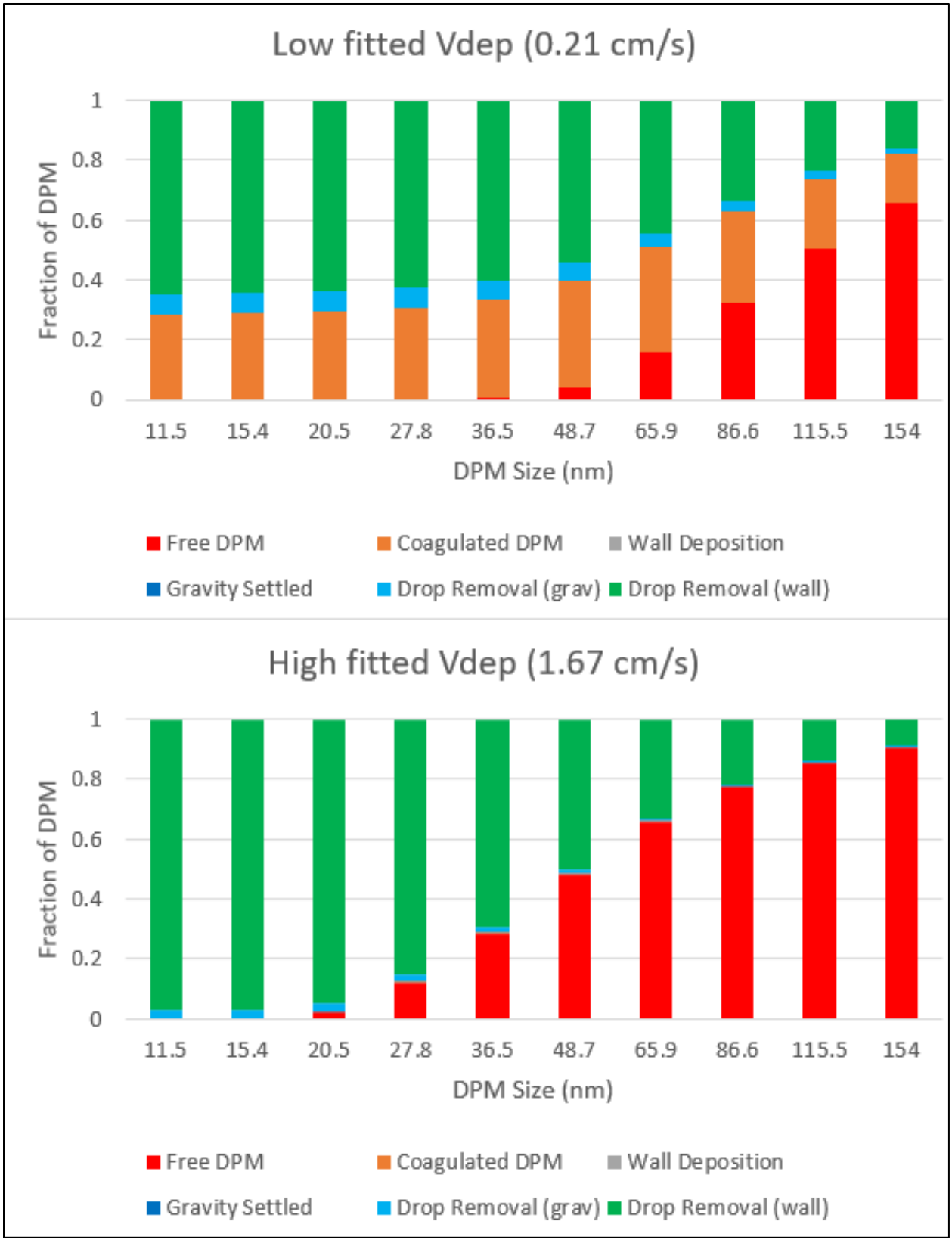

Figure 2.15. Simulated fractions of the DPM (by size bin) in all possible classes for inlet DPM and fog drop concentrations measured in Test 6 in Chapter 1. Results are shown using the a) low and b) high fitted V_{dep_d} values determined in Figure 2.5.

Even though the results of the model using both the low and high fitted V_{dep_d} agree with the experimental results, the lower fitted V_{dep_d} value seems more plausible based on the evaluation of the total drop removal. As discussed in Chapter 1, E_d is expected to be similar to E if DPM removal does indeed proceed by DPM-drop coagulation followed by drop removal. Figure 2.7 shows the simulated E_d values (for the smooth-walled, lower fitted and higher fitted V_{dep_d} cases) versus the E_D values (for particles in bins between 20.7-35.6 nm) determined for each test from Chapter 1. The model shows very good agreement between the simulated E_d and experimental E_D when using the lower fitted V_{dep_d} values. On the other hand, the model predicts nearly complete removal of the drops ($E_d \approx$100%) when using the higher fitted V_{dep_d} values, which is inconsistent with visual observations of fog at the scrubber outlet during the field testing.

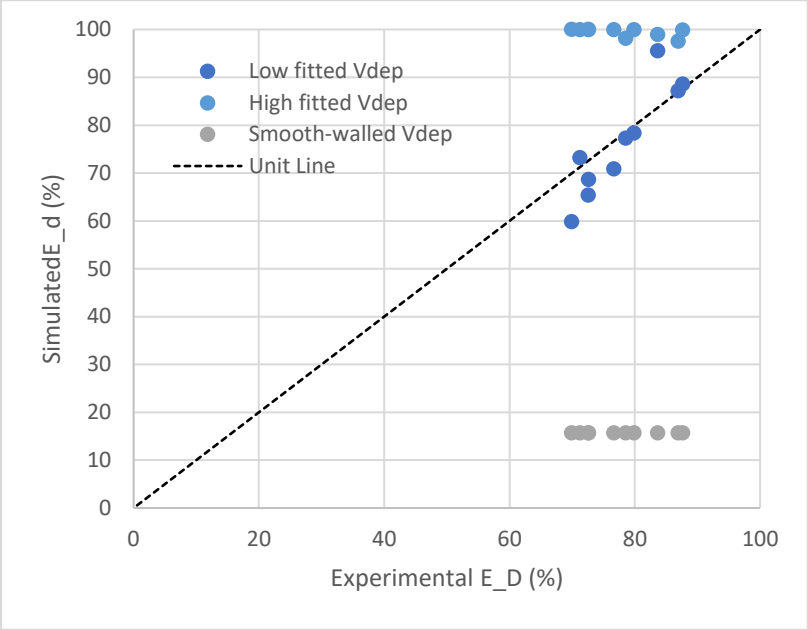

Figure 2.16. Simulated E_d versus experimental E_D (for particles in bin sizes 20.5, 27.8 and 36.5 nm). Simulated E_d values are shown using V_{dep_d} calculated for the smooth-wall case (i.e., Equations 2.10 and 2.14) and the lower- and higher-fitted V_{dep_d} values shown in Table B.2 in Appendix B.

When comparing E_D from the lower fitted V_{dep_d} model to the experimentally measured E_D it can be seen that the two values are mostly similar across all DPM size bins. Figure 2.8 shows the lower fitted V_{dep_d} modeled and experimental E_D values for all tests except 9 for each DPM size bin. Figure 2.8 shows that the majority of the size bin data for simulated and experimental E_D values fall along the unit line showing similarity between the two values across the size bins for each test. In Figure 2.8 several experimental points show a negative removal efficiency. This tends to be the case for size bins that report low inlet concentrations (in the range of 10^4 #/cm^3). Table A.3 in Appendix A shows the inlet concentrations for all size bins in each test and it can be seen that the size ranges which report a negative removal efficiency in Figure 2.8 typically show low inlet concentrations in Table A.3.

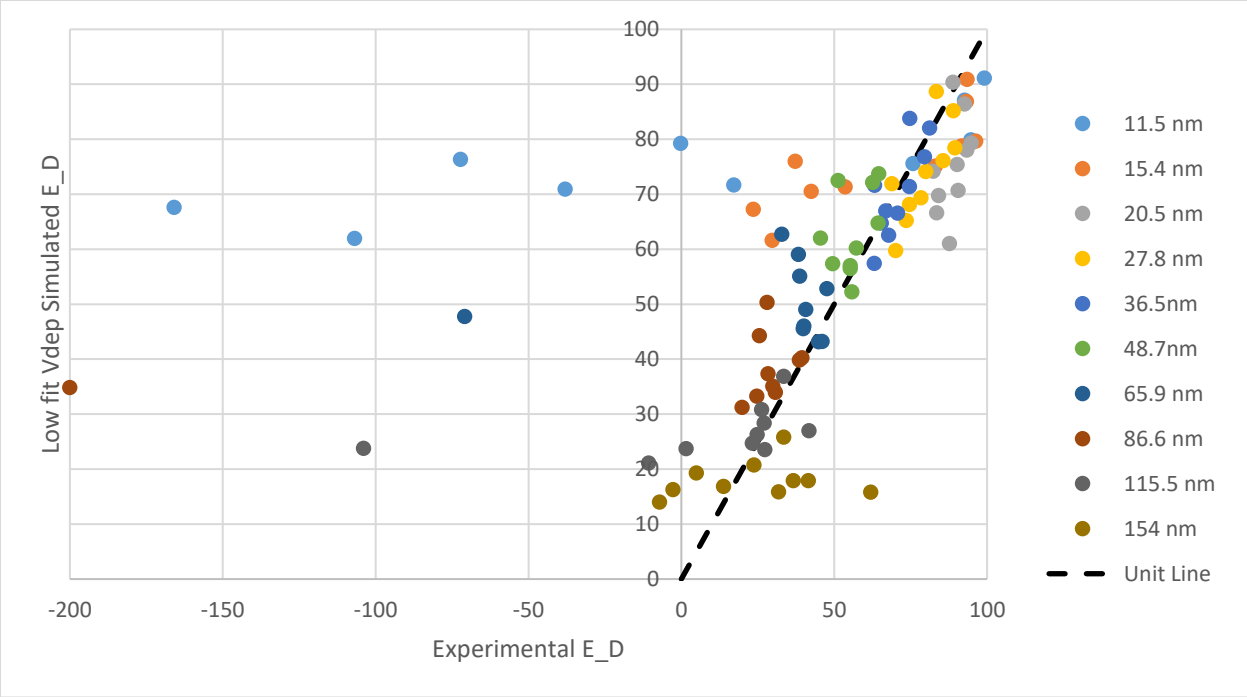

Figure 2.17. E_D values for experimental and the low fitted V_{dep_d} model data for each test separated by size bin.

The effective (fitted) V_{dep_d} values predicted for the scrubber were also assessed based on the available literature, which includes a number of studies pertaining to particle deposition from turbulent flow through rough, ribbed or wavy tubes. Most studies focus on a dimensionless form of V_{dep_d} (denoted as V_{dep}^{+}) as a function of dimensionless relaxation time (τ^{+}), which is proportional to particle size (Lu and Wang, 2019; Hayati et al., 2019). Equations 2.16 and 2.17 define V_{dep}^{+} and τ^{+}, respectively.

$$V_{dep}^{+} = \frac{V_{dep_d}}{u^*} \tag{2.16}$$

$$\tau^{+} = \frac{C_c S (d_d)^2 u^{*2}}{18\, v^2} \tag{2.17}$$

Where C_c is the Cunningham correction factor (defined in Equation 2.3), which is effectively 1.0 for micron-scale particles such as the fog drops considered here; S is the density ratio between the particles and the carrying fluid (air), which is taken to be 814 here; v is the kinematic viscosity of air (1.48×10^{-5} m^2/s); and u^* is the frictional velocity (m/s) as defined by Equation 2.18:

$$u^* = U_{avg}\sqrt{\frac{f}{2}} \tag{2.18}$$

Where U_{avg} is the average air speed velocity (0.5 m/s); and f is a dimensionless friction factor value determined by the tube and flow geometry. Although various empirical equations have been derived to find f for a ribbed tube, f_{rib} (e.g., see Gradziel and Majewski, 2019), none appear to be valid for the particular geometry inherent to the scrubber apparatus.

As an alternative approach to directly computing a value for f_{rib}, other researchers have indicated that f_{rib} can be reasonably estimated by multiplying the friction factor of a smooth-walled tube, f_{smo}, by an enhancement constant, R_f, as shown in Equation 2.19. Work by Gradziel and Majewski (2019) and Lai et al. (1999) has shown that an R_f of about 3-4 is expected for ribbed tubes.

$$f_{smo} = (R_f) f_{smo} \tag{2.19}$$

To determine f_{smo}, a number of equations are reported in the literature, including Equations 2.20 and 2.21, which are the common Moody equations for friction factor in turbulent flow (microscale roughness) and turbulent flow in a smooth pipe, respectively.

$$f_{smo} = \left[1.14 + 2 \log\left(\frac{\varepsilon}{d_t}\right)\right]^{-2} \tag{2.20}$$

$$f_{smo} = \frac{0.316}{Re^{0.25}} \tag{2.21}$$

In Equation 2.20, ε is the roughness height, which is estimated to be 0.0015 mm for Mylar tubing (Engineering ToolBox, 2003).

Based on the above equations, Table 2.3 shows a range of values for f_{smo} and f_{rib} (assuming R_f=3) for the scrubber tube, and $\tau^+$for the fog drops. To find corresponding values for V_{dep}^+, works by Lu and Wang (2019) and Hyati et al. (2019) were consulted. As shown in Figures 2.8 and 2.9, respectively, these researchers compiled data from numerous other studies on the relationship between V_{dep}^+ and τ^+ in smooth ducts or channels. The shaded areas superimposed on their figures can be used to approximate a range of expected V_{dep}^+ values for the fog drops in the scrubber based on the calculated τ^+ values (Table 2.3). Then, using the limits of the shaded areas as a maximum and minimum V_{dep}^+, the maximum and minimum expected V_{dep_d} values can also be determined using Equation 2.11 (Table 2.3). The blue shaded areas in Figures 2.8 and 2.9 show the range of V_{dep}^+ and τ^+ values for a smooth walled tube and the red shaded areas show the range V_{dep}^+ and τ^+ values for the ribbed tube case (Table 2.3).

Expectations based on prior work in smooth tubes appear to significantly underestimate the effect of V_{dep_d} to remove the DPM-laden fog drops from the ribbed scrubber tube. As shown in Table 2.3, the maximum expected value for V_{dep_d} according to the literature compiled in Figures 2.8 and 2.9 was determined to be about 0.01 cm/s. This is much less than the lower fitted V_{dep_d} values from the simulated scrubber results, which ranged from about 0.15-0.45 cm/s when the model used inlet DPM and drop concentrations for the tests reported in Chapter 1. This order-of-magnitude discrepancy in V_{dep_d} implies an R_f value for the ribbed scrubber tube of 40-350 (Figure B.37 in Appendix B), as opposed to a value of 3-4 based on the available literature (Gradziel and Majewski, 2019; Lai et al.,1999).

However, the results of Hayati et al. (2019) shown in Figure 2.9 for wavy-walled channels appear to be consistent with the simulated scrubber results. Their study showed dramatic increases in V_{dep}^+ between flat

and wavy wall conditions, which provides some support for what appears to be a very significant enhancement of depositional velocity here due to the ribbed scrubber walls.

Table 2.5. Summary table of results from literature investigation.

Quantity	Smooth tube case	Ribbed tube case	Source
f range	7.1×10^{-3} to 4.8×10^{-2}	2.1×10^{-2} to 1.45×10^{-1}	f_{smo}: Equation 2.20 (min) and Equation 2.21 (max). And $R_f = 3$.
τ^+ range	4.3×10^{-3} to 2.9×10^{-2}	1.28×10^{-2} to 8.7×10^{-2}	Equation 2.10
Expected V_{dep}^+ range (Lu and Wang, 2019)	9×10^{-6} to 2×10^{-3}	7×10^{-6} to 8×10^{-4}	Values determined from Figure 1 in Lu and Wang (2019)
Expected V_{dep_d} range (Lu and Wang, 2019) (cm/s)	2.7×10^{-5} to 1.56×10^{-2}	6.4×10^{-5} to 1.08×10^{-2}	Determined using Equation 2.16
Expected V_{dep}^+ range (Hayati et al., 2019)	4×10^{-5} to 1.3×10^{-3}	1×10^{-4} to 1.2×10^{-3}	Values determined from Figure 13 in Hayati et al. (2019)
Expected V_{dep_d} range (Hayati et al., 2019) (cm/s)	1.2×10^{-4} to 1.02×10^{-2}	5.2×10^{-4} to 1.6×10^{-2}	Determined using Equation 2.16
Simulated V_{dep_d} (cm/s)	1.29×10^{-5}	1.47×10^{-1} to 4.5×10^{-1}	Smooth simulated V_{dep_d} from Equation 2.10. (R_f = 1.0). Ribbed values from range of low fitted V_{dep_d} (R_f = 11,000-35,000) as indicated by Figures B.19-B.27 in Appendix B.

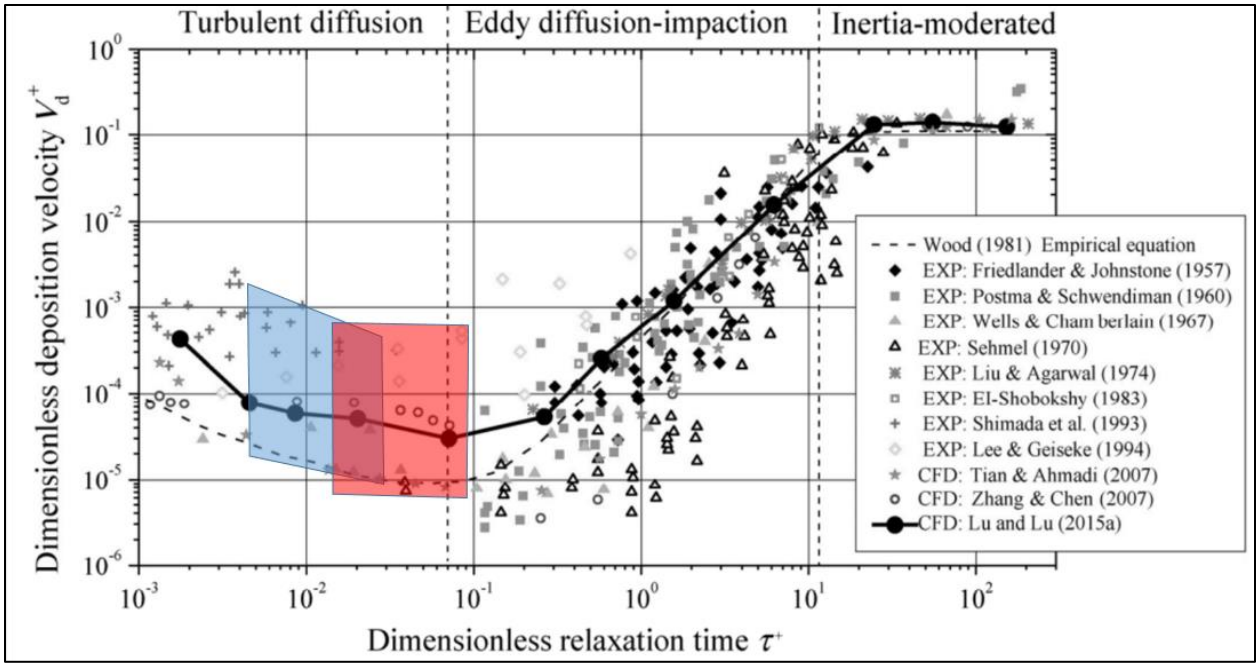

Figure 2.18. Adapted from Lu and Wang (2019), who compiled V_{dep}^+ versus τ^+ data from previous studies of smooth tubes and ducts. The shaded areas show the range of expected values for V_{dep}^+ and τ^+ for a smooth tube (blue) and for a ribbed tube (red) based on Equations 2.15-2.20. The range of V_{dep}^+ values derived from the simulated scrubber results with the low fitted V_{dep_d} could not be added due to the limitations of the y axis; these would fall in the range of 1.09-8.76.

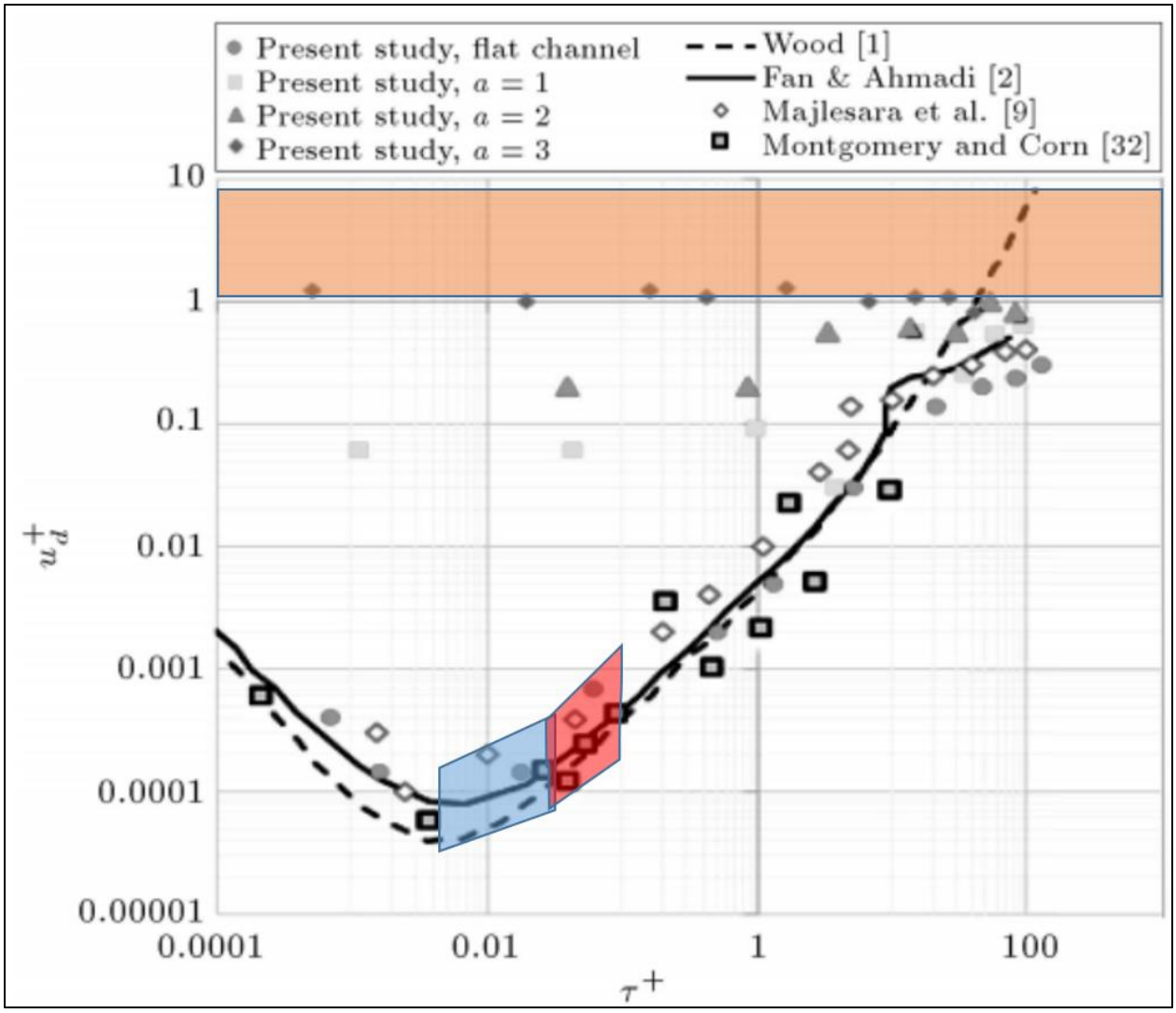

Figure 2.19. Adapted from Hayati et al. (2019), who compiled V_{dep}^+ versus τ^+ data from previous studies of flat channels (V-shaped trend) and wavy-walled channels. The shaded areas show the range of expected values for V_{dep}^+ and τ^+ for a smooth tube (blue) and for a ribbed tube (red) based on Equations 2.15-2.20; and the range of V_{dep}^+ values derived from the simulated scrubber results with the low fitted V_{dep_d} values (orange).

2.4 Conclusions

A fogging scrubber was previously tested in the field to determine its efficacy for removing DPM from a vehicle exhaust. To better understand the predominant removal mechanisms, a model was developed and used here to simulate the scrubber using DPM and fog drop concentrations indicated from the field tests. Results support the notion that DPM removal largely dependent on early coagulation of DPM with the fog drops, which are subsequently removed from the air flow. Moreover, the model indicates that while gravitational settling of drops does account for some drop (and hence DPM) removal, drop removal by inertial impaction is likely a much bigger factor.

The relative effect of inertial impaction is controlled by the depositional velocity of fog drops (V_{dep_d})—a quantity that cannot be directly measured, but rather is initially approximated by conceptualizing the

scrubber as a smooth-walled tube. However, the model suggests that this approximation is far from the actual V_{dep} imparted by the ribbed tubing currently utilized for the scrubber. In fact, the simulated results show that V_{dep} is enhanced by a factor of about 15,000-35,000 versus what is expected for a smooth-wall case. Such an enhancement in consistent with modeled results of wavy channels by Hayati et al. (2019), but deserves further investigation.

Considering the effective V_{dep_d} values indicated by the model, the simulated results for total particle removal in the scrubber generally agree quite well with experimental observations from Chapter 1. It also yielded reasonable agreement with observed trends with respect to bin size. Further, the model results suggest that DPM removal by the scrubber could be improved by additional enhancement of V_{dep}. This may be possible with modifications to the scrubber geometry and operation, and the model provides a tool for initial exploration and sensitivity analysis.

References

1) Virtanen, A, Ristimaki, J, et al. (2002). *Effective Density of Diesel Exhuast Particles as a Function of Size.* SAE Technical Paper. 2002-01-0056.
2) Pruppacher, H, and Klett, J. (1978). Microphysics of Clouds and Precipitation. Dordrecht: Reidel Publishing Company.
3) Hinds, W. C. (1999). *Aerosol Technology: Properties, Behavior, and Measurement of Airborne Particles, 2nd Edition.* New York: Wiley-Interscience.
4) Merrell, T. M. and Saylor, J. R. (2017a). *Demisting using an Ultrasonic Standing Wave Field*. Journal of the Acoustical Society of America. Vol 141. Pages 171-182.
5) Chamberlain, A. C., Garland, J. A., and Wells, A.C. (1984) *Transport of Gases and Particles to Surfaces with Widely Spaced Roughness Elements,* Boundary Layer Meteor. Vol 29. Pages 343-360.
6) El-Shobokshy, M. S. and Ismail I. A. (1979). *Deposition of Aerosol Particles from Turbulent Flow onto Rough Pipe Wall*. Atmospheric Environment. Vol 14. Pages 297-304.
7) Sippola, M. R. and Nazaroff, W. W. (2010) *Experiments Measuring Particle Deposition from Fully Developed Turbulent Flow in Ventilation Ducts.* Aerosol Science and Technology. Vol 38(9). Pages 914-925.
8) Lu, H and Lu, L. (2015). *Effects of Rib Spacing and Height on Particle Deposition in Ribbed Duct Air Flows.* Building and Environment Vol 92. Pages 317-327.
9) Lu, H and Lu, L. (2016). *CFD Investigation on Particle Deposition in Aligned and Staggered Ribbed Duct Air Flows.* Building and Environment Vol 93. Pages 697-706.
10) Lai, A. C. K., Bryne, M. A., and Goddard, A. J. H. (1999). *Measured Deposition of Aerosol Particles on a Two-Dimensional Ribbed Surface in a Turbulent Duct Flow.* Journal of Aerosol Science. Vol 30(9). Pages 1201-1214.
11) Lu, H and Wang, Y. (2019). *Particle Deposition in Ventilation Ducts: A Review*. Building Simulation. Vol 12(5). Pages 723-734.
12) Hayati, H., Goharrizi, A. S., Salmanzadeh, M., and Ahmadi, G. (2019). *Numerical Modeling of Particle Motion and Deposition in Turbulent Wavy Channel Flows.* Scientia Iranica. Vol 26(4). Pages 2229-2240.

13) Gradziel, S and Majewski, K. (2019). *Experimental Determination of the Friction Factor in a Tube with Internal Helical Ribs.* Energies. Vol 12(2). Pages 257-274.

14) Engineering ToolBox, (2003). *Roughness & Surface Coefficinets.* [online] Available at: https://www.engineeringtoolbox.com/surface-roughness-ventilation-ducts-d_209.html. [Accessed 03 June 2020]

Chapter 3: Lessons Learned and Recommendations for Future Work

3.1. Lessons Learned

DPM is a known health hazard and due to the enclosed spaces of underground mine workings, miners often face higher exposure risks. Previous work by Rojas-Mendoza et al. (2017) showed the efficacy of a fog-based scrubber treatment for removing DPM from an exhaust stream in a controlled laboratory setting. The goal of the current work was to investigate the efficacy and applicability of a fog-based DPM treatment in a more practical setting. A field apparatus was built and deployed in an underground stone mine and data was gathered on the inlet and outlet concentrations of DPM for control and treatment cases. To better understand how DPM is removed by a combination of DPM-fog drop coagulation and removal of the drops, a model was developed in to simulate the scrubber apparatus. The experimental results were compared to the simulated results to investigate the predominant mechanisms responsible for the removal of DPM.

The results of the experimental testing showed that the fog treatment removed more DPM particles than when the treatment was not employed. The treatment was highly effective at removing the smallest DPM particles from the air, however it was less efficient for the larger particles. The average total particle removal efficiency was determined to be 7.5% for the control and 65% when the fog treatment was applied. The removal of DPM took place over the course of a 100-ft settling tube and used an average 2 L of deionized water per hour. This DPM treatment was only tested on light duty vehicles, a scaled up version for larger vehicles could present challenges if additional space and deionized water are required to treat an even larger source of DPM.

One particular limitation of the field experiments was the inability to measure the concentration of droplets. Having to estimate the droplet concentration based on the water consumption and an average drop size limits the understanding of the exact mechanisms of the Droplet and DPM. A lack of knowledge about DPM and droplet interaction, limits the conclusions able to be pulled from the data. It also limits the ability to optimize this treatment.

The mechanistic model developed in Chapter 2 provided key insights to how the scrubber works, including the likely importance of fog drop removal by inertial impaction. The simulated results initially under predicted the DPM removal compared to what was measured in the field. An investigation of the enhancement of the friction factor and the depositional velocity was conducted using previously published research. Previous literature showed that significant enhancement of the depositional velocity needed to allow the simulated outlet concentration to match the experimentally measured outlet concentration is possible. However further investigation on particle deposition enhancement in “wavy” or helically ribbed tubes still needs to be conducted for definitive proof. Additionally, the model has potential to be used for optimizing the fog treatment by investigating how changing input variables such as tube geometry and fog characteristics will maximize DPM removal.

3.2. Recommendations for Future Work

The work completed during this investigation has proved that a fog-based treatment can effectively reduce the DPM concentration in a concentrated diesel exhaust stream. However, the scrubber tested here requires a large amount of space and clean water with the current setup. Future work on the fog-based treatment could seek ways for practical applications of the concepts proved in this work and in Rojas-Mendoza (2017). A likely application for this fog treatment would be to implement it as a tailpipe scrubber to effectively remove the reduce the amount of DPM ultimately emitted. A promising result from the experimental results shows that the fog treatment is most effective at removing small DPM particles. Currently, diesel particulate filters (DPFs) are used in some operations to reduce the DPM emitted from equipment. However, while DPFs can be highly effective for removing the largest sized DPM particles, they are less efficient for the small particles escape. By coupling a DPF and fog-based treatment, the DPM removal would be effective for both sides of the particle size distribution.

The mechanistic model provides an excellent resource to simulate and optimize the removal of DPM. In addition to optimization of DPM removal, the model could have potential in future work to scale up the fog treatment for larger equipment.

Future work on the particle deposition of droplets in a helical-ribbed, large opening duct is needed to prove the application of the fog treatment. Chapter 2 highlighted the importance of the deposition velocity and the removal of drops in the removal of DPM. Further testing done on different tube and rib geometries could help identify conditions to remove DPM more rapidly. Additionally, the use of baffles and other large obstruction elements to increase droplet removal could be investigated to provide new avenues for optimization.

3.3 References

1. Rojas-Mendoza, Lucas, et al. (2017). Removal of DPM from an Airstream Using Micron-Scale Droplets. *Aerosol and Air Quality Research.* Vol 17. Pages 1865-1874.

Appendix A

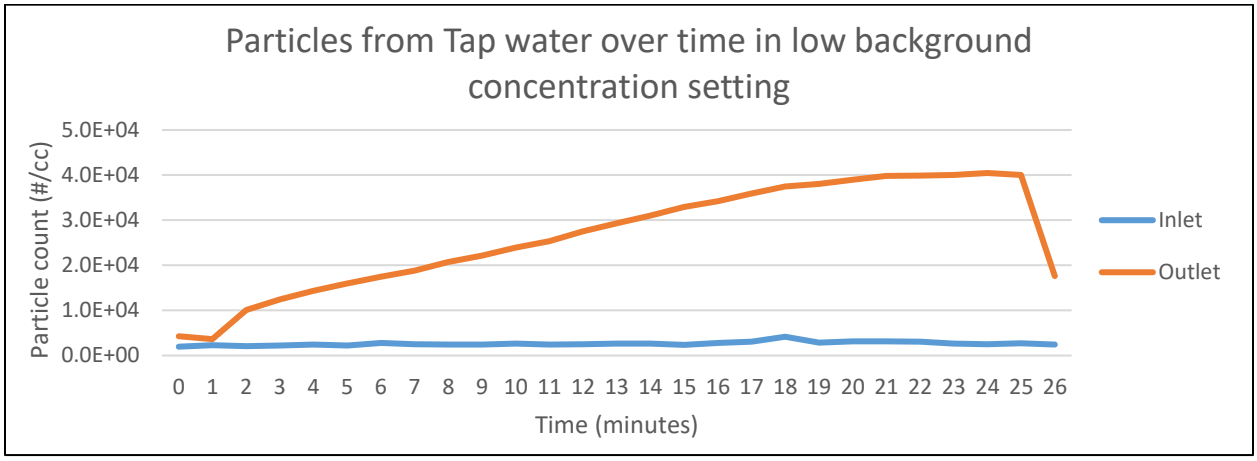

Figure A.20. Lab Test with Tap Water. Total concentration of particles in the inlet and outlet during a test in a low particle background, using tap water which has a higher concentration of dissolved particles.

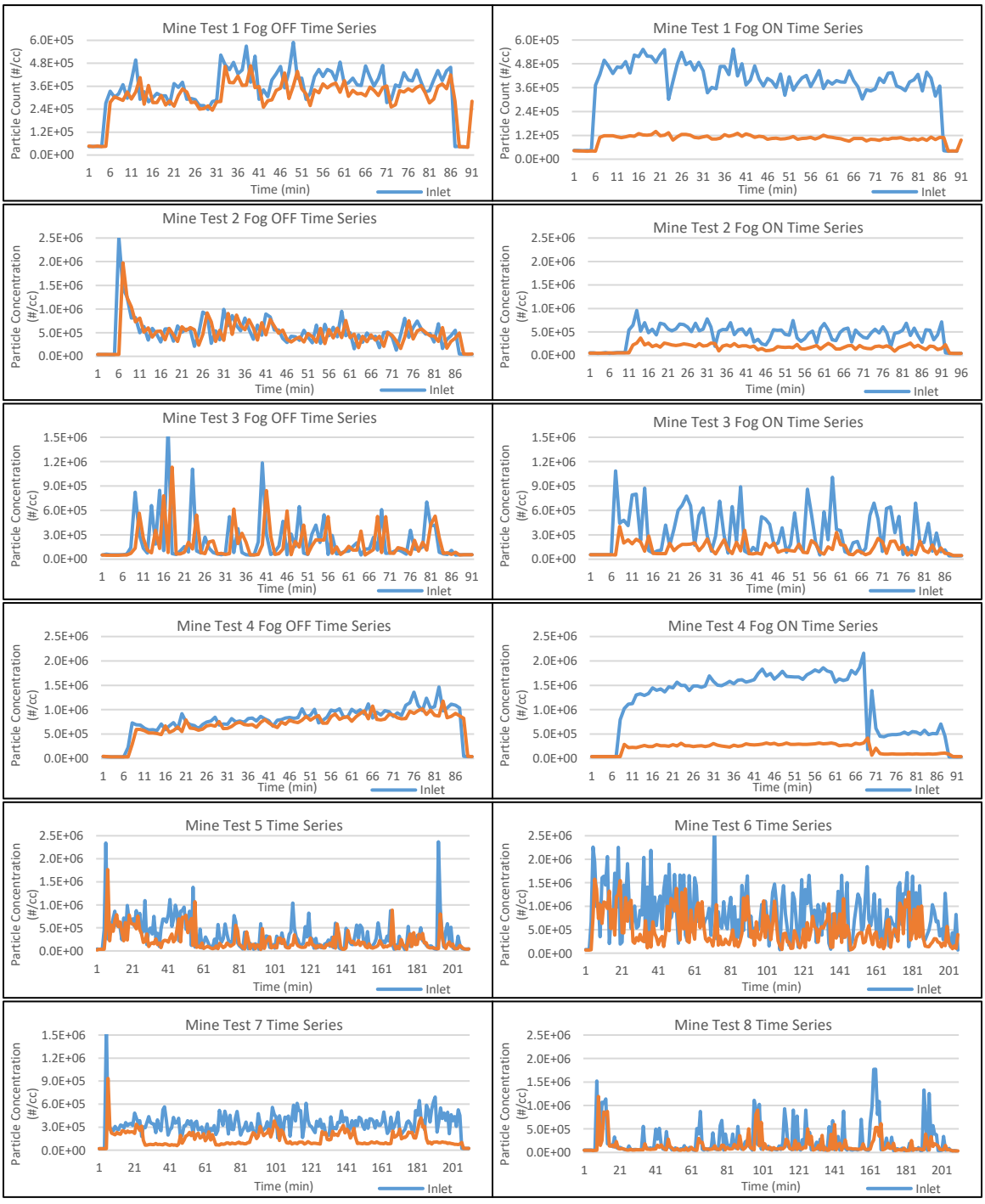
Mine Test 1 Fog OFF Time Series
Particle Count (#/cc)
6.0E+05
4.8E+05
3.6E+05
2.4E+05
1.2E+05
0.0E+00
1 6 11 16 21 26 31 36 41 46 51 56 61 66 71 76 81 86 91
Time (min)
Inlet
Mine Test 1 Fog ON Time Series
Particle Count (#/cc)
6.0E+05
4.8E+05
3.6E+05
2.4E+05
1.2E+05
0.0E+00
1 6 11 16 21 26 31 36 41 46 51 56 61 66 71 76 81 86 91
Time (min)
Inlet
Mine Test 2 Fog OFF Time Series
Particle Concentration (#/cc)
2.5E+06
2.0E+06
1.5E+06
1.0E+06
5.0E+05
0.0E+00
1 6 11 16 21 26 31 36 41 46 51 56 61 66 71 76 81 86
Time (min)
Inlet
Mine Test 2 Fog ON Time Series
Particle Concentration (#/cc)
2.5E+06
2.0E+06
1.5E+06
1.0E+06
5.0E+05
0.0E+00
1 6 11 16 21 26 31 36 41 46 51 56 61 66 71 76 81 86 91 96
Time (min)
Inlet
Mine Test 3 Fog OFF Time Series
Particle Concentration (#/cc)
1.5E+06
1.2E+06
9.0E+05
6.0E+05
3.0E+05
0.0E+00
1 6 11 16 21 26 31 36 41 46 51 56 61 66 71 76 81 86 91
Time (min)
Inlet
Mine Test 3 Fog ON Time Series
Particle Concentration (#/cc)
1.5E+06
1.2E+06
9.0E+05
6.0E+05
3.0E+05
0.0E+00
1 6 11 16 21 26 31 36 41 46 51 56 61 66 71 76 81 86
Time (min)
Inlet
Mine Test 4 Fog OFF Time Series
Particle Concentration (#/cc)
2.5E+06
2.0E+06
1.5E+06
1.0E+06
5.0E+05
0.0E+00
1 6 11 16 21 26 31 36 41 46 51 56 61 66 71 76 81 86
Time (min)
Inlet
Mine Test 4 Fog ON Time Series
Particle Concentration (#/cc)
2.5E+06
2.0E+06
1.5E+06
1.0E+06
5.0E+05
0.0E+00
1 6 11 16 21 26 31 36 41 46 51 56 61 66 71 76 81 86 91
Time (min)
Inlet
Mine Test 5 Time Series
Particle Concentration (#/cc)
2.5E+06
2.0E+06
1.5E+06
1.0E+06
5.0E+05
0.0E+00
1 21 41 61 81 101 121 141 161 181 201
Time (min)
Inlet
Mine Test 6 Time Series
Particle Concentration (#/cc)
2.5E+06
2.0E+06
1.5E+06
1.0E+06
5.0E+05
0.0E+00
1 21 41 61 81 101 121 141 161 181 201
Time (min)
Inlet
Mine Test 7 Time Series
Particle Concentration (#/cc)
1.5E+06
1.2E+06
9.0E+05
6.0E+05
3.0E+05
0.0E+00
1 21 41 61 81 101 121 141 161 181 201
Time (min)
Inlet
Mine Test 8 Time Series
Particle Concentration (#/cc)
2.5E+06
2.0E+06
1.5E+06
1.0E+06
5.0E+05
0.0E+00
1 21 41 61 81 101 121 141 161 181 201
Time (min)
Inlet

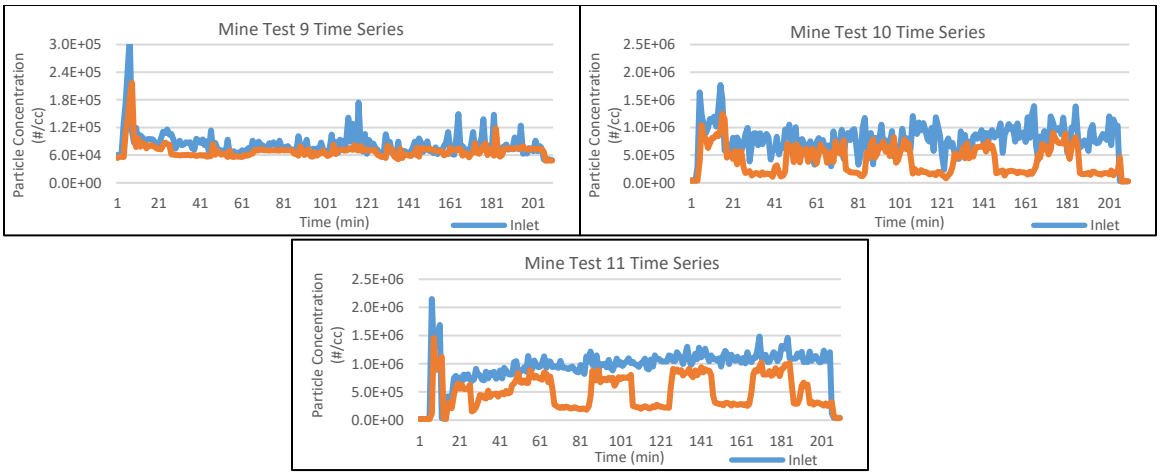

Figure A.21. Time Data. The total concentrations at the inlet and outlet of the experimental apparatus for all field tests.

Table A.6. Mine Test Data. The relevant data for all successful field tests conducted for this research project.

Field Test Number	Continuous (or) Periodic	DPM Source	Scaling Factor	Average Water Consumption (L/min)	Average Droplet Concentration (#/cm^3)	Average Control Trial Inlet DPM Concentration (#/cm^3)	Average Treatment Trial Inlet DPM Concentration (#/cm^3)	Total Average E_D (Control)	Total Average E_D (Treatment)
1	Continuous	Buggy	0.931	0.065	3.68×10^5	3.47×10^5	3.82×10^5	12.08%	73.48%
2	Continuous	Long Bus	1.022	0.049	2.66×10^5	5.62×10^5	5.04×10^5	4.38%	61.35%
3	Continuous	Short Bus	0.974	0.039	2.21×10^5	2.44×10^5	3.70×10^5	12.98%	63.99%
4	Continuous	Roxor Mine Jeep	1.031	0.042	2.38×10^5	7.71×10^5	1.16×10^6	11.06%	81.87%
5	Periodic	Long Bus	1.03	0.044	2.47×10^5	3.59×10^5	3.58×10^5	16.04%	56.89%
6	Periodic	Short Bus	0.989	0.045	2.53×10^5	9.26×10^5	7.98×10^5	19.85%	59.90%
7	Periodic	Buggy	1.001	0.049	2.77×10^5	3.40×10^5	3.79×10^5	34.08%	76.36%
8	Periodic	Short Bus	1.01	0.045	2.66×10^5	2.33×10^5	2.64×10^5	22.47%	56.75%
9	Periodic	Buggy	1.011	0.037	2.49×10^5	8.52×10^4	8.33×10^4	17.70%	17.84%
10	Periodic	Buggy	1.011	0.037	2.06×10^5	8.13×10^5	8.31×10^5	23.65%	78.13%
11	Periodic	Brown Truck	0.9935	0.033	1.84×10^5	9.97×10^5	9.92×10^5	25.61%	69.00%

Table A.7. Side by side scaling factors (SF) of each size bin and total concentrations for each field test per Equation 1.3.

	11.5nm	15.4nm	20.5nm	27.4nm	35.6nm	48.7nm	64.9nm	86.6nm	115.5nm	154nm	Total
MT1	1.142	0.922	0.681	0.752	0.966	1.400	1.188	0.991	0.853	0.793	0.931
MT2	0.991	1.257	1.471	1.154	0.995	1.020	1.131	1.051	1.051	1.004	1.022
MT3	1.014	2.078	1.669	1.127	1.086	1.195	1.081	1.031	0.977	0.888	0.981
MT4	1.474	2.251	1.463	1.269	1.303	1.154	1.292	1.165	1.072	0.973	1.031
MT5	1.265	1.956	1.183	1.052	0.966	1.077	1.175	1.158	1.090	0.998	1.030
MT6	1.265	1.956	1.183	1.052	0.966	1.077	1.175	1.158	1.090	0.998	1.030
MT7	0.974	1.185	1.183	0.927	0.927	1.702	1.190	1.200	1.087	0.959	1.001
MT8	1.184	1.319	0.909	1.565	1.552	1.400	1.199	1.101	1.027	0.937	1.010
MT9	1.112	0.945	1.156	1.326	1.218	1.094	1.065	1.049	1.010	0.937	1.011
MT10	1.832	1.173	0.644	0.759	1.447	1.464	1.214	1.050	0.950	0.850	0.962
MT11	1.220	0.934	0.772	1.149	1.090	1.251	1.117	1.087	1.032	0.948	0.994

Table A.8. Average particle concentrations (#/cm^3) measured by inlet and outlet NanoScans for nominal size bins (11.5 to 154 nm).

Test		DPM Bin (nm)									
		11.5	15.4	20.5	27.8	36.5	48.7	65.9	86.6	115.5	154
1	Inlet	35286	48465	38110	56051	59444	48611	35442	28397	21066	10309
	Outlet	1859	1831	1985	5907	12157	23714	23806	20433	14008	6855
2	Inlet	1739	3075	22746	64299	87795	88150	72126	52093	30205	10248
	Outlet	2995	1931	2234	12882	22324	31421	37813	31555	22013	9749
3	Inlet	2131	6157	30943	59943	65888	55367	39611	28890	20318	12122
	Outlet	2941	3541	4909	15226	22807	27991	23809	20015	14766	8267
4	Inlet	163737	293744	178037	132011	97425	72028	64299	67887	58678	31544
	Outlet	1454	19177	19802	21965	24676	26955	39381	41669	34185	18440
5	Inlet	1722	7687	27982	59201	73026	68273	52392	35890	20398	7901
	Outlet	4579	5882	4618	15656	23525	30573	31408	25152	15672	6808
6	Inlet	10588	19040	51281	116244	152703	152182	121538	82662	48280	22986
	Outlet	8774	8849	4868	25126	44718	65023	72068	59236	36292	14582
7	Inlet	54571	76715	44944	47013	43724	32697	23189	20229	17051	9952
	Outlet	4057	5216	3337	5199	8233	11594	14301	15067	12583	7595
8	Inlet	2362	7594	18694	38363	49511	48500	38999	27910	17223	9483
	Outlet	4886	5339	2309	11482	18257	21443	21516	21015	16961	9748
9	Inlet	4531	5699	3478	5125	6184	7584	10062	12818	13076	9806
	Outlet	2307	3082	2077	3326	4438	6074	8535	11075	11763	9628
10	Inlet	9199	74494	148813	231317	200104	101350	12976	281	2271	10901
	Outlet	9218	6229	9918	33226	73596	55264	22175	842	4633	4148
11	Inlet	23140	83966	135264	218965	222250	161094	84394	38125	16312	6676
	Outlet	5607	14223	23856	68183	73555	72164	45564	30550	18056	7154

Appendix B

Table B.9. $K_{1,2}$ values computed for each combination of nominal DPM size (10 bins between 11.5 and 154 nm) and the mean drop size (4800 nm). Values for each combination of DPM-drop coagulation are highlighted in yellow.

Particle Diameter (nm)	11.5	15.4	20.5	27.4	36.5	48.7	64.9	86.6	115.5	154	4800
11.5	3.26	3.29	3.48	3.85	4.40	5.20	6.29	7.79	9.81	12.52	341.53
15.4		3.18	3.22	3.41	3.76	4.30	5.07	6.14	7.59	9.55	249.09
20.5			3.12	3.16	3.35	3.70	4.23	4.99	6.04	7.47	184.00
27.4				3.07	3.12	3.31	3.65	4.18	4.92	5.96	136.05
36.5					3.04	3.09	3.28	3.62	4.14	4.88	101.40
48.7						3.01	3.07	3.26	3.60	4.11	75.74
64.9							2.99	3.05	3.24	3.58	56.86
86.6								2.98	3.04	3.23	42.79
115.5									2.97	3.03	32.35
154										2.96	24.57
4800											2.93

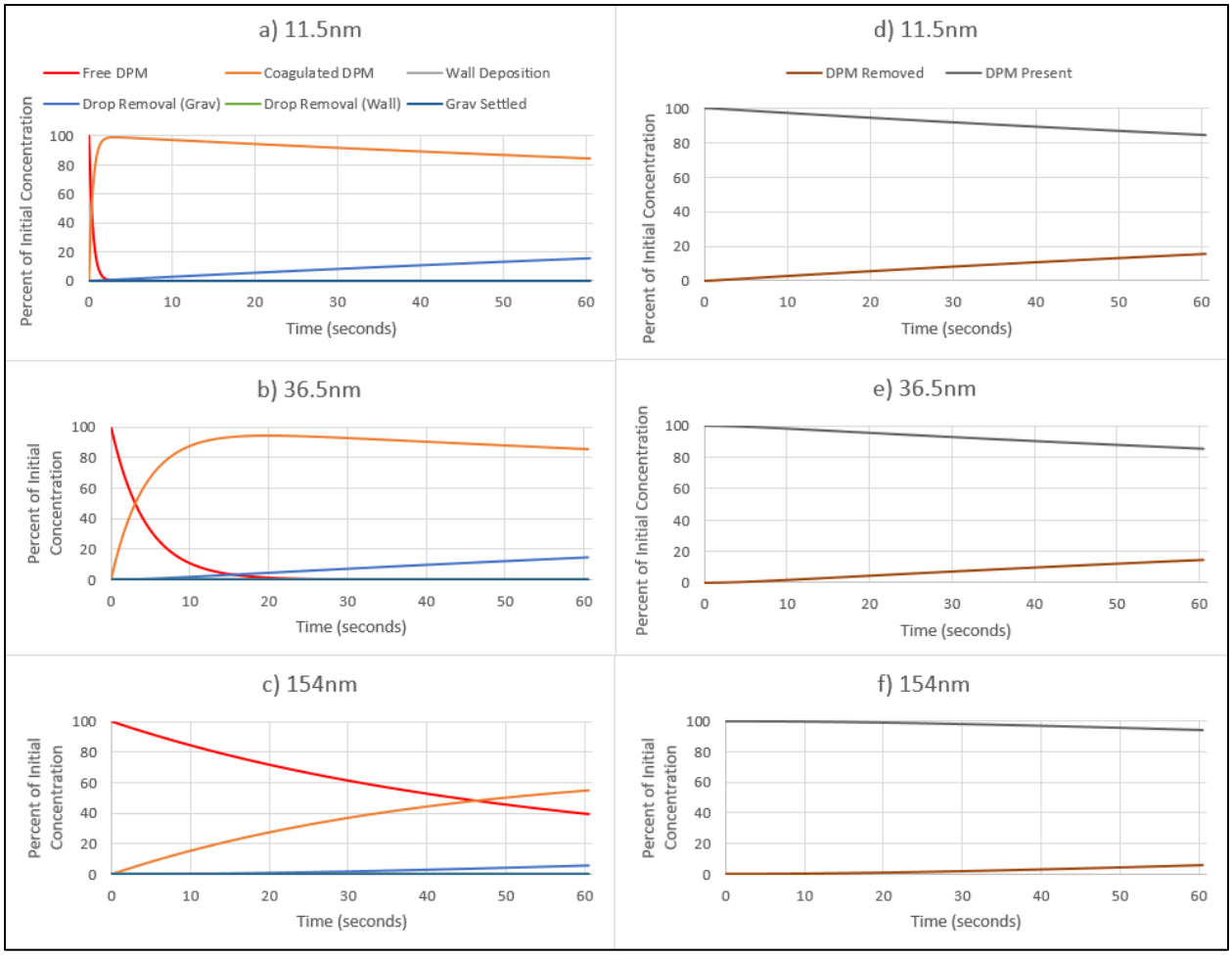

Figure B.22. Modeled DPM classes shown across the length of the scrubber tube using initial conditions from Test 1. a), b) and c) show results for the 11.5, 36.5, and 154 nm size bin, respectively, with particles fractionated between the six possible DPM classes defined in Table 2.2. d), e) and f) show the total DPM removed and still suspended in the air flow for the same three size bins.

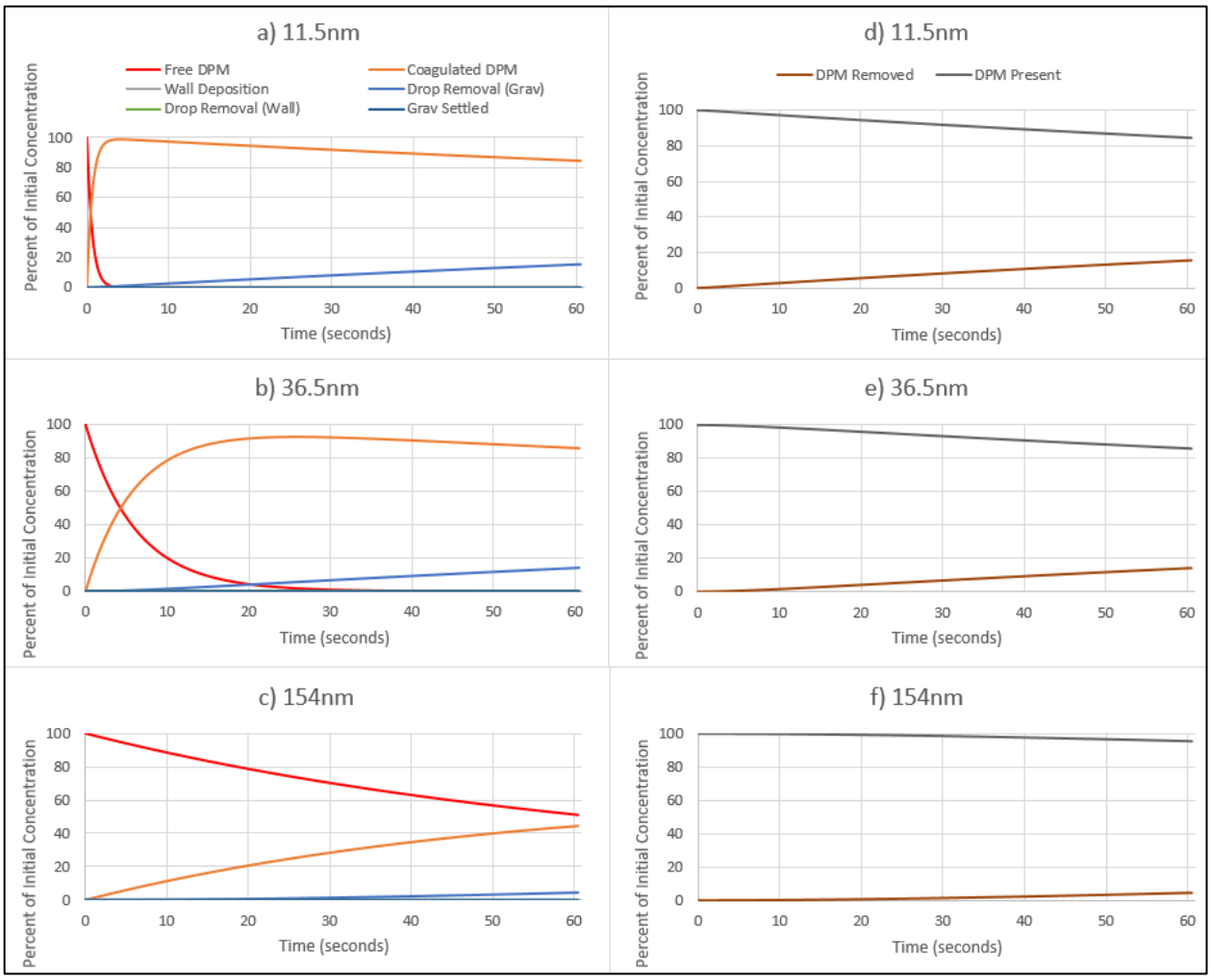

Figure B.23. Modeled DPM classes shown across the length of the scrubber tube using initial conditions from Test 2. a), b) and c) show results for the 11.5, 36.5, and 154 nm size bin, respectively, with particles fractionated between the six possible DPM classes defined in Table 2.2. d), e) and f) show the total DPM removed and still suspended in the air flow for the same three size bins.

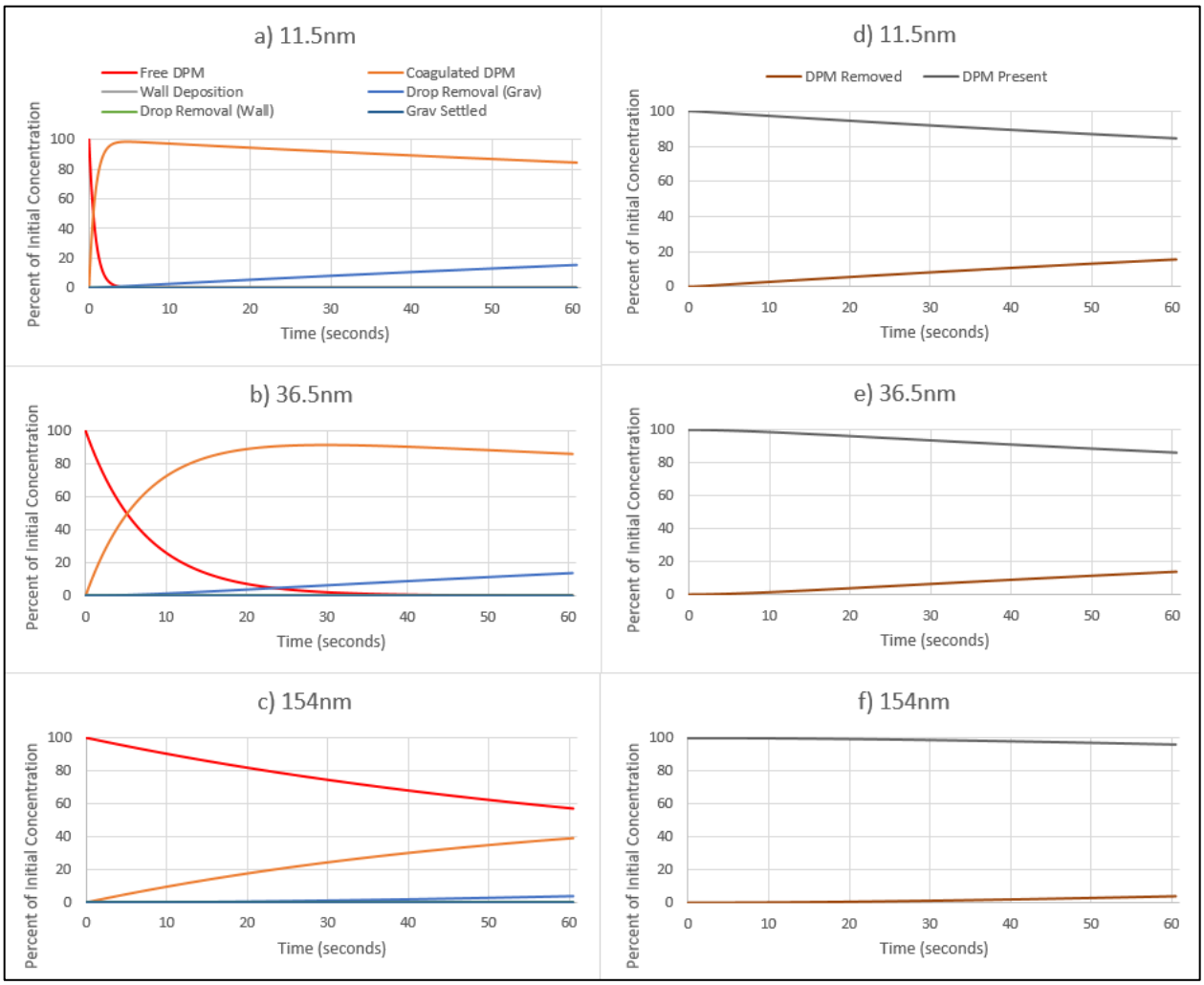

Figure B.24. Modeled DPM classes shown across the length of the scrubber tube using initial conditions from Test 3. a), b) and c) show results for the 11.5, 36.5, and 154 nm size bin, respectively, with particles fractionated between the six possible DPM classes defined in Table 2.2. d), e) and f) show the total DPM removed and still suspended in the air flow for the same three size bins.

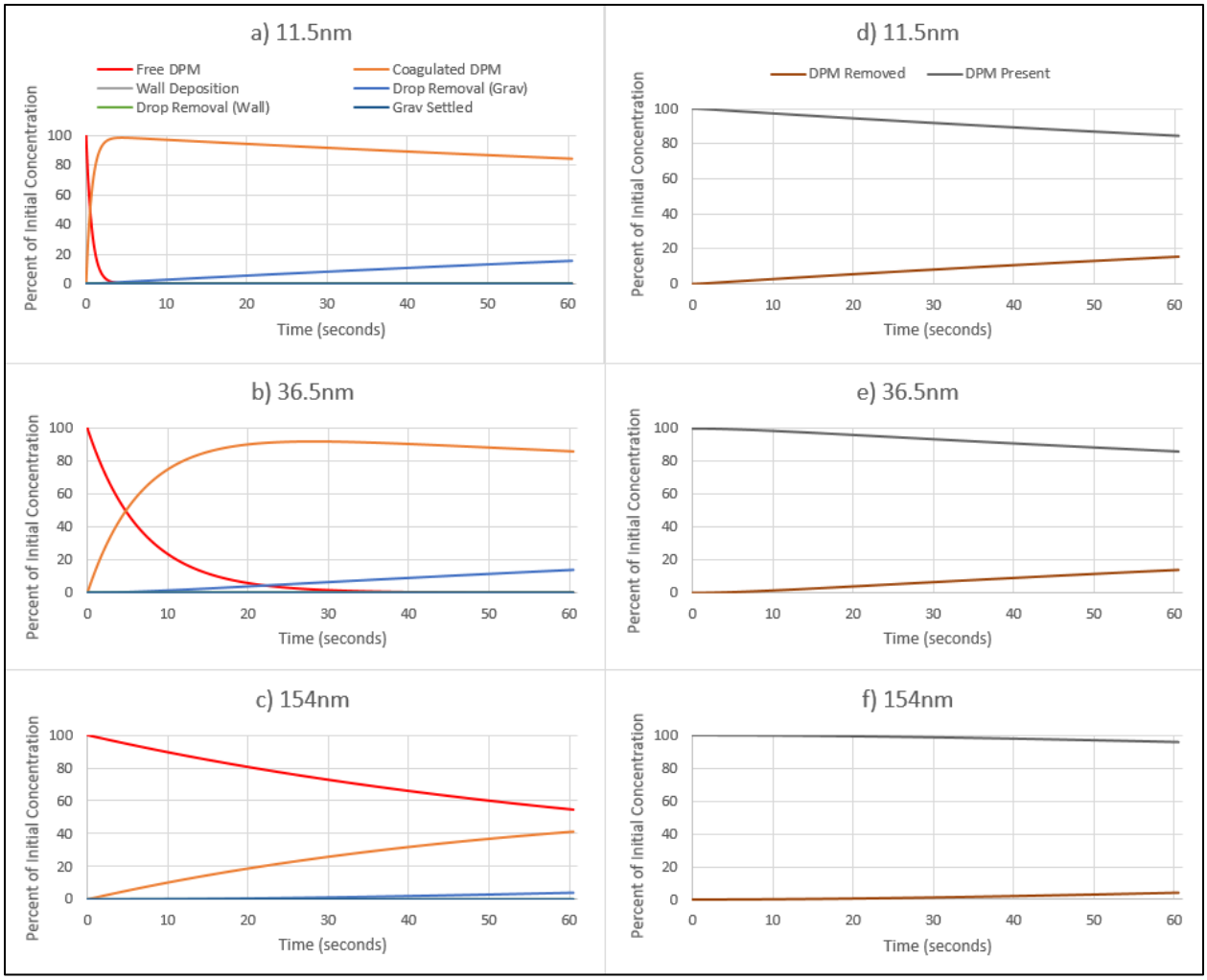

Figure B.25. Modeled DPM classes shown across the length of the scrubber tube using initial conditions from Test 4. a), b) and c) show results for the 11.5, 36.5, and 154 nm size bin, respectively, with particles fractionated between the six possible DPM classes defined in Table 2.2. d), e) and f) show the total DPM removed and still suspended in the air flow for the same three size bins.

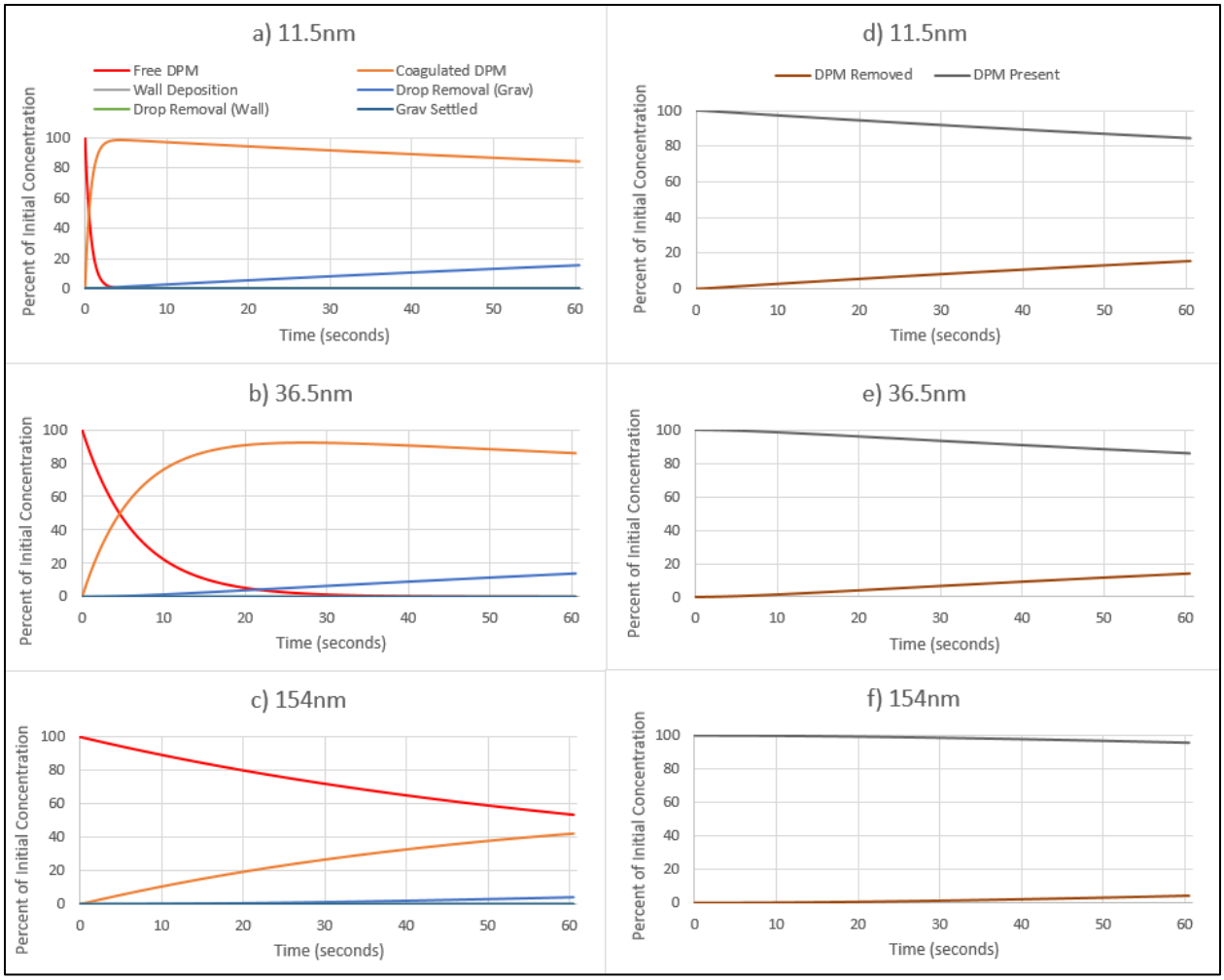

Figure B.26. Modeled DPM classes shown across the length of the scrubber tube using initial conditions from Test 5. a), b) and c) show results for the 11.5, 36.5, and 154 nm size bin, respectively, with particles fractionated between the six possible DPM classes defined in Table 2.2. d), e) and f) show the total DPM removed and still suspended in the air flow for the same three size bins.

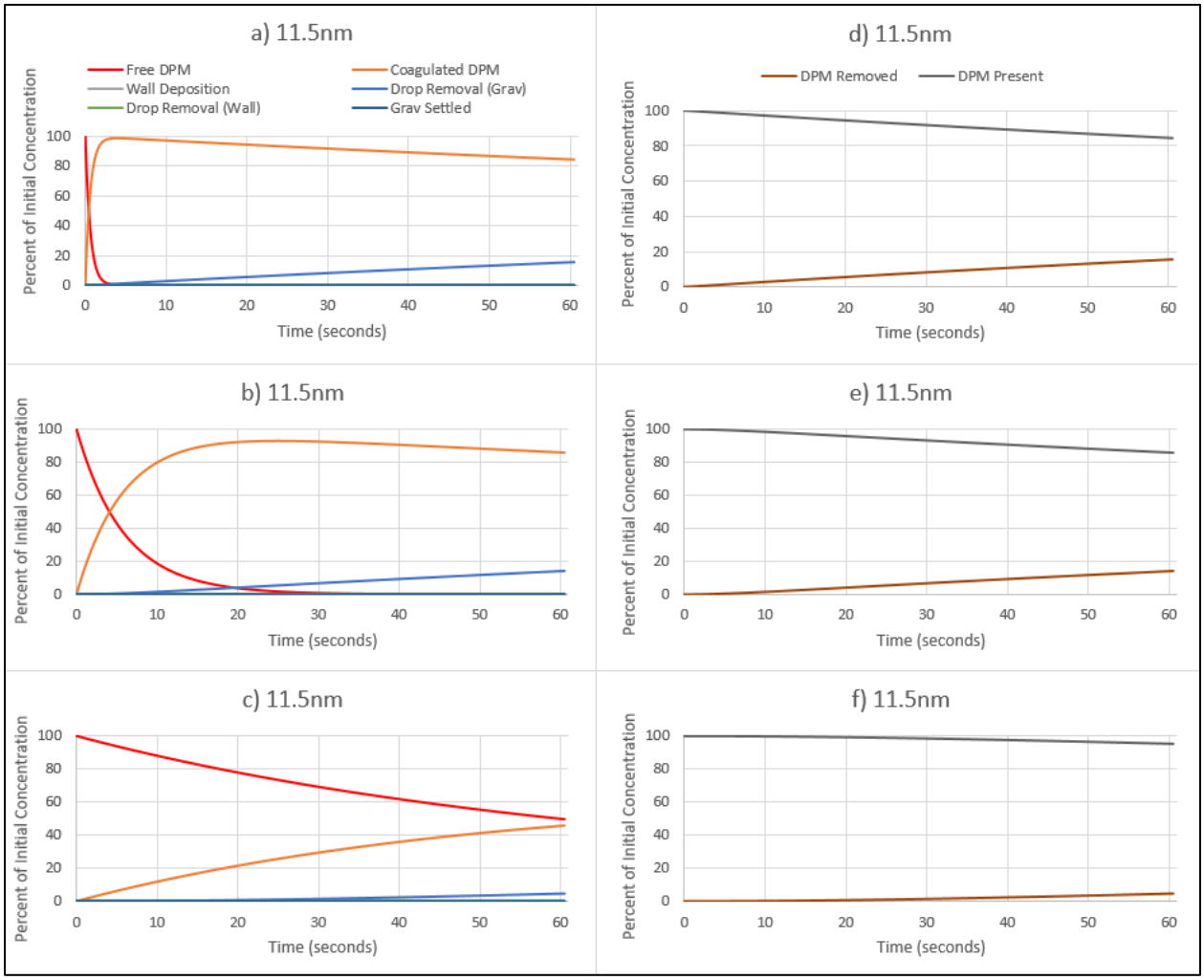

Figure B.27. Modeled DPM classes shown across the length of the scrubber tube using initial conditions from Test 7. a), b) and c) show results for the 11.5, 36.5, and 154 nm size bin, respectively, with particles fractionated between the six possible DPM classes defined in Table 2.2. d), e) and f) show the total DPM removed and still suspended in the air flow for the same three size bins.

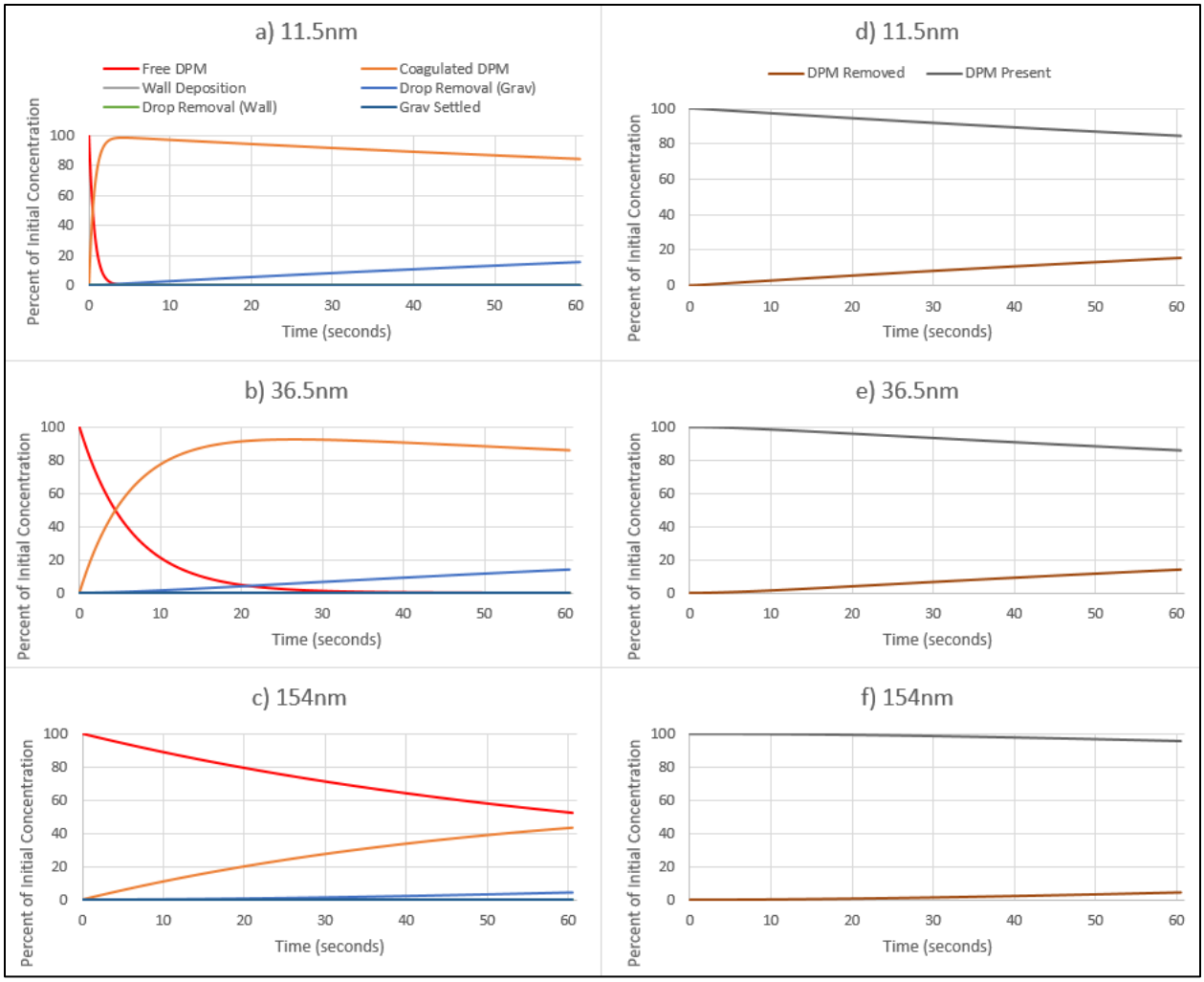

Figure B.28. Modeled DPM classes shown across the length of the scrubber tube using initial conditions from Test 8. a), b) and c) show results for the 11.5, 36.5, and 154 nm size bin, respectively, with particles fractionated between the six possible DPM classes defined in Table 2.2. d), e) and f) show the total DPM removed and still suspended in the air flow for the same three size bins.

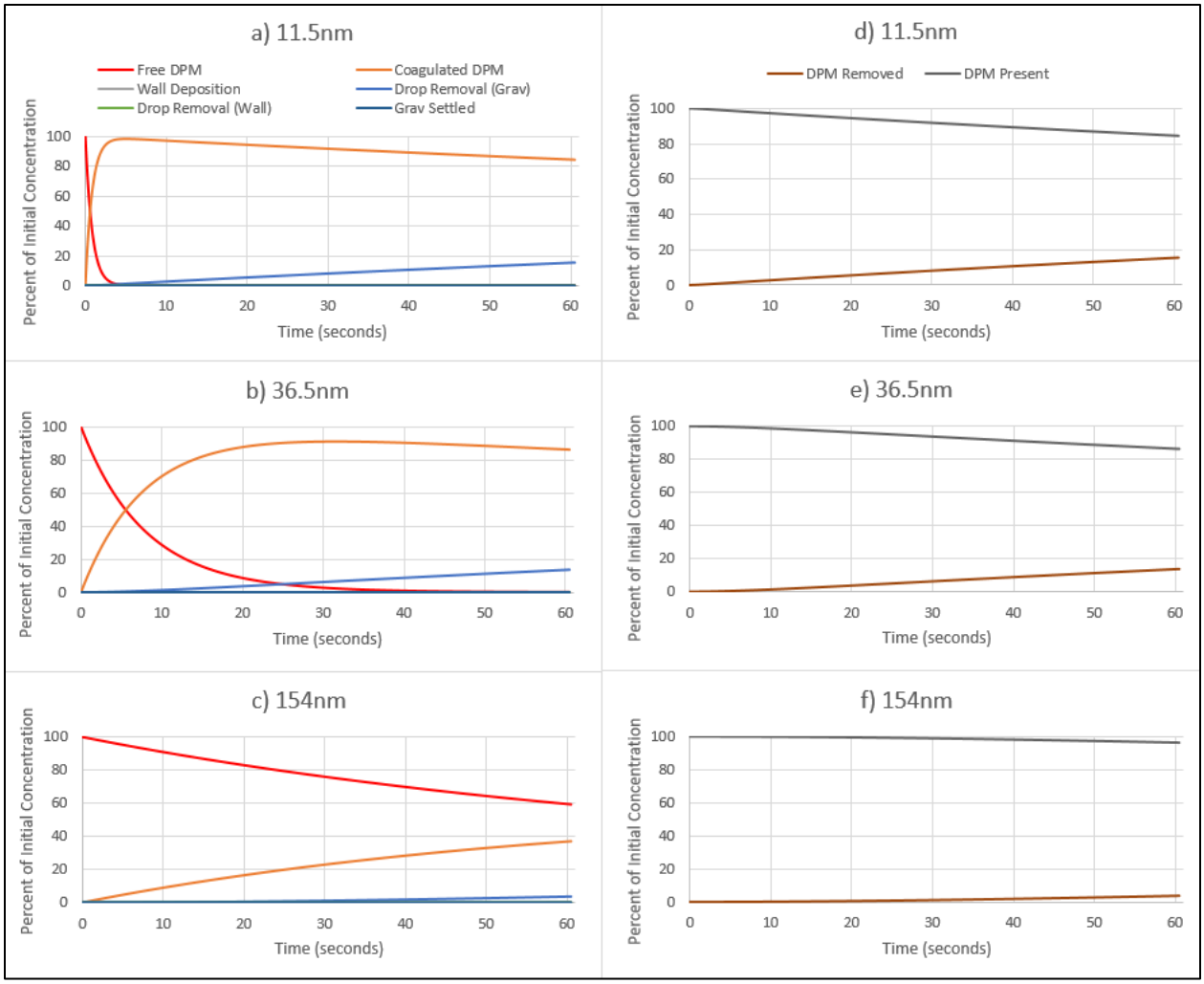

Figure B.29. Modeled DPM classes shown across the length of the scrubber tube using initial conditions from Test 10. a), b) and c) show results for the 11.5, 36.5, and 154 nm size bin, respectively, with particles fractionated between the six possible DPM classes defined in Table 2.2. d), e) and f) show the total DPM removed and still suspended in the air flow for the same three size bins.

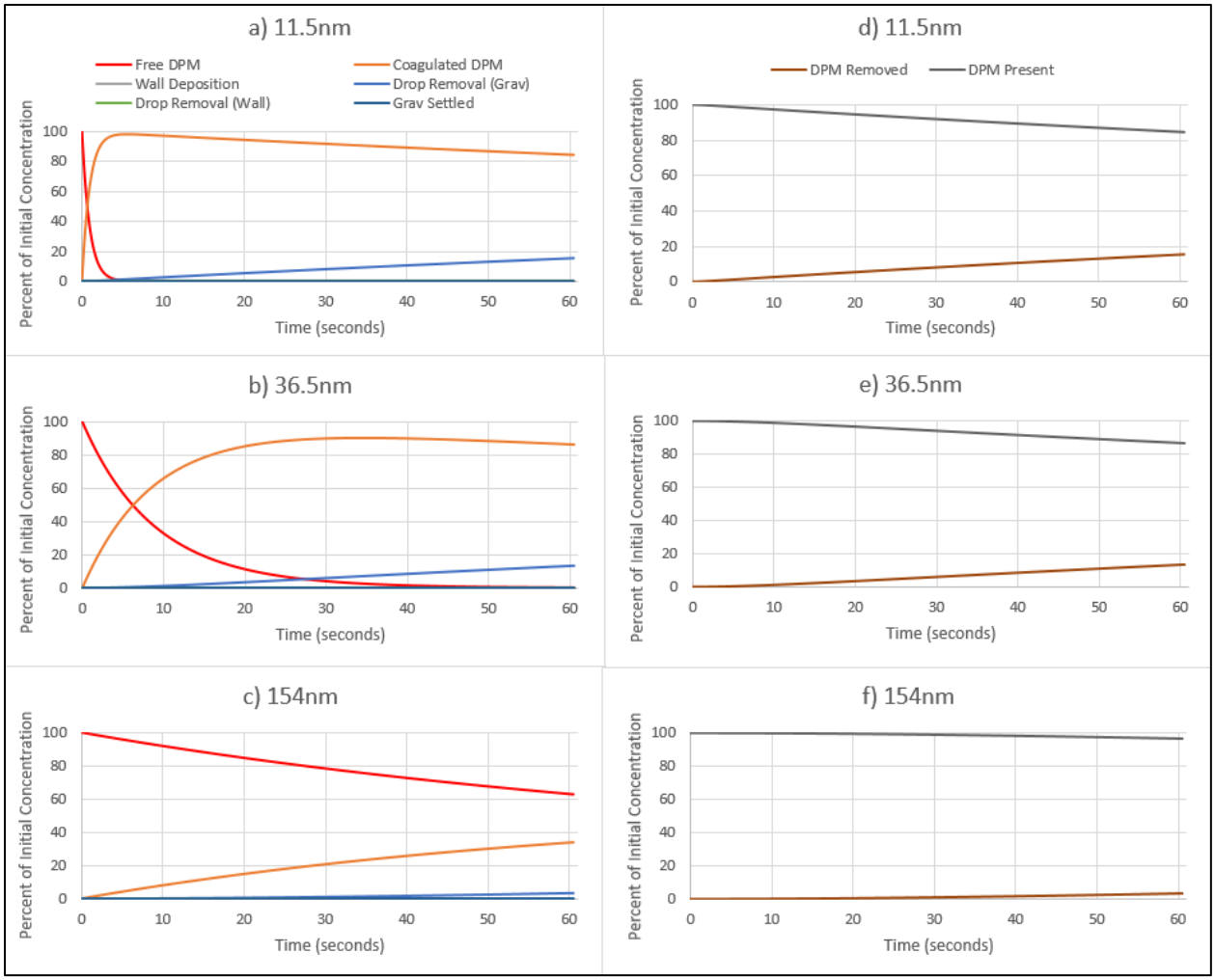

Figure B.30. Modeled DPM classes shown across the length of the scrubber tube using initial conditions from Test 11. a), b) and c) show results for the 11.5, 36.5, and 154 nm size bin, respectively, with particles fractionated between the six possible DPM classes defined in Table 2.2. d), e) and f) show the total DPM removed and still suspended in the air flow for the same three size bins.

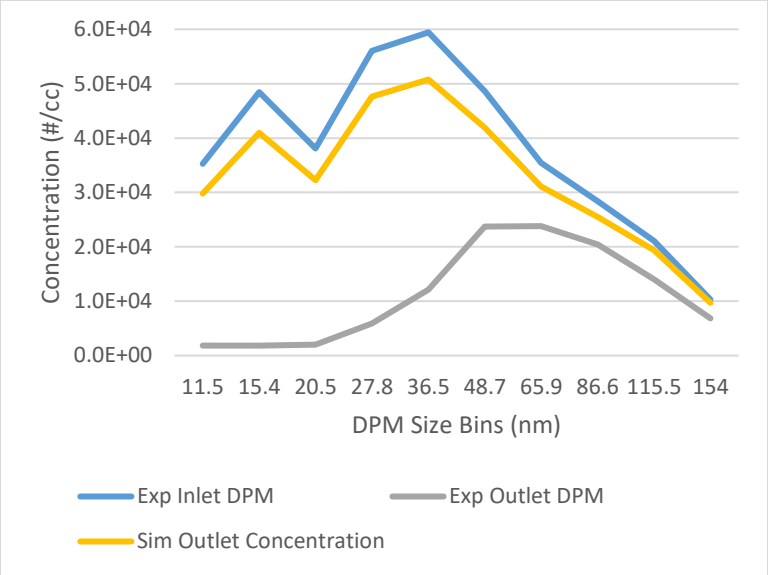

Figure B.31. Experimental and modeled scrubber outlet DPM concentration by size bin for inlet conditions measured in Test 1 in Chapter 1. The measured inlet DPM concentration by size bin is also shown, and the inlet fog drop concentration was taken as $3.68 \times 10^5 \#/cm^3$ *per Chapter 1.*

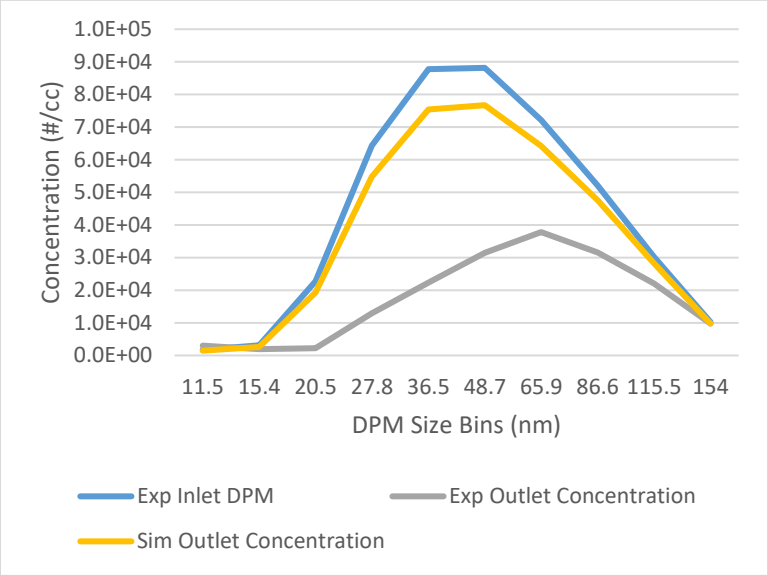

Figure B.32. Experimental and modeled scrubber outlet DPM concentration by size bin for inlet conditions measured in Test 2 in Chapter 1. The measured inlet DPM concentration by size bin is also shown, and the inlet fog drop concentration was taken as $2.66 \times 10^5 \#/cm^3$ *per Chapter 1.*

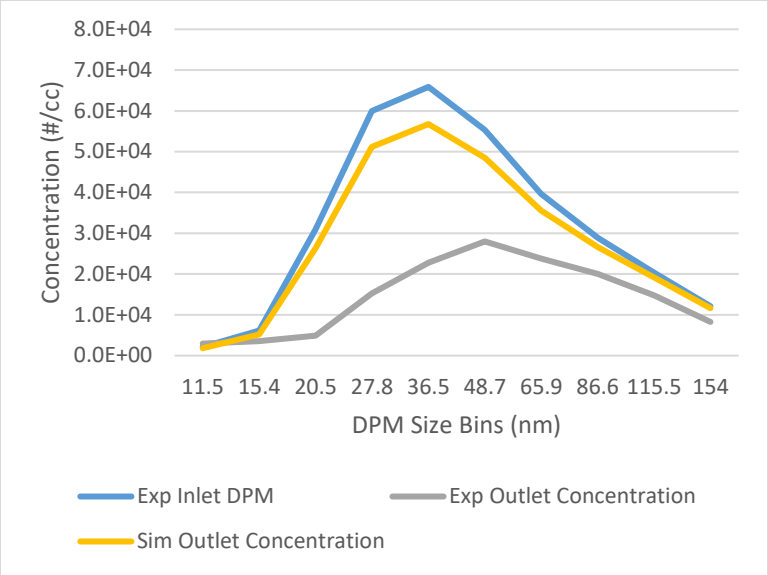

Figure B.33. Experimental and modeled scrubber outlet DPM concentration by size bin for inlet conditions measured in Test 3 in Chapter 1. The measured inlet DPM concentration by size bin is also shown, and the inlet fog drop concentration was taken as $2.21 \times 10^5 \#/cm^3$ *per Chapter 1.*

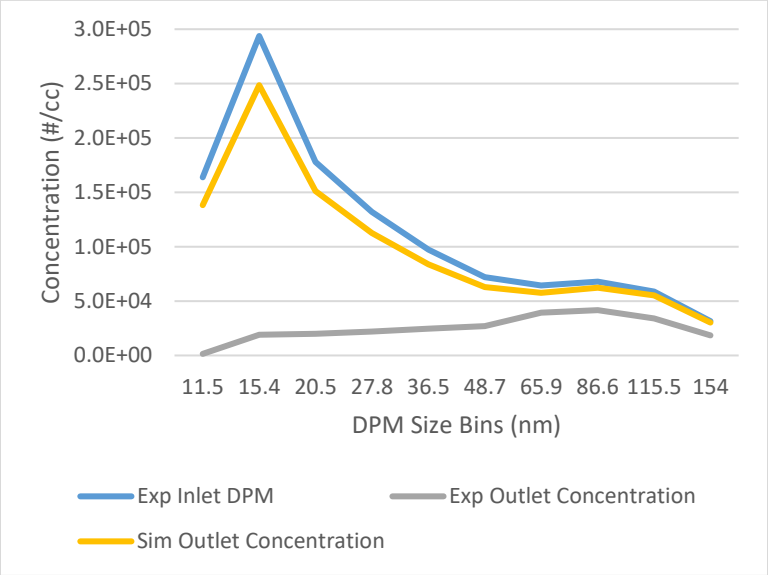

Figure B.34. Experimental and modeled scrubber outlet DPM concentration by size bin for inlet conditions measured in Test 4 in Chapter 1. The measured inlet DPM concentration by size bin is also shown, and the inlet fog drop concentration was taken as $2.38 \times 10^5 \#/cm^3$ *per Chapter 1.*

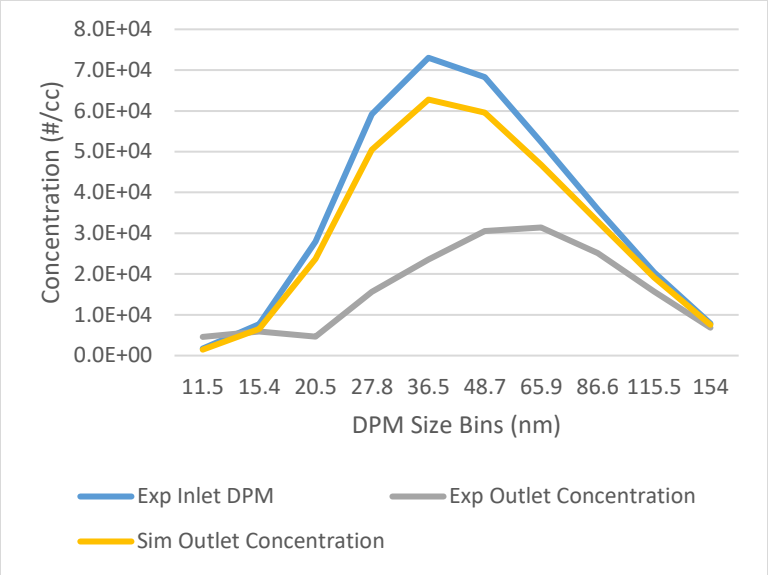

Figure B.35. Experimental and modeled scrubber outlet DPM concentration by size bin for inlet conditions measured in Test 5 in Chapter 1. The measured inlet DPM concentration by size bin is also shown, and the inlet fog drop concentration was taken as $2.47 \times 10^5 \#/cm^3$ *per Chapter 1.*

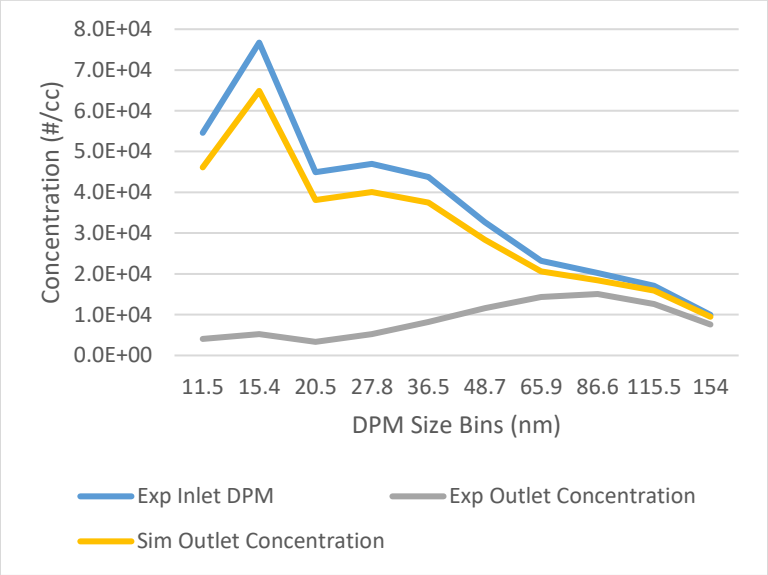

Figure B.36. Experimental and modeled scrubber outlet DPM concentration by size bin for inlet conditions measured in Test 7 in Chapter 1. The measured inlet DPM concentration by size bin is also shown, and the inlet fog drop concentration was taken as $2.77 \times 10^5 \#/cm^3$ *per Chapter 1.*

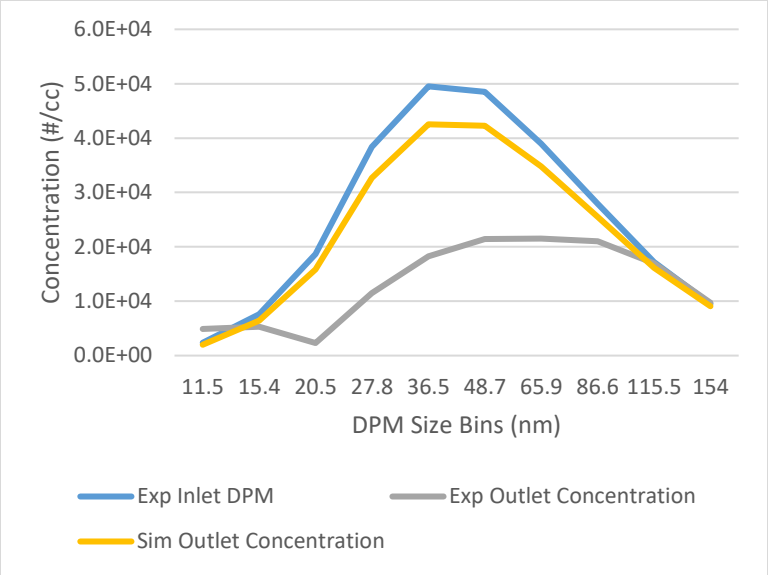

Figure B.37. Experimental and modeled scrubber outlet DPM concentration by size bin for inlet conditions measured in Test 8 in Chapter 1. The measured inlet DPM concentration by size bin is also shown, and the inlet fog drop concentration was taken as $2.66 \times 10^5\ \#/cm^3$ *per Chapter 1.*

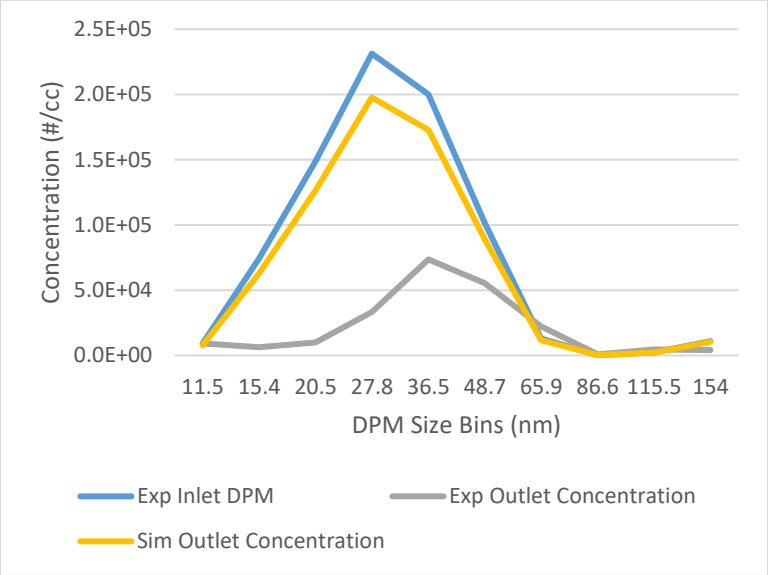

Figure B.38. Experimental and modeled scrubber outlet DPM concentration by size bin for inlet conditions measured in Test 10 in Chapter 1. The measured inlet DPM concentration by size bin is also shown, and the inlet fog drop concentration was taken as $2.06 \times 10^5\ \#/cm^3$ *per Chapter 1.*

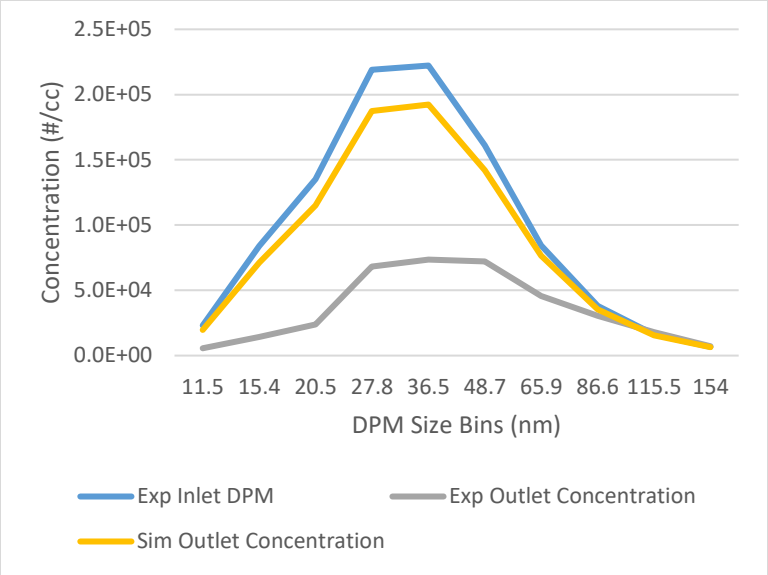

Figure B.39. Experimental and modeled scrubber outlet DPM concentration by size bin for inlet conditions measured in Test 11 in Chapter 1. The measured inlet DPM concentration by size bin is also shown, and the inlet fog drop concentration was taken as $1.84 \times 10^5 \, \#/cm^3$ *per Chapter 1.*

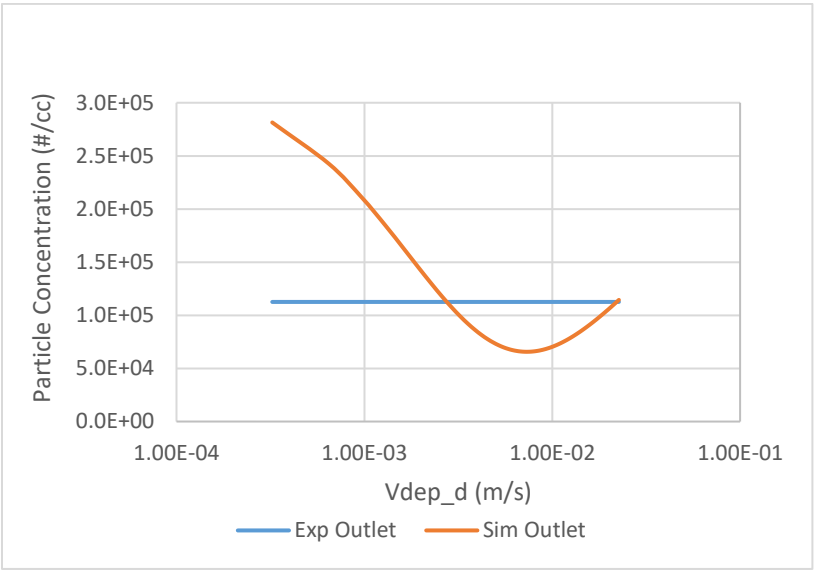

Figure B.40. Modeled DPM concentration at the scrubber outlet as a function of V_{dep_d} *for the inlet DPM and fog drop concentrations measured in Test 1 in Chapter 1. The experimental outlet concentration is also shown.*

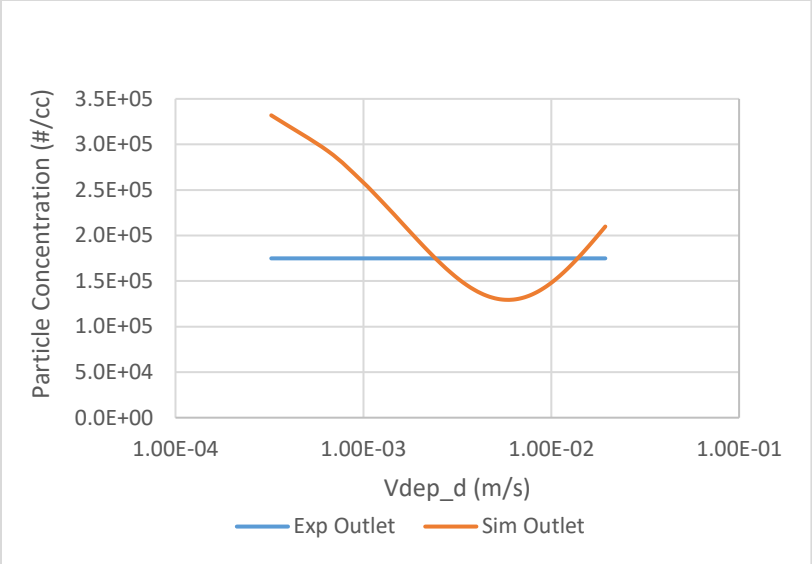

Figure B.41. Modeled DPM concentration at the scrubber outlet as a function of V_{dep_d} for the inlet DPM and fog drop concentrations measured in Test 2 in Chapter 1. The experimental outlet concentration is also shown.

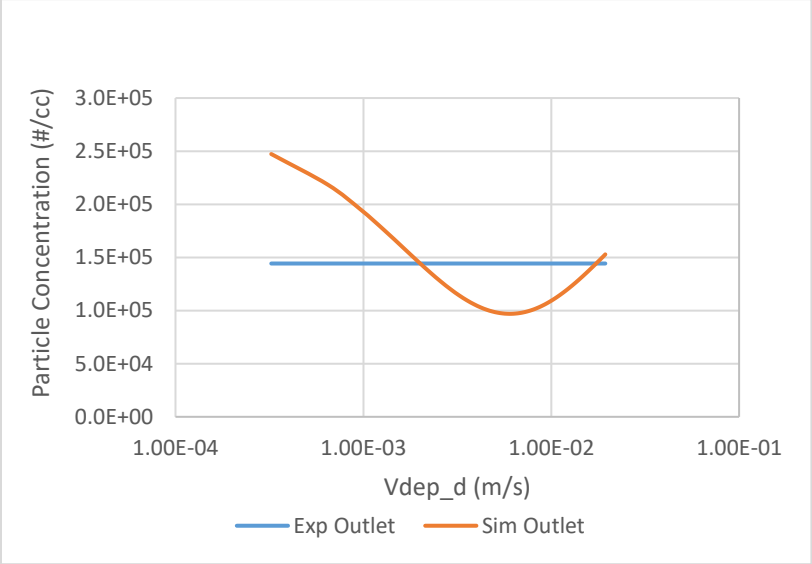

Figure B.42. Modeled DPM concentration at the scrubber outlet as a function of V_{dep_d} for the inlet DPM and fog drop concentrations measured in Test 3 in Chapter 1. The experimental outlet concentration is also shown.

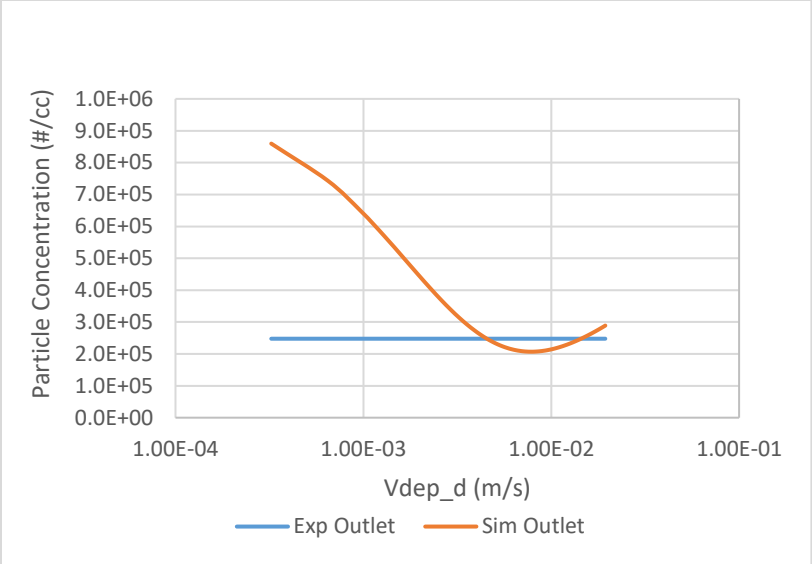

Figure B.43. Modeled DPM concentration at the scrubber outlet as a function of V_{dep_d} for the inlet DPM and fog drop concentrations measured in Test 4 in Chapter 1. The experimental outlet concentration is also shown.

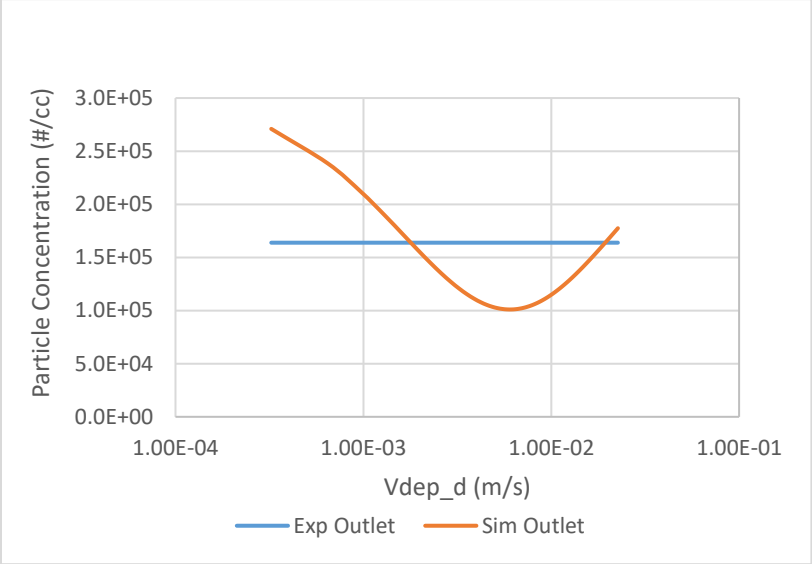

Figure B.44. Modeled DPM concentration at the scrubber outlet as a function of V_{dep_d} for the inlet DPM and fog drop concentrations measured in Test 5 in Chapter 1. The experimental outlet concentration is also shown.

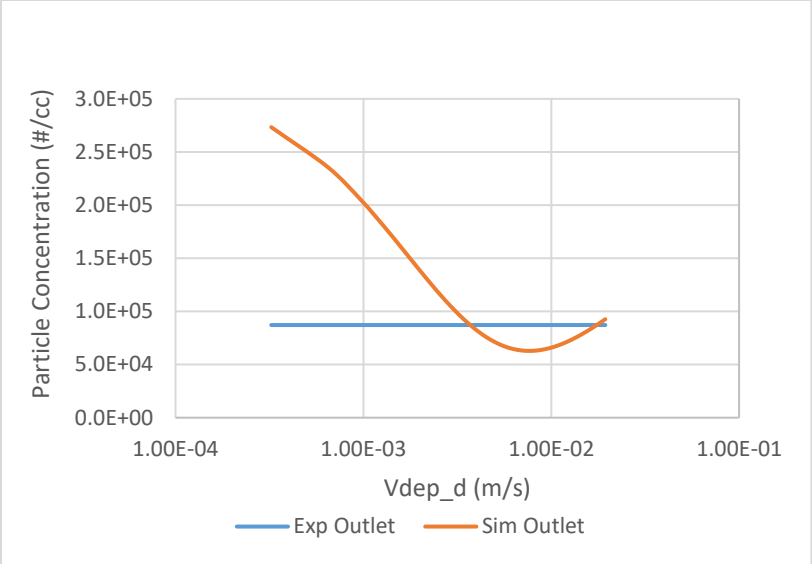

Figure B.45. Modeled DPM concentration at the scrubber outlet as a function of V_{dep_d} for the inlet DPM and fog drop concentrations measured in Test 7 in Chapter 1. The experimental outlet concentration is also shown.

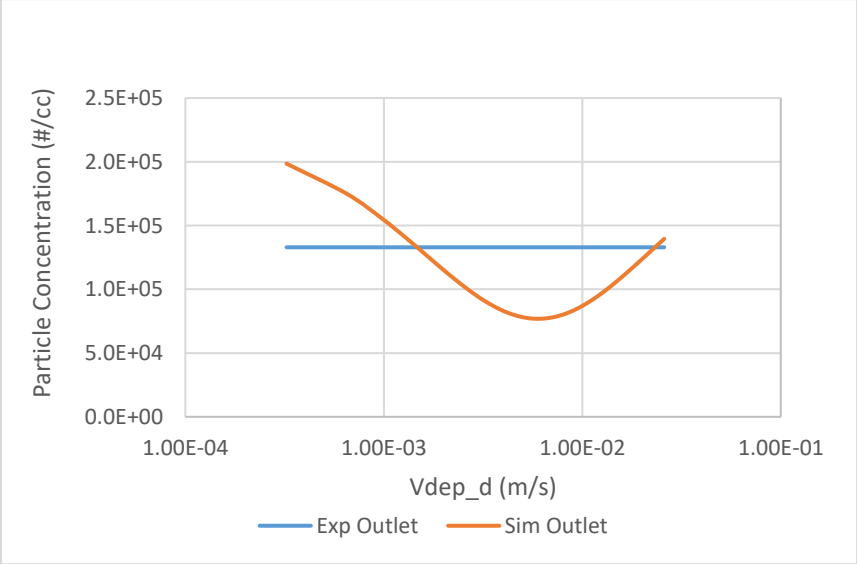

Figure B.46. Modeled DPM concentration at the scrubber outlet as a function of V_{dep_d} for the inlet DPM and fog drop concentrations measured in Test 8 in Chapter 1. The experimental outlet concentration is also shown.

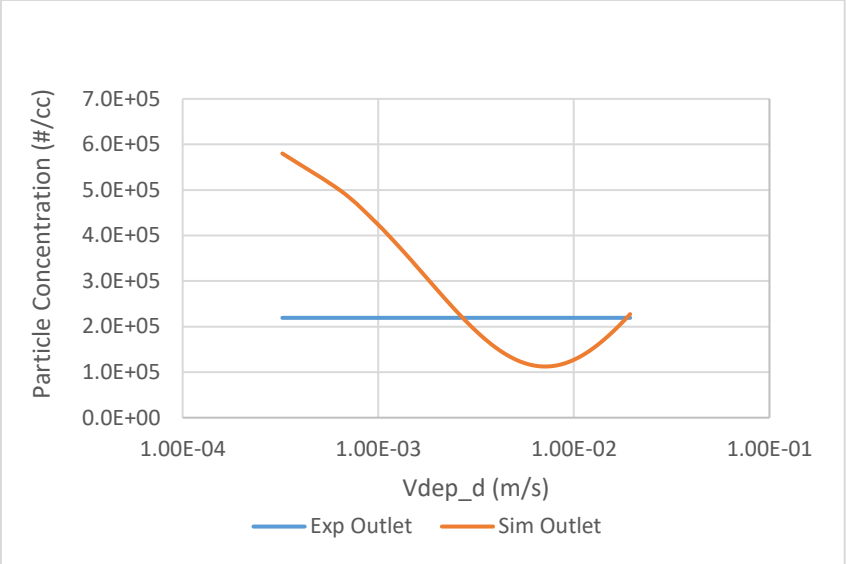

Figure B.47. Modeled DPM concentration at the scrubber outlet as a function of V_{dep_d} for the inlet DPM and fog drop concentrations measured in Test 10 in Chapter 1. The experimental outlet concentration is also shown.

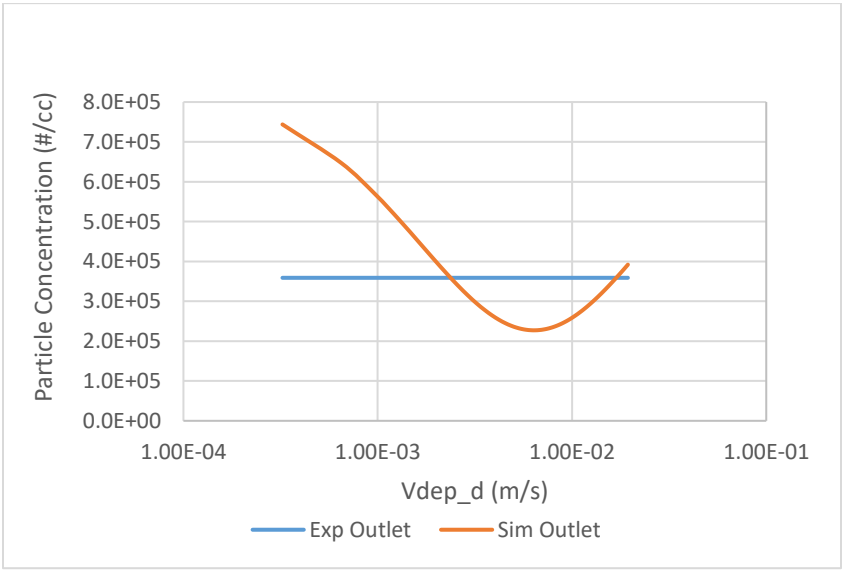

Figure B.48. Modeled DPM concentration at the scrubber outlet as a function of V_{dep_d} for the inlet DPM and fog drop concentrations measured in Test 11 in Chapter 1. The experimental outlet concentration is also shown.

Table B.10. Values of V_{dep_d} in cm/s for the smooth walled case, low fitted V_{dep_d} case, and high fitted V_{dep_d} case for all field tests (except test 9).

	Smooth walled	Low fitted $V_{dep_{drop}}$	High fitted $V_{dep_{drop}}$
Test 1	1.29E-05	0.275	2.20
Test 2	1.29E-05	0.243	1.38
Test 3	1.29E-05	0.201	1.73
Test 4	1.29E-05	0.455	1.44
Test 5	1.29E-05	0.180	1.94
Test 6	1.29E-05	0.206	1.67
Test 7	1.29E-05	0.371	1.75
Test 8	1.29E-05	0.148	2.32
Test 10	1.29E-05	0.271	1.86
Test 11	1.29E-05	0.238	1.69

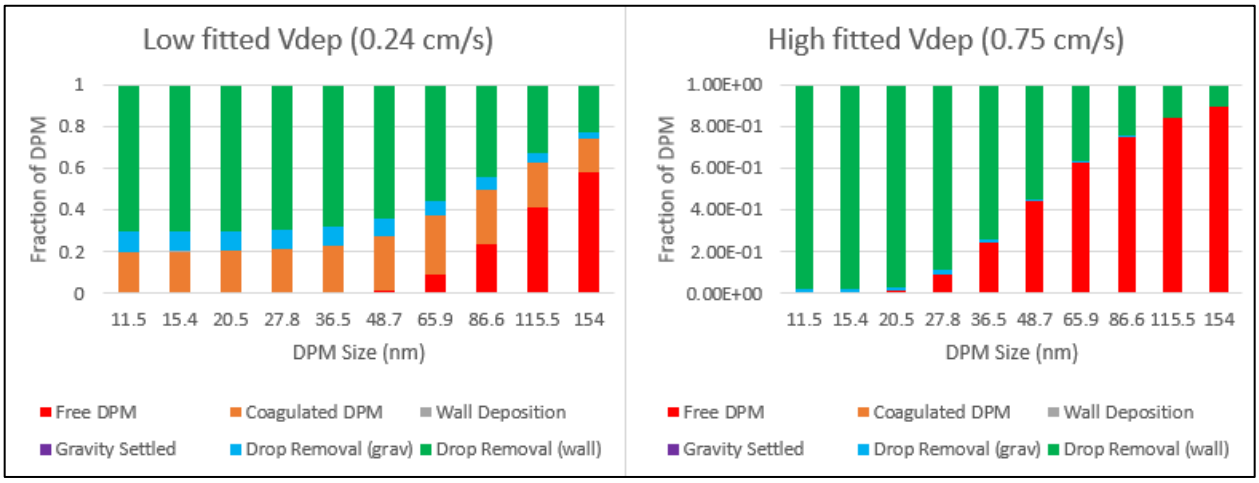

Figure B.49. Modeled fractions of the DPM (by size bin) in all possible classes for inlet DPM and fog drop concentrations measured in Test 1 in Chapter 1. Results are shown using the a) low and b) high fitted V_{dep_d} values determined in Figure B.19.

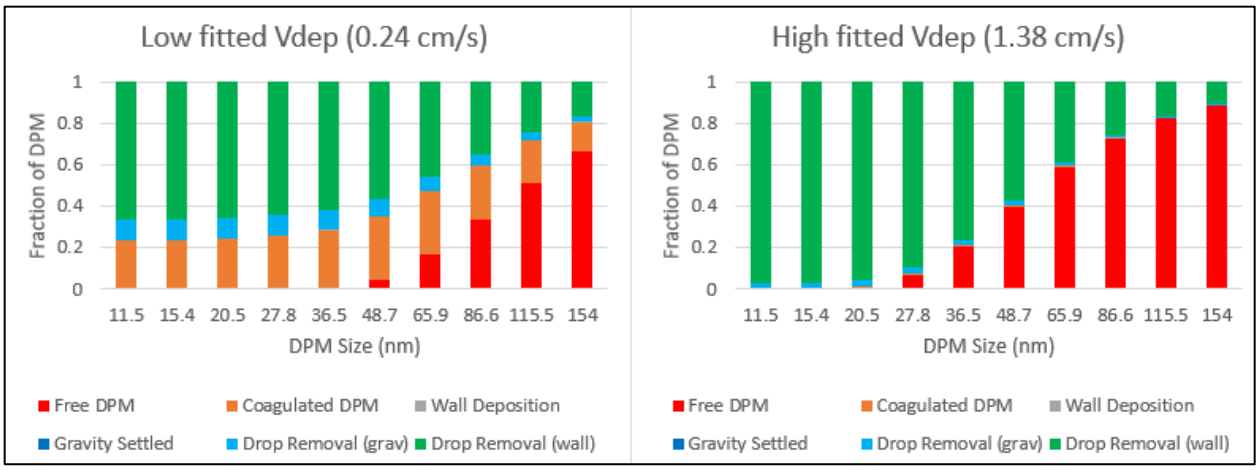

Figure B.50. Modeled fractions of the DPM (by size bin) in all possible classes for inlet DPM and fog drop concentrations measured in Test 2 in Chapter 1. Results are shown using the a) low and b) high fitted V_{dep_d} values determined in Figure B.20.

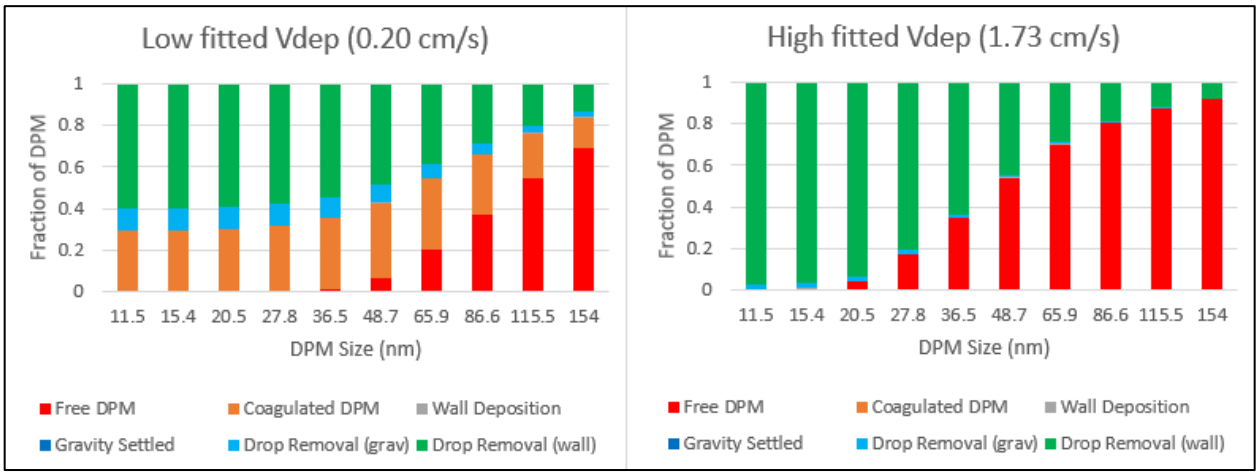

Figure B.51. Modeled fractions of the DPM (by size bin) in all possible classes for inlet DPM and fog drop concentrations measured in Test 3 in Chapter 1. Results are shown using the a) low and b) high fitted V_{dep_d} values determined in Figure B.21.

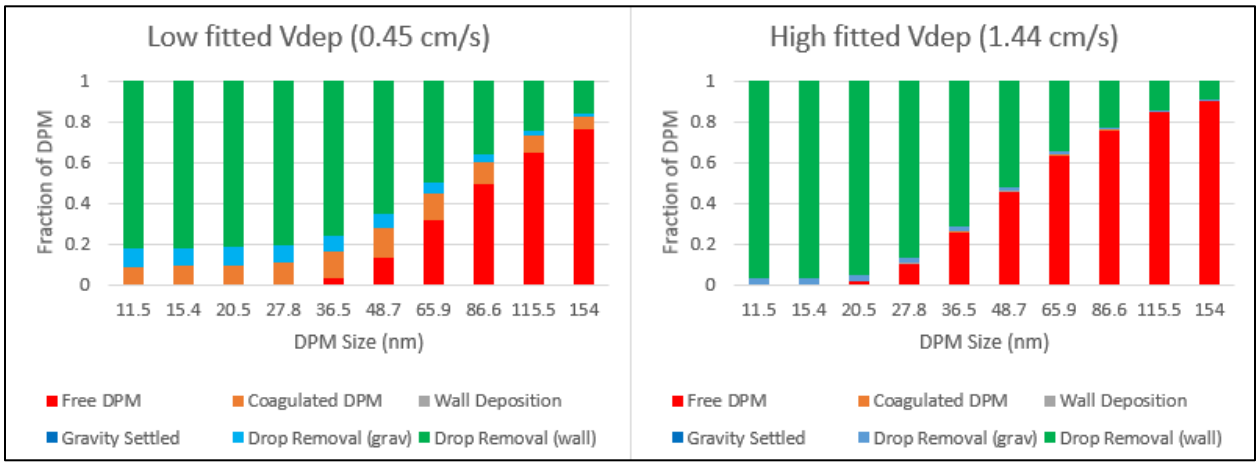

Figure B.52. Modeled fractions of the DPM (by size bin) in all possible classes for inlet DPM and fog drop concentrations measured in Test 4 in Chapter 1. Results are shown using the a) low and b) high fitted V_{dep_d} values determined in Figure B.22.

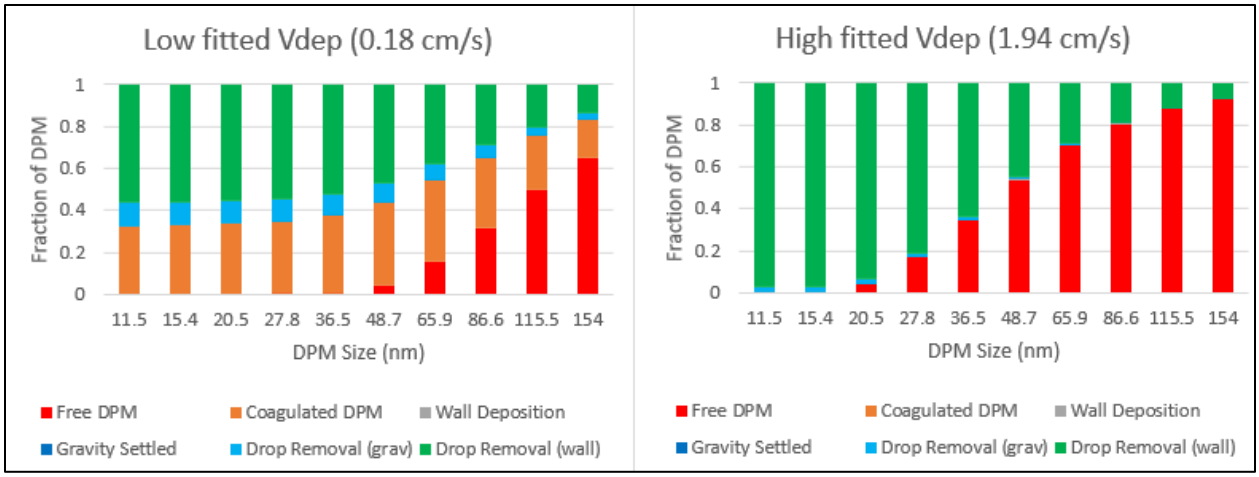

Figure B.53. Modeled fractions of the DPM (by size bin) in all possible classes for inlet DPM and fog drop concentrations measured in Test 5 in Chapter 1. Results are shown using the a) low and b) high fitted V_{dep_d} values determined in Figure B.23.

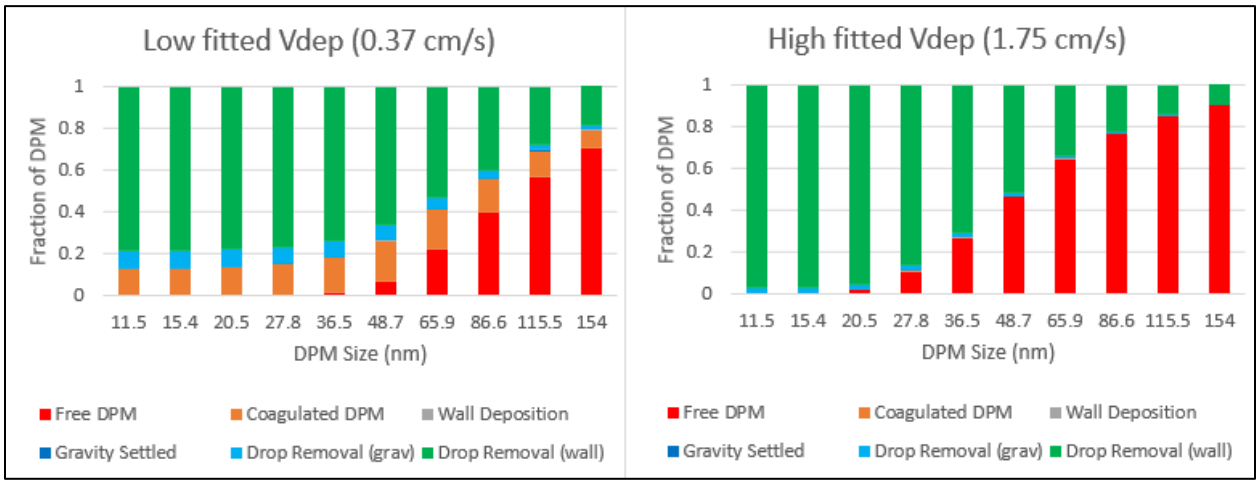

Figure B.54. Modeled fractions of the DPM (by size bin) in all possible classes for inlet DPM and fog drop concentrations measured in Test 7 in Chapter 1. Results are shown using the a) low and b) high fitted V_{dep_d} values determined in Figure B.24.

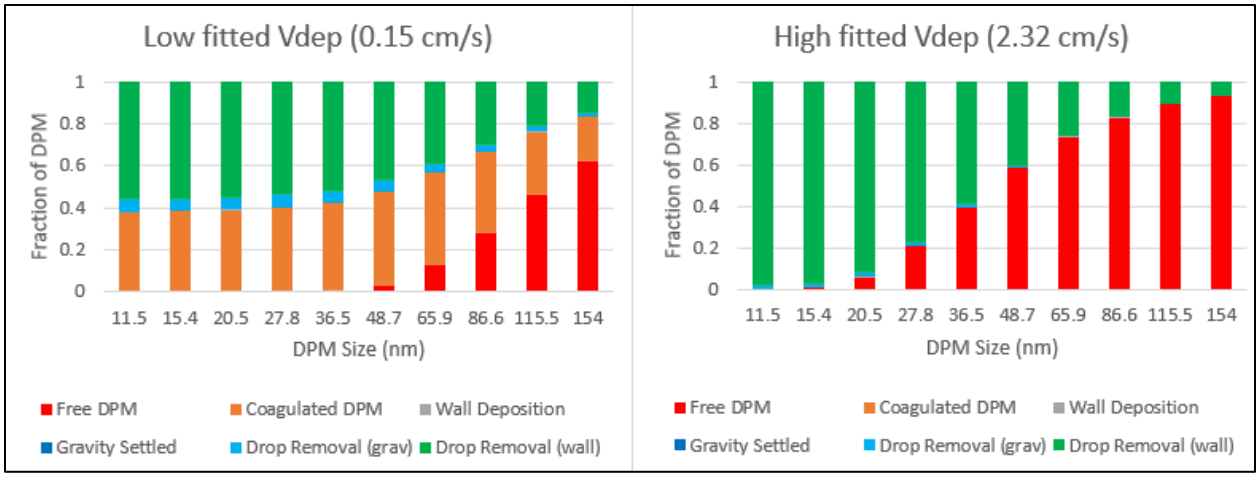

Figure B.55. Modeled fractions of the DPM (by size bin) in all possible classes for inlet DPM and fog drop concentrations measured in Test 8 in Chapter 1. Results are shown using the a) low and b) high fitted V_{dep_d} values determined in Figure B.25.

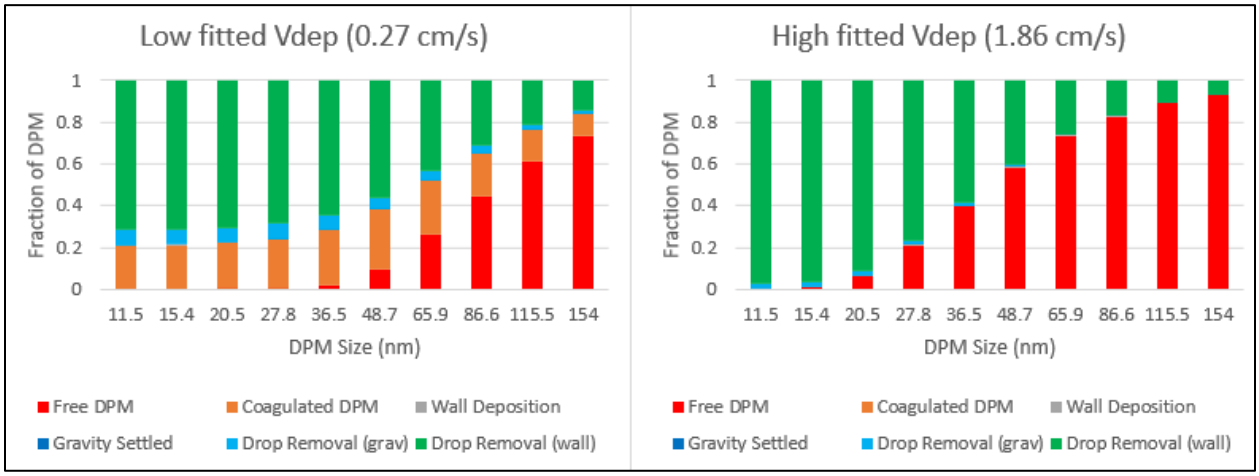

Figure B.56. Modeled fractions of the DPM (by size bin) in all possible classes for inlet DPM and fog drop concentrations measured in Test 10 in Chapter 1. Results are shown using the a) low and b) high fitted V_{dep_d} values determined in Figure B.26.

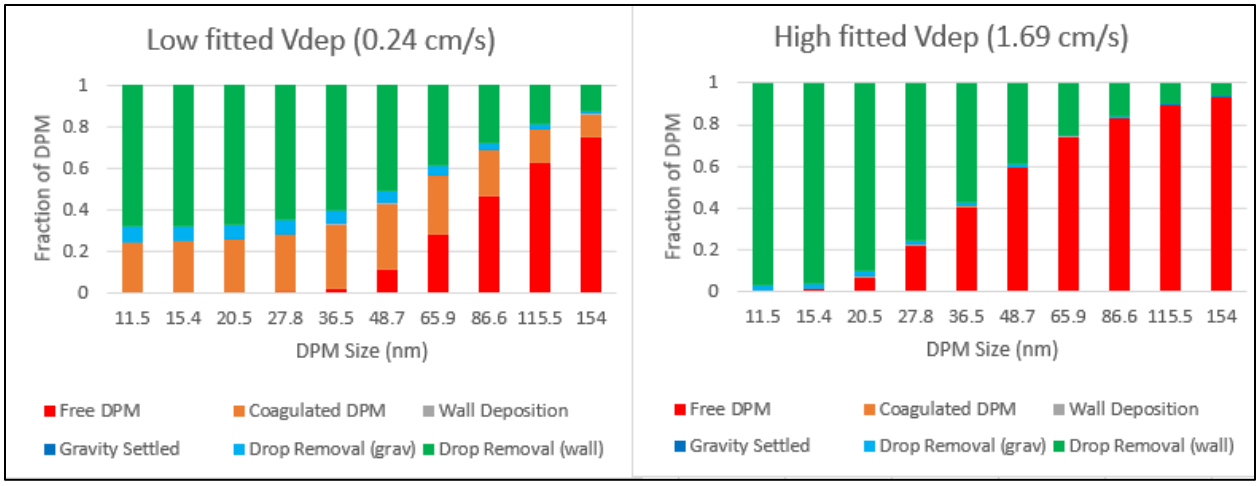

Figure B.57. Modeled fractions of the DPM (by size bin) in all possible classes for inlet DPM and fog drop concentrations measured in Test 11 in Chapter 1. Results are shown using the a) low and b) high fitted V_{dep_d} values determined in Figure B.27.

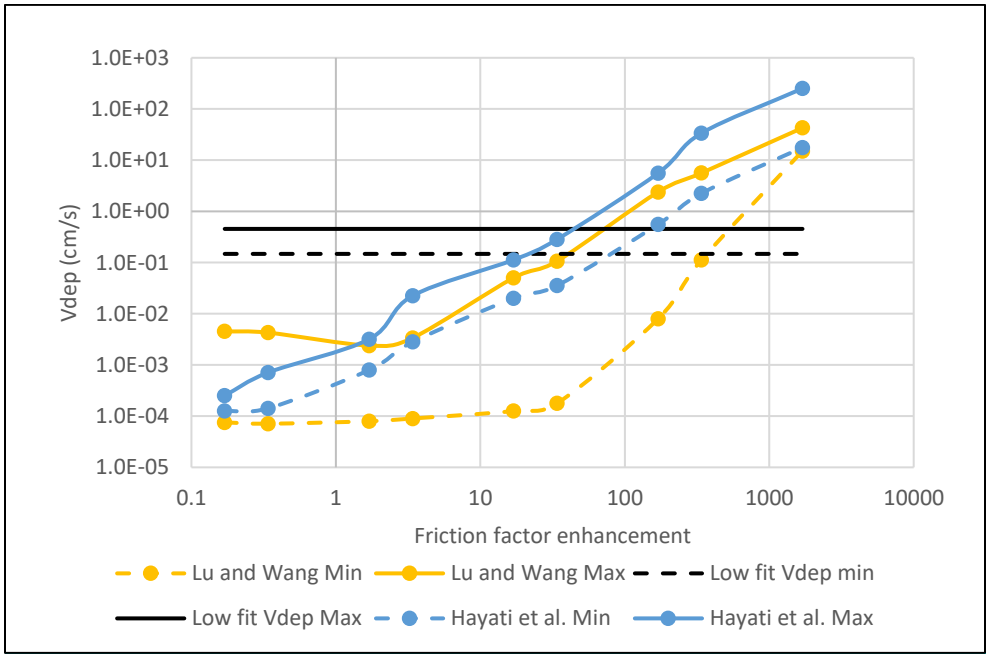

Figure B.58. V_{dep_d} vs f enhancement. The minimum and maximum values of the V_{dep_d} values that allow the modeled DPM removal to match the experimental DPM removal are compared to the minimum and maximum values for V_{dep_d} from Figure 2.9 and 2.10.

Appendix C

```
n = 0; %Loop counter (No.)
lt = 30.48; %tube length (m)
dt = 0.3556; %Tube diameter (m)
At = 1.068; %m
Q = 106 * 0.0283188; %m3/min
t = 0; %Time (s)
ts = 0.005; %Loop time step (s)
diamdpm = (10^-9)*[11.5 15.4 20.5 27.8 36.5 48.7 65.9 86.6 115.5 154]; %DPM diameter
(m)
diamdrop = [0.000001117 0.000001391 0.000001732 0.000002156 0.000002685 0.000003343
0.000004162 0.000005182 0.000006451 0.000008031 0.00001]; %Droplet size bins (m)
velt = Q/(3.1415926 *((dt/2)^2))/60; %Air speed in the tube (m/s)
rt = lt/velt; %Residence time in the tube (s)
Re = 12154; %Reynolds Number in the tube (unitless)
mfp = 0.000000068; %mean free path of air (m)

%The following is the concentration data for all size bins from each test
DPM = [35286.26032      48465.27409      38110.05482      56050.68911
        59444.39748      48610.80494      35441.55134      28396.65469
        21065.54326      10309.41546;     1738.567642      3074.511947
        22746.06845      64299.39131      87794.94625      88149.64503
        72125.89179      52092.63734      30204.77639      10247.94978;
       2130.607432      6157.032289      30942.5181       59943.46554
        65887.87734      55366.58008      39611.13967      28889.7734
        20318.27918      12122.44502;     163737.3935      293744.3395
        178036.5118      132010.724       97425.46505      72028.42777
        64298.66997      67886.67697      58677.8518       31543.69098;
       1721.706405      7686.804372      27982.41831      59201.23938
        73025.64764      68273.43691      52391.80981      35890.27059
        20397.72402      7900.860247;     10587.58725      19039.56617
        51280.92111      116244.4872      152702.8298      152182.228
        121538.2953      82661.87733      48279.77031      22985.95762;
         54570.6964      76715.45312      44944.33935      47012.65472
        43724.08179      32696.73198      23188.97813      20229.12864
        17050.88492      9952.44275;      2361.758262      7594.247199
        18694.43512      38363.00194      49510.61839      48500.2854
        38999.47294      27909.81208      17223.16389      9483.291513;
       4530.644383      5698.596347      3477.761348      5124.75047
        6184.069667      7584.211232      10061.91914      12818.10674
        13076.01546      9805.561625;     9199.353678      74494.32274
        148812.7762      231317.2095      200103.8617      101350.0368
        12975.92365      280.523762       2270.998486      10900.85719;
       23139.84688      83965.52017      135264.469       218965.3234
        222250.4421      161093.7046      84393.86934      38125.43104
        16312.17591      6675.938415];
cd = [0.147965924 0.106597608 0.089057069 0.0958688 0.099224208 0.101797073
0.111258265 0.102857131 0.082876055 0.082875833 0.073796852]; %the droplet
concentration adjustment for each test.
```

```
%The following allocates memory for the simulation.
    I_i = [0 0 0 0 0 0 0 0 0 0 0];
    tsave = [0 0 0 0 0 0 0 0 0 0 0];
    Difdpm = [0 0 0 0 0 0 0 0 0 0 0];
    ScavDPM = [0 0 0 0 0 0 0 0 0 0 0];
    CapDPM = [0 0 0 0 0 0 0 0 0 0 0];
    WallDPM = [0 0 0 0 0 0 0 0 0 0 0];
    CoagDPM = [0 0 0 0 0 0 0 0 0 0 0];
    Walldep = [0 0 0 0 0 0 0 0 0 0 0];
    Gdi = [0 0 0 0 0 0 0 0 0 0 0];
    Gravdrops = [0 0 0 0 0 0 0 0 0 0 0 0];
    Wdi = [0 0 0 0 0 0 0 0 0 0 0];
    Walldrops = [0 0 0 0 0 0 0 0 0 0 0 0];
    GravDPM = [0 0 0 0 0 0 0 0 0 0 0];
    GDPMi = [0 0 0 0 0 0 0 0 0 0 0];
    vdrop = zeros(1,length(diamdrop));
    ddist = zeros(1,length(diamdrop));
    gravseti = zeros(1,length(diamdrop));
    veldepdrop = zeros(1,length(diamdrop));
    Pendrop = zeros(1,length(diamdrop));
    Difdrop = zeros(1,length(diamdrop));
    Vd_avg = zeros(pmax,1);
    OutletDPM = zeros(pmax,1);

    test = 6; %selects which test data to simulate
    ConcDPM = DPM(test,:)*10^6;
    SR = 1; %this is the enhancement factor for surface roughness.
    i = 0;
    for i = 1:10
        concdrop = cd(1,test)*[33511.23175 52217.39683 127592.7619 202468.5667
220666.5 249575.8889 327822.9095 414766.6206 506754.2048 334958.8206 44615.5127]*10^6;
%Concentration of the droplets (#/m3)
        t=0;
        n=0;
        Gdi = 0;
        Wdi = 0;
        vDPM =1225*(diamdpm(1,i))^2*9.81/(18*(1.81*10^-5)); %Stoke's settling velocity
of DPM particles
        DPMdist = vDPM * ts; %Settling distance for DPM particles
        gravsetDPM = (1-((dt^2)/2*acos(DPMdist/dt)-(DPMdist/2)*sqrt(dt^2-
DPMdist^2))/((dt/2)^2*3.14159265358979323846264338 32)); %sets the gravitational DPM
loss per time step as a fraction.

        while t <= rt %from t=0 to t=residence time by increments of the time step.
            t = t+ts; %increases the time by ts.
            n = n+1; %loop counter

            Cc = 1 + ((mfp/diamdpm(1,i))*(2.34 + 1.05*exp(-0.39*(diamdpm(1,i)/mfp))));
%Cunningham correction factor for DPM
            Difdpm(1,i) = 1.38064852*10^-23*288.7*Cc/(3*3.1415926*(1.81*10^-
5)*diamdpm(1,i)); %Diffusion coefficient for the DPM (m2/s)
```

```
            dwidth = [0.247 0.3075 0.3825 0.4765 0.5935 0.7385 0.9195 1.1445 1.4245
1.7745 1.969]*(10^-6); %width of each bin (m).
            for l = 1:length(diamdrop)
                dheight(1,l) = concdrop(1,l)/dwidth(1,l); %(m^-4) The height of the
size bins whose areas equal total concentration.
                I_i(1,l) = (diamdrop(1,l)^2*dheight(1,l)); %(m^-2) The discrete
integral d*N(d) d(d) for each bin.
            end
            I = sum(I_i);
            Lamb = (2*3.1415926.*Difdpm(1,i)*(I)); %Lambda_c from the Scavenging
equation (s^-1)
            Scav = 1-exp(-Lamb*ts); %the scavenging efficiency as a fraction
(unitless)

            holddrops = concdrop; %the following loop calculates the drops removed in
this time step due to inertial impaction and gravitational settling.
            for j = 1:length(diamdrop)
                Difdrop(1,j) = 1.38064852*10^-23*288.7/(3*3.1415926*(1.81*10^-
5)*diamdrop(1,j));
                vdrop(1,j) =997*(diamdrop(1,j))^2*9.81/(18*(1.81*10^-5));
                ddist(1,j) = vdrop(1,j) * ts;
                gravseti(1,j) = (1-((dt^2)/2*acos(ddist(1,j)/dt)-
(ddist(1,j)/2)*sqrt(dt^2-ddist(1,j)^2))/((dt/2)^2*3.1415926)); %sets the initial
droplet loss per time step as a fraction.
                veldepdrop(1,j) =
SR*(0.04*velt)/(Re^0.25)*(1.225*Difdrop(1,j)/(1.81*10^-5))^(2/3);
                Pendrop(1,j) = exp((-4*veldepdrop(1,j)*ts)/(dt));
                Gdi(1,j) = (concdrop(1,j)*(gravseti(1,j)));
                Gravdrops(1,j) = Gravdrops(1,j)+Gdi(1,j);
                concdrop(1,j) = concdrop(1,j) - Gdi(1,j);
                Wdi(1,j) = (concdrop(1,j)*(1-Pendrop(1,j)));
                Walldrops(1,j) = Walldrops(1,j)+Wdi(1,j);
                concdrop(1,j) = concdrop(1,j)- Wdi(1,j);
            end

            %The following adjust the concentration of DPM in each of the DPM
categories.
            dps = (sum(holddrops)-sum(concdrop))/sum(holddrops); %fraction of drops
removed in the time step.
            CoagDPM(1,i) = CoagDPM(1,i) + (ConcDPM(1,i)*(Scav));
            CapDPM(1,i) = CapDPM(1,i) + (ConcDPM(1,i)*(Scav));
            ConcDPM(1,i) = ConcDPM(1,i)*(1-Scav); %Concentration of DPM after
scavenging for the time step (#/m3)

            ScavDPM(1,i) = ScavDPM(1,i) + (dps*CapDPM(1,i));
            CapDPM(1,i) = CapDPM(1,i) - (dps*CapDPM(1,i));

            veldepdpm = (0.04*velt)/(Re^0.25)*(1.225*Difdpm(1,i)/(1.81*10^-5))^(2/3);
            Pendpm = exp((-4*veldepdpm*ts)/(dt));
            Walldep(1,i) = ConcDPM(1,i)*(1-Pendpm);
            ConcDPM(1,i) = ConcDPM(1,i) - Walldep(1,i);
```

```
        WallDPM(1,i) = WallDPM(1,i) + Walldep(1,i);

        GDPMi(1,i) = (ConcDPM(1,i)*(gravsetDPM));
        GravDPM(1,i) = GravDPM(1,i)+GDPMi(1,i);
        GravDPM(1,i) = GravDPM(1,i) + GDPMi(1,i);
        ConcDPM(1,i) = ConcDPM(1,i) - GDPMi(1,i);


    end

end
Vd_avg1 = mean(veldepdrop); %determines the average drop depositional velocity.
```